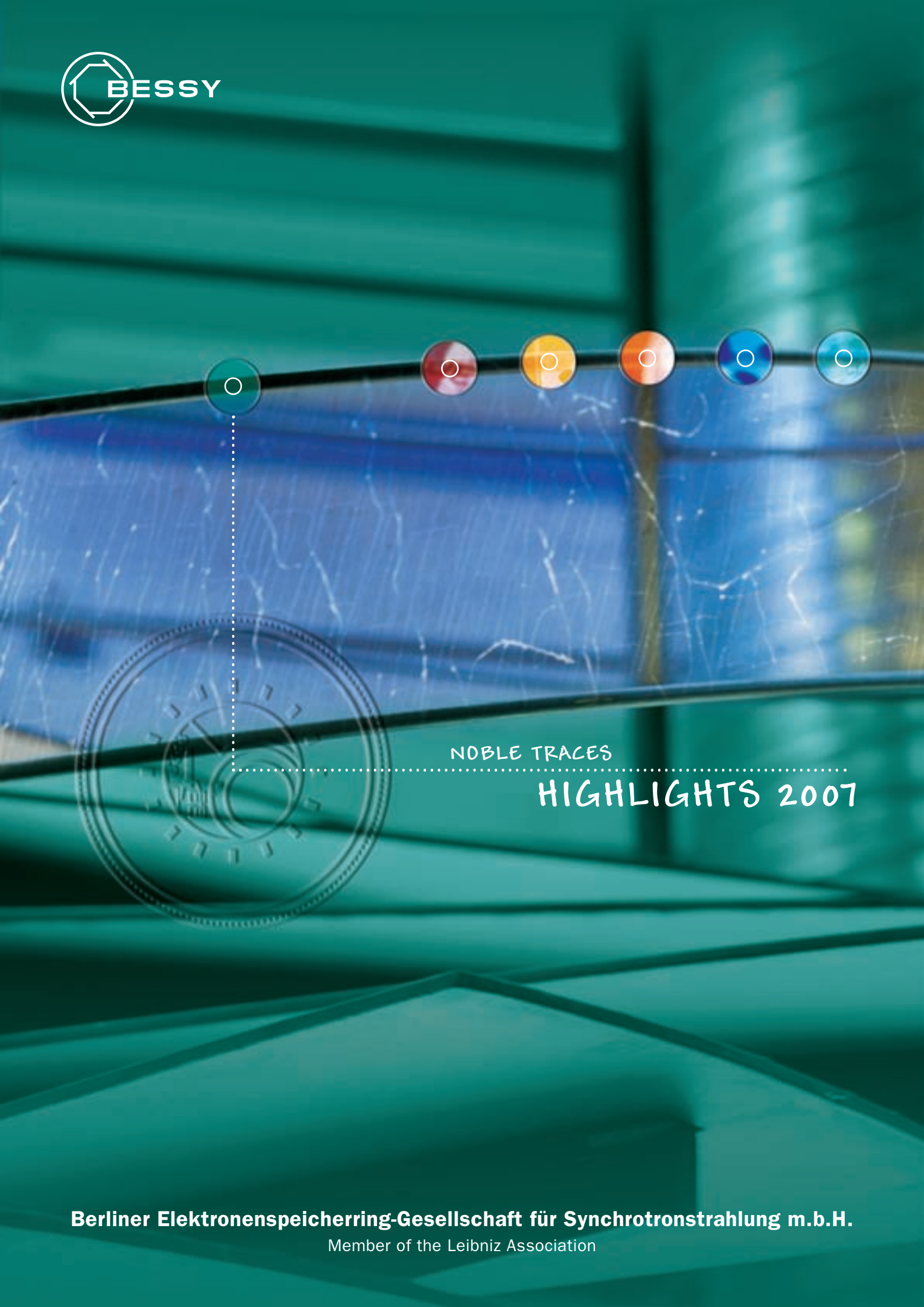

Berliner Elektronenspeicherring-Gesellschaft für Synchrotronstrahlung m.b.H.

Member of the Leibniz Association

PUBLISHED BY:

Berliner Elektronenspeicherring-Gesellschaft für
Synchrotronstrahlung m.b.H. – BESSY

Albert-Einstein-Straße 15
12489 Berlin, Germany
phone +49 (0)30 / 6392 2999
fax +49 (0) 30 / 6392 2990

www.bessy.de
info@bessy.de

Board of Directors:
Prof. Dr. Dr. h.c. Wolfgang Eberhardt,
Prof. Dr. Eberhard Jaeschke,
Thomas Frederking

Editor:
Dr. Markus Sauerborn

Layout:
Annette Weber, Stitz & Betz GmbH, Berlin

ISSN Number: 1611-6127

NOBLE TRACES

INTRODUCTION

Dear BESSY-Users and Friends,

It does not happen often that you are lucky twice in a row. Sometimes it happens in real life when you play lottery or when you are expecting twins. But in science…

Then last year we were 'hit' by the announcements from Stockholm that Peter Grünberg and – just one day after – Gerhard Ertl would receive the Nobel Prize in physics and in chemistry, respectively. We have been thrilled for several reasons, not least owing to our long lasting and very successful collaborations with the Forschungszentrum Jülich and the Fritz-Haber-Institut in Berlin, but more importantly, due to the awardees enormous impact on two major research fields at BESSY during the last 15-20 years. In fact, joint studies, then still at BESSY-I, revealed the basis of the mechanism of Grünbergs giant magnetoresistance discovery - the discrete quantized electronic structure of the interlayer. And already in 1986, Ertl and his co-workers at FHI started to use synchrotron radiation to study heterogeneous catalysis. Today, scientists study more complex catalytic reactions under realistic conditions (see article) and many researchers work on new layered systems, which still have some surprises in stock.

Many recent studies have been presented at the VUV-XV conference, which took place in the 'Konzerthaus am Gendarmenmarkt' in Berlin in the summer. The conference was organized by BESSY in collaboration with the Technische Universität Berlin. More than 500 participants gathered in the centre of Berlin to present and discuss their latest research results, mainly achieved by using synchrotron radiation sources world wide. We would like to thank all participants and the organizing team at BESSY to make this extraordinary event possible.

But last year held another, however less surprising, issue. After being solely a synchrotron radiation facility for almost 30 years, BESSY is about to merge with the Hahn-Meitner-Institut to form a new 'Helmholtz Centre Berlin for Materials and Energy'. The new centre will operate two large scale facilities (BESSY-II and Ber-II) to provide synchrotron radiation and neutrons with a state-of-the-art experimental infrastructure. The merger will strengthen our joint research programs on modern materials and will also improve opportunities and services for our users. In particular, we encourage research projects taking advantage of the complementary use of photons and neutrons.

We hope that our user community will largely benefit from the merger. Please keep on putting forward challenging experiments. We are indebted to all our users, who have been, and still are, the main reason for the BESSY story of success. However, without the drive and the enthusiasm of our staff to make things possible, many ideas would stay just ideas.

Enjoy following our 'noble traces'…

Prof. Dr. Dr. h.c. Wolfgang Eberhardt

Prof. Dr. Eberhard Jaeschke

Thomas Frederking

NOBLE TRACES

SCIENTIFIC HIGHLIGHTS

The digital octopus – or dual career for porphyrins

H. Wende[1], M. Bernien[2], J. Luo[2], C. Weis[1], N. Ponpandian[2], J. Kurde[2], J. Miguel[2], M. Piantek[2], X. Xu[2,3], Ph. Eckhold[2], W. Kuch[2], K. Baberschke[2], P. Srivastava[1,4]

1 Universität Duisburg-Essen
2 Freie Universität Berlin
3 Fudan University, Shanghai, People's Republic of China
4 IIT Delhi, New Delhi, India

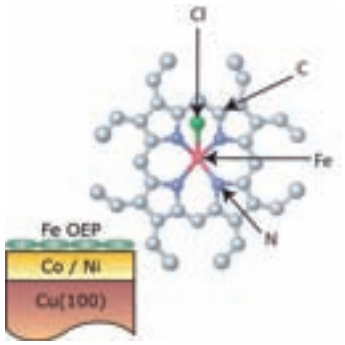

Fig. 1: Schematic representation of Fe octaethylporphyrin (OEP) chloride and the sample setup.

It's not only that they look like molecular octopuses – they also have 'their tentacles everywhere': the Fe-porphyrins investigated here have eight legs as their counterpart in the fauna. Fascinatingly, porphyrins are parts of numerous biologically active molecules. A member of this family with magnesium in the centre is chlorophyll – the green colour of leaves – which insures that plants can use sun light to store energy. In haemoglobin Fe-porphyrins take care of the oxygen transport in our blood. The latter have aroused the interest of physicists, since with iron in the centre these molecules act as tiny magnets, a prerequisite on the way to achieve molecular spintronics. This technology utilizes the electron spin additionally to its charge. To make the porphyrin useful for spintronics, it is essential to investigate the interaction of the porphyrin with surfaces and, even more challenging, to manipulate or switch its iron spin direction.

In this experiment we studied a single layer (monolayer: ML) of porphyrins on epitaxially grown ferromagnetic cobalt and nickel layers on Cu(100) [1,2]. From our measurements we observe that the Fe-porphyrins adsorb flat on the surface like octopuses 'accidentally' reaching the beach and drying in the sun. We find that the Fe spin of the porphyrins couples ferromagnetically to magnetic films (the beach in our picture). The promising result for spintronics is that the iron centres of the porphyrins can be switched by changing the magnetic direction of the underlying magnetic film. This might be used in the future for spin-dependent electric transport through biomolecular devices.

The results were obtained with X-ray absorption spectroscopy (XAS) and X-ray magnetic circular dichroism (XMCD) measurements at the beamline UE56/2-PGM2. Thereby we were able to discriminate the magnetic effects of all the key players in this game. The samples were prepared by sublimating Fe-octaethylporphyrin chloride (OEP) under UHV conditions on a 5 ML Co film and a 15 ML Ni film epitaxially grown on Cu(100) (schematic representation in Fig. 1). One advantage of the X-ray absorption spectroscopy is that the information on the electronic structure and the magnetism can be gained in an element-specific manner by tuning the photon energy to the absorption edges of the elements in the molecule (e.g. Fe, N, C) and the underlying film (Co or Ni) (see labels in Fig. 1).

To determine the orientation 'of the octopus on the beach' we analyzed the Near-Edge X-ray Absorption Fine Structure (NEXAFS) at the nitrogen K-edge versus the incidence angle of the incoming light with linear polarization [1]. These spectra exhibit a prominent angular dependence (Fig. 2). This reveals a well defined orientation of the molecules on the surface. The detailed fine structures can be assigned to typical molecular electronic structures – the antibonding π^*- and σ^*-resonances (labelled in Fig. 2). The σ^*-resonances are scattering resonances probing the antibonding states oriented in direct connection from atom to atom. For the case of the N K-edge these are the N-Fe and N-C σ^*-states. Since the σ^*-resonances are strong at normal X-ray incidence and the ϖ^*-resonances dominate at grazing X-ray incidence it can be safely concluded that the octopus is basically lying flat on the beach.

Next we tune the photon energy to the Fe $L_{2,3}$ absorption edges to probe the magnetic properties (spin direction, magnetic moment) of the Fe atom in the molecule – the head of the octopus – in comparison to the magnetic properties of the Ni or Co film [1,2]. In Fig. 3 the Fe XAS and XMCD spectra are shown for the Ni film and Co film substrates. Since a 5 ML Co film exhibits an in-plane magnetization whereas that of a 15 ML Ni film is out-of-plane, the temperature-dependent measurements were carried out at grazing or normal X-ray incidence, respectively (see inset of Fig. 3). For both cases a clear XMCD signal can be seen at room temperature (Fig. 3 b, d) which demonstrates that the Fe spins in the porphyrins are ordered. Furthermore, it turns out that on the Co substrate all spins in the molecules are oriented in-plane whereas on the Ni film they are all oriented out-of-plane. A magnetic field of only ~10 mT was applied to saturate the magnetic films, although at 300 K this field is far from being sufficient to order the paramagnetic Fe-porphyrin molecules. Hence, there must exist a further coupling mechanism of the spin in the molecule to the ferromagnetic films. Interestingly, there

References:

[1] H. Wende et al., Nature Materials **6**, 516 (2007).

[2] M. Bernien et al., Phys. Rev. B **76**, 214406 (2007).

Acknowledgements:

We want to thank P.M. Panchmatia, B. Sanyal, P.M. Oppeneer and O. Eriksson (Uppsala University, Sweden) for their enlightening DFT+U calculations, which revealed the coupling mechanism. P.S. wishes to thank the DFG (SFB 658) for financial assistance and the University of Duisburg-Essen for hospitality and support. Supported by BMBF and DFG (SFB 658, Heisenberg-Programm).

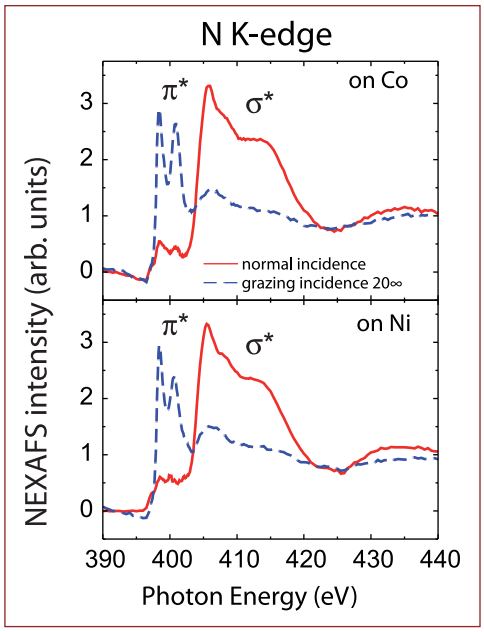

Fig. 2:
Angular dependence of NEXAFS (linear polarization) of Fe-OEP at the N K-edge for the Co and Ni substrates. X-rays at normal and grazing incidence (20°) were applied to determine the molecule's orientation (Fig. taken from [1]).

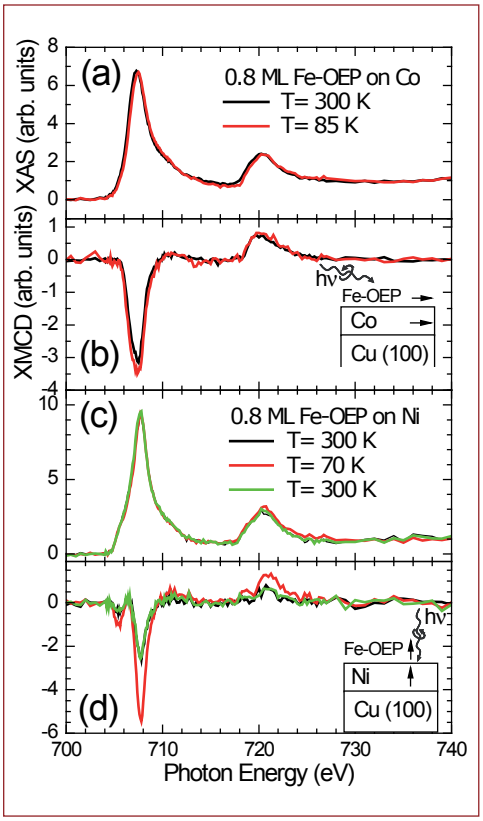

Fig. 3:
XAS and XMCD spectra (applied field 10 mT) for 0.8 ML Fe-OEP molecules on Co (a, b) recorded at 300 K and 85 K and on Ni (c, d) at 300, 70 and 300 K (Fig. taken from [2]).

is hardly any change of the Fe XMCD intensity when cooling down the Co substrate to 85 K. However, when the Ni film is cooled down, a dramatic increase of the Fe XMCD signal can be seen in Fig. 3 (d). This reveals that the coupling of the Fe spins to the Ni film is considerably weaker than the one for Co [2].

What is the nature of this coupling phenomenon? To answer this question we collaborated with O. Eriksson and P. M. Oppeneer at Uppsala University, Sweden. Their density functional theory (DFT+U) calculations for the porphyrins on the Co film revealed that there is no direct hybridization between the Fe atom in the molecule and the Co film below [1]. However, the Fe-surrounding N atoms interact with the surface. By combining these results we conclude that a 90° indirect coupling mechanism is responsible for the observed phenomena [1].

To investigate the coupling in greater detail we measured element-specific hysteresis curves by tuning the photon energy to the Fe XMCD maximum or to the ones of the respective ferromagnetic films and swept the magnetic field. The result for the Ni substrate is presented in Fig. 4. The hysteresis curve of Fe in the molecule directly follows the one of the ferromagnetic film. This shows that the coupling is ferromagnetic. Even more fascinating is that the two hysteresis curves have the same shape, which demonstrates that the

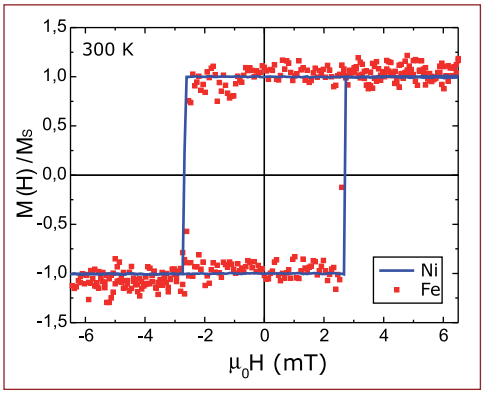

Fig. 4:
Element-specific hysteresis curves of the porphyrin Fe atom and the Ni film at the L_3-edge XMCD maximum of Fe OEP on Ni/Cu(100) at 300 K (Fig. taken from [1]).

Fe spin of the molecule directly follows the magnetization of the film. Hence, the spin of the molecule can be switched by reversing the magnetization of the film. The spin can point either left/right (as in the photograph) or up/down – a real digital octopus. The switching of the spin direction might open new possibilities for molecular devices for spintronics, where e.g. spin-dependent electric transport is utilized.

Contact:
Heiko Wende
heiko.wende@uni-due.de

Soft landing required!

How XAS can help to monitor the conditions after touching gold

M. Fonin[1], S. Voss[1], M. Burgert[1], Yu. S. Dedkov[2], U. Groth[1], U. Rüdiger[1]

1 Universität Konstanz
2 Technische Universität Dresden

Single-molecule magnets (SMMs) are one possible approach to nanomagnets (or nanoscale magnetic particles). These molecules contain a finite number of interacting spin centres (e.g. transition metal ions), and thus provide ideal opportunities to study basic concepts of magnetism and quantum mechanics such as quantum tunneling of magnetization and quantum phase interference. Moreover, SMMs exhibit the conventional properties of a magnet (e.g. magnetic hysteresis loop) below a blocking temperature (T_B) of a few Kelvin. Hence, they might promise the realization of the smallest practical unit for magnetic memories.

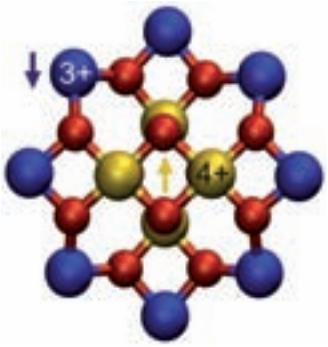

Fig. 1: Representative image of the Mn_{12} core comprising eight Mn^{3+} (blue) and four Mn^{4+} (yellow) ions viewed along the c-axis. O ions are depicted in red. A deviation from the 8:4 ratio of the Mn ions can be used as an indication of degradation.

The most widely investigated class of SMMs is the Mn_{12} group, comprised of Mn_{12}-acetate and its derivatives [1,2]. The synthesis and crystallographic structure of Mn_{12}-acetate have been reported in 1980, followed then by the discovery of its fascinating magnetic properties in 1993 [3]. The Mn_{12} core contains an inner tetrahedron of four Mn^{4+} (S = 3/2) surrounded by an outer ring of eight Mn^{3+} (S = 2) ions with spins strongly coupled via the superexchange interaction through oxygen ions (Fig. 1). The Mn^{4+} spins are coupled antiferromagnetically to the Mn^{3+} spins resulting in a ground state spin S=10. When crystallized, Mn_{12}-acetate forms a tetragonal lattice with the easy magnetization axes of individual Mn_{12} molecules oriented along the c-axis. The high-spin ground state and a large uniaxial magnetic anisotropy give rise to a magnetic bistability below the blocking temperature T_B (about 3.5 K for Mn_{12}-acetate).

To date, experiments on the magnetic properties of Mn_{12} have been performed mostly on bulk-like material while the magnetic as well as the electronic properties of the individual molecules or SMM monolayers on a surface remain unknown to a large extent. Nonetheless, 'molecular magnetists' expect an interesting interplay between quantum tunneling, phase interference effects and electronic correlations in the transport properties of isolated SMM clusters.

One of the most promising strategies to access individual Mn_{12} molecules is to organize the clusters on conducting surfaces and to use scanning tunneling microscopy (STM) in order to address the electronic and magnetic properties of Mn_{12} molecules (Fig. 2). With respect to this, there has been a variety of approaches to graft Mn_{12} molecules on different surfaces [4]. Although depositing and investigating molecules on surfaces is nearly routine nowadays, the conservation of the structural, electronic and magnetic properties of Mn_{12} clusters upon deposition on surfaces could not be unambiguously confirmed so far. Moreover, when using synchrotron techniques for the investigation of Mn_{12} monolayers a special attention should be paid to the fact of possible influence (or damage) due to synchrotron radiation itself.

We have implemented X-ray absorption spectroscopy (XAS) at room temperature to study the electronic properties of individual Mn_{12} single molecule magnets, both in the crystalline and monolayer environment. Synchrotron radiation from RGBL-PGM and PM-3 beamlines at was used in these experiments. We used several Mn_{12} derivatives: Mn_{12}-thiophenecarboxylate (Mn_{12}-th), Mn_{12}-biphenylcarboxylate (Mn_{12}-biph) and Mn_{12}-parafluorobenzoate (Mn_{12}-pfb) and studied two 'landing' conditions of Mn_{12} monolayers on a gold surface (Fig. 3).

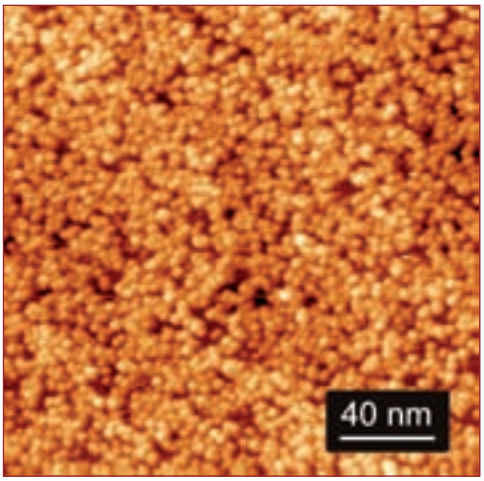

Fig. 2: 200x200 nm² scanning tunneling microscopy image of Mn_{12} molecules on the functionalized Au(111) surface.

References:

[1] D. Gatteschi and R. Sessoli, Angew. Chem. Int. Ed. **42**, 268 (2003).

[2] G. Christou et al., MRS Bull. **25**, 66 (2000).

[3] R. Sessoli et al., Nature **365**, 141 (1993).

[4] S. Voss et al., Dalton Trans., **499** (2008).

[5] R. Moroni et al., Phys. Rev. B **68**, 064407 (2003).

Acknowledgements:

Supported by DFG, SFB 513.

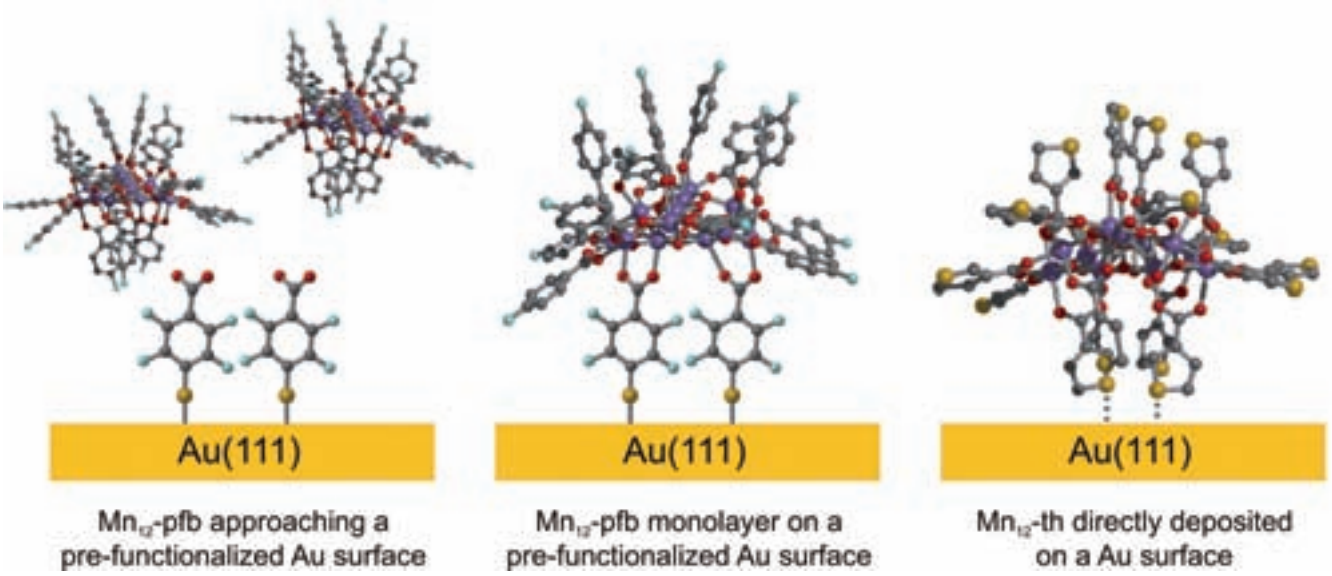

Fig. 3:
Sketches of the used deposition techniques.

The Mn $L_{2,3}$ XAS spectra obtained from Mn_{12}-th, Mn_{12}-pfb, Mn_{12}-biph single crystals (Fig. 4, upper panel) revealed a multiplet structure, which is in good agreement with previous measurements [5]. Then we compared those spectra with XAS spectra from Mn_{12}-monolayers on Au surface. To monitor induced damages we also measured spectra with radiation damaged Mn_{12}-pfb single crystals (a) and Mn_{12}-pfb single crystals that have been Ar^+ sputtered (c) to induce damage. The lower panels of Fig. 4 shows a comparison of the typical XAS line shapes.

When Mn_{12}-th monolayers have been directly deposited on Au the shape of spectrum (d) is very similar to the Ar+ sputtered sample indicating a degradation of the molecules during the deposition due to the sole Mn^{2+} contribution. However, when we 'landed' Mn_{12}-pfb in monolayers on the pre-functionalized Au(111) surface by ligand exchange, the spectrum (b) allows the interpretation that an intact layer of molecules has been damaged under the influence of X-ray-radiation due to its similarity to spectrum (a). Assuming that the spectral shape is a consequence of radiation-induced degradation rather than degradation during the deposition, the need for functionalization layers corroborates the necessity to decouple the molecule from the substrate to avoid a possible damage during the monolayer preparation.

The different signatures from monolayers damaged during the deposition or by X-ray radiation, respectively, indicate a possibility to examine the success of the deposition by a straightforward XAS measurement while STM studies alone cannot corroborate the presence of intact Mn_{12} molecules on a surface (Fig. 2). Thus, despite the radiation sensitivity of Mn_{12}, XAS is a useful technique significantly contributing to the progress in investigation of SMM monolayers, which is necessary to realize the vision of implementing Mn_{12} in quantum computing devices.

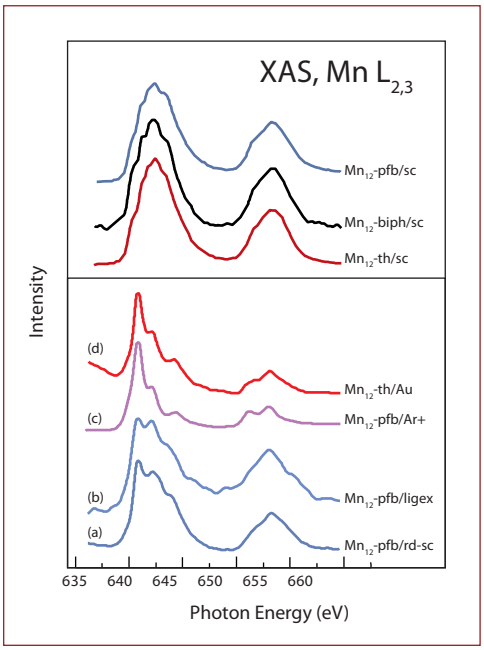

Fig. 4:
Upper panel: XAS spectra obtained from Mn_{12}-th, Mn_{12}-biph, and Mn_{12}-pfb single crystals. Lower panel: XAS spectra obtained from (a) radiation-damaged Mn_{12}-pfb single crystals and (b) Mn_{12}-pfb monolayers on the pre-functionalized Au(111) surface that look like those in the STM image (Fig. 2), (c) Ar^+-sputtered Mn_{12}-pfb single crystals and (d) Mn_{12}-th monolayers deposited directly on Au(111).

Contact:
Mikhail Fonin
mikhail.fonin@uni-konstanz.de

Cool magnetite: Frozen electrons below the Verwey temperature

J. Schlappa[1,*], C. Schüßler-Langeheine[1], C. F. Chang[1], H. Ott[1], A. Tanaka[2], Z. Hu[1], M. W. Haverkort[1], E. Schierle[3], E. Weschke[3], G. Kaindl[3], L. H. Tjeng[1]

1
Universität zu Köln

2
ADSM, Hiroshima University

3
Freie Universität Berlin

* present adress:
Swiss Light Source

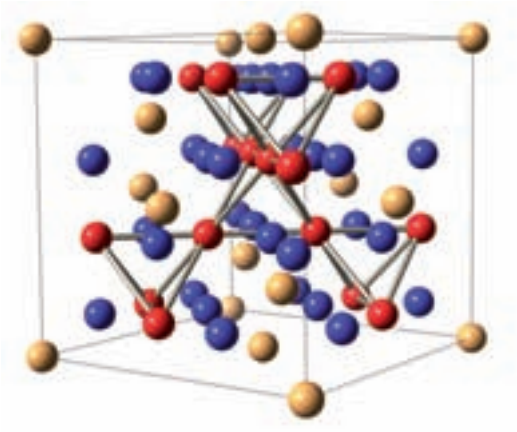

Fig. 1:
Magnetite room temperature crystal structure. Blue balls denote oxygen sites, yellow balls iron A-sites and red balls iron B-sites.

Magnetite (Fe_3O_4) is known to the humanity for more than 2,000 years and still keeps intriguing and suprising us with its unusual properties. As a natural magnet it not only has been already used by ancient Chinese navigatiors as a compass, it also turns out that small magnetite particles inside migratory bird's beaks allow these animals to use the earth's magnetic field to find their way. In these days magnetite is considered for spintronic applications, because all electrons carrying electrical current in this material have the same spin orientation.

In 1939 the Dutch physicist E. J. W. Verwey found that when magnetite is cooled to temperatures below 120 K, its properties change quite drastically (Verwey transition). Its crystalline structure turns from highly symmetric to a complex low-symmetry phase and the electrical resistivity grows by a factor of hundred [1]. What exactly happens at this transition has been debated now for almost 70 years and it requires modern structural and spectroscopic tools to find the well-hidden order in the low-temperature phase [2,3].

At room temperature magnetite crystallizes in the cubic inverse-spinell structure. One-third of the iron-atoms are surrounded by 4 oxygen ions (the so-called A-sites, blue balls in Fig. 1), whereas two-thirds are surrounded by 6 oxygen ions (B-sites, red balls). The B-site irons are mixed valen,t which means that on average two iron sites share one extra electron. Verwey suggested that below 120 K these extra electrons freeze to an ordered arrangement of half divalent (2+) and half trivalent (3+) sites and therefore can no longer transport current. Such a kind of charge order has in the meantime been found in various compounds, but the Verwey transition in magnetite and especially the interplay between the crystalline and electronic structure is still not understood.

In a recent powder-diffractometry experiment the crystalline structure of magnetite at low temperatures could mostly be solved and signatures of charge order were indeed found [2]. Based on this crystal structure, band structure calculations predict an additional ordering of orbitals (i.e. ordering in the arrangement of charge around the ions) for the low-temperature phase [4]. Typically charge and/or orbital order lead to a displacement of neighbouring oxygen ions and to the appearance of superstructure reflections, which can be probed by e.g. neutron diffraction. In the case of magnetite, though, the orbital order is well hidden, because it involves only the t_{2g} orbitals, which interact very little with oxygen neighbours. The aim of our work was to investe the connection between the formation of low-temperature superstructure in magnetite and the electronic state of the Fe ions. For this purpose we used the technique of resonant soft X-ray diffraction (RSXD) [5], which directly combines spectroscopy with diffraction. We applied photons with energies at the Fe $L_{2,3}$ resonance, where the scattered signal is most sensitive to the electronic states of the Fe ions.

For the experiment we chose magnetite thin films rather than bulk crystal, because films allow us to pick up intensity from the (001) reflection, which cannot be reached at the iron $L_{2,3}$ resonance directly, as the wavelength is too large. The broadening of reflections in thin films transfers enough intensity into the reachable momentum space such that the diffraction signal can be still picked up. Our magnetite films had a thickness of 40 nm and showed a sharp Verwey transition at 115 K (see Fig. 2). RSXD experiments were carried out at beamline UE52-SGM, using the UHV diffractometer built at the Freie Universität Berlin.

References:

[1] E. J. W. Verwey, Nature **144**, 327 (1939).

[2] J. P. Wright, et al., Phys. Rev. Lett. **87**, 266401 (2001).

[3] J. Schlappa, et al., Phys. Rev. Lett. **100**, 026406 (2008).

[4] I. Leonov, et al., Phys. Rev. Lett. **93**, 146404 (2004).

[5] C. W. M. Castleton and M. Altarelli, Phys. Rev. B **62**, 1033 (2000).

Acknowledgements:

We gratefully appreciate helpful discussions with M. Braden, H.-H. Hung, P. G. Radaelli, P. Abbamonte, G. A. Sawatzky, D. Khomskii. Funded by the DFG through SFB 608.

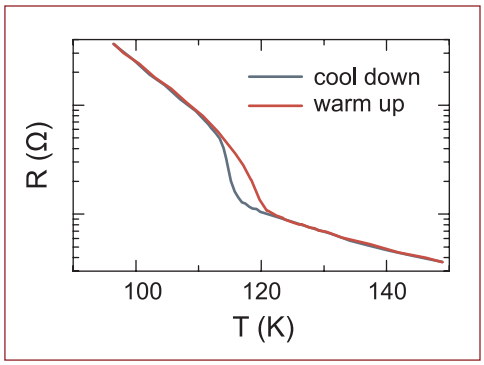

Fig. 2:
Electrical resistivity of a 40-nm magnetite thin film as a function of temperature.

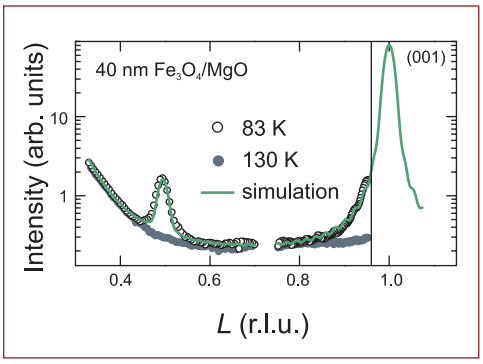

Fig. 3:
Scans along [001] (L): Open (filled) symbols are experimental data taken below (above) the Verwey temperature, the green line is a simulation.

Fig. 3 shows the diffraction scan at a photon energy of 708.5 eV along the L-direction. Below the Verwey temperature we see two diffraction peaks: (00½) and (001), the second one visible as an onset. Both reflections disappear above the Verwey temperature, demonstrating their relation to the low-temperature phase. To investigate the origin of these reflections we studied their intensity across the Fe $L_{2,3}$ resonance and compared it with X-ray absorption (XAS) data. For this study we decomposed the XAS signal into the contributions of the three different Fe sites, making use of cluster model calculations. Fig. 4(a) displays XAS with the single contributions, from B-site Fe^{2+} (red solid line), A-site Fe^{2+} (orange dotted line) and B-site Fe^{3+} (red dashed line) irons, together with the (00½) and (001) diffraction spectra.

The (00½) reflection shows a strong resonance coinciding with the position of the absorption signal of B-site Fe^{2+} Ion. The (00½) reflection is hence a result of order involving only these B-site Fe^{2+} ions. The only degree of freedom, which can make one 2+ site different from another, is the orientation of the t_{2g} orbitals, implying an orbital order in the system. This result is in fact the first direct observation of orbital order in magnetite.

In contrast, the (001) reflection shows a double-peak structure, which decreases sharply toward low and high-energy sides. The two maxima are well-separated and their position coincides with the position of the maxima of the absorptions signals belonging to the two B-site irons, the first peak to the maximum of

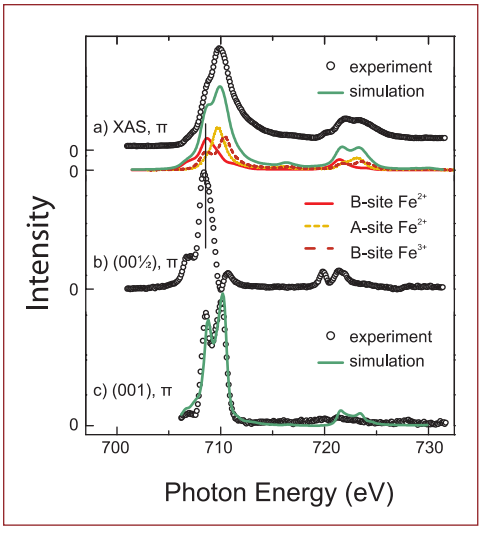

Fig. 4:
XAS and RSXD spectra around the Fe $L_{2,3}$ resonance: (a) experimental XAS spectrum (symbols) with a simulation (green line) showing the separate contribution of the different Fe sites. (b) (00½) RSXD spectrum and (c) (001) RSXD spectrum with a B-site charge-order simulation (green line).

Fe^{2+} and the second peak to Fe^{3+}. A simulation using the charge order scenario proposed in Ref. [3] gives a very good agreement with the experimental findings. From this result we can safely conclude that the (001) reflection is indeed a result of the charge order of the B-site iron ions.

In conclusion, using resonant soft X-ray diffraction from a magnetite thin film we find clear spectroscopic evidence for charge and orbital order.

Contact:
Justina Schlappa
Justina.Schlappa@psi.ch

The hole is important!
The quest for ferromagnetism in doped ZnO.

T. Tietze[1], M. Gacic[2], G. Schütz[1], G. Jakob[2], S. Brück[1], E. Goering[1]

1 Max-Planck-Institut für Metallforschung, Stuttgart

2 Johannes Gutenberg-Universität, Mainz

Zinc oxide is a widely used mineral. Tons of it are added to the vulcanization process to improve our tyres. It makes cement resistant to moisture and protects our skin from the UV light. However, Zinc oxide is also transparent and semiconducting, indispensible properties for the combination of optics and electronics. In addition, ZnO doped with moderate amounts of a transition metal (Co, Mn,…), its magnetic properties are dramatically enhanced [1]. The combination of these material properties makes ZnO a promising candidate for spin electronic applications. These 'Spintronic' applications utilize the charge and the spin of an electron to build new functional systems. ZnO is not the only candidate of the diluted magnetic semiconductors (DMS) family.

Up to now, enormous efforts have been made to verify the intrinsic mechanism for ferromagnetism (FM) in this system and to exclude extrinsic ferromagnetism, like cluster of the doping transition metal (TM). Theoretical models explain this room temperature ferromagnetism (RT-FM) by ferromagnetic ordering of the magnetic TM ions, for example Co or Mn, which is mediated via the doping modified ZnO host.

This has been recently questioned for several reasons: No significant charge carrier enhanced FM has been observed, as in the low temperature DMS system GaMnAs [2]. In contrast, other non-stoichiometric variations as O-vacancies have shown dramatic influence on the ferromagnetism [3, 4]. And, most striking, ferromagnetism can be found in undoped ZnO [5], and also in ZnO doped with typical non-magnetic ions (C, Sc, Cu and Al [6]). These observations clearly challenge the role of the 'magnetic' TM ions in ZnO and other DMS systems. If this is true, where is the ferromagnetism from?

In order to find the element specific origin of RT-FM in Co doped ZnO, we performed X-ray magnetic circular dichroism (XMCD) experiments at the Co $L_{2,3}$ and O K edges. We prepared slightly Co doped (5%) samples as well as layered samples and Li (10%) co-doped layered samples to enhance FM.

The XMCD measurements were performed at the bending magnet beamline PM-3 and UE56-2 beamline in total electron yield (TEY), total fluorescence yield (TFY), and reflection-mode, in order to provide surface, bulk, and interface sensitivity. A fast switching superconducting magnet system has been used to flip the magnetic field between ±2T at each data point to minimize drift phenomena.

Very high sensitivity of the XMCD signal up to 10^{-6} with respect to the full absorption signal has been achieved and allowed us to determine very small element specific magnetic projected spin and orbital moments even for the diluted TM ion down to approximately 10^{-4} μ_B (10^{-5} μ_B for pure TM).

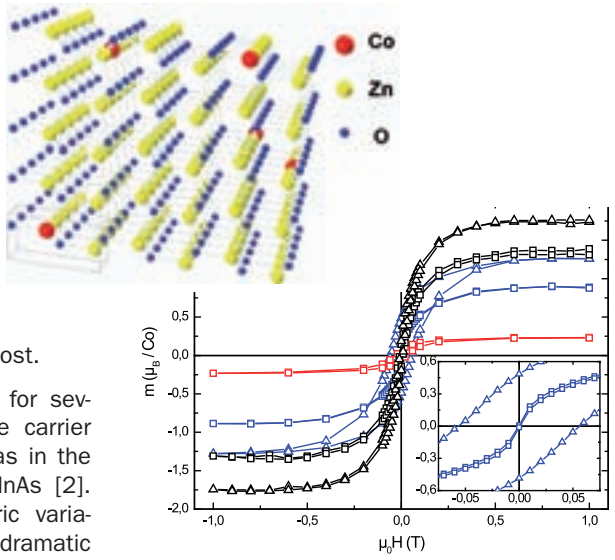

Fig. 1:
Structure of 5% Co doped ZnO. Comparison of SQUID measurements of single layered (black), triple layered (blue) and Li co-doped (red) samples (square: RT; triangle: low temperature)

Our magnetometry (SQUID) results clearly exhibit FM (Fig. 1). The triple layered sample provides an enhanced coercivity at low temperatures (5K and 15K) for additional remanence measurements. From the SQUID we expected Co XMCD effects at room temperature in the order of 20-40% with respect to the Co L_3 white line intensity.

References:

[1] T. Dietl et al., Science **287**, 1019 (2000).

[2] D. Chakraborti et al., J.Appl. Phys. **102**, 113908 (2007).

[3] D. A. Schwartz et al., Adv. Mater. **16**, 2115 (2004).

[4] T. Zhu et al., Appl. Phys. Lett. **89**, 022508 (2006).

[5] S. Banerjee et al., Appl. Phys. Lett. **91**, 182501 (2007).

[6] J. M. D Coey, Solid State Sciences **7**, 660 (2005).

[7] A. Barla et al., Phys. Rev. B **76**, 125201 (2007).

[8] M. Gacic et al., Phys. Rev. B **75**, 205206 (2007).

[9] J. M. D Coey, J. Appl. Phys. **97**, 10D313-1 (2005).

[10] T. Tietze et al., New Journal of Physics in press (2008).

Acknowledgements:

We thank T. Kachel, W. Mahler, and B. Zada for kind support during the beamtime.

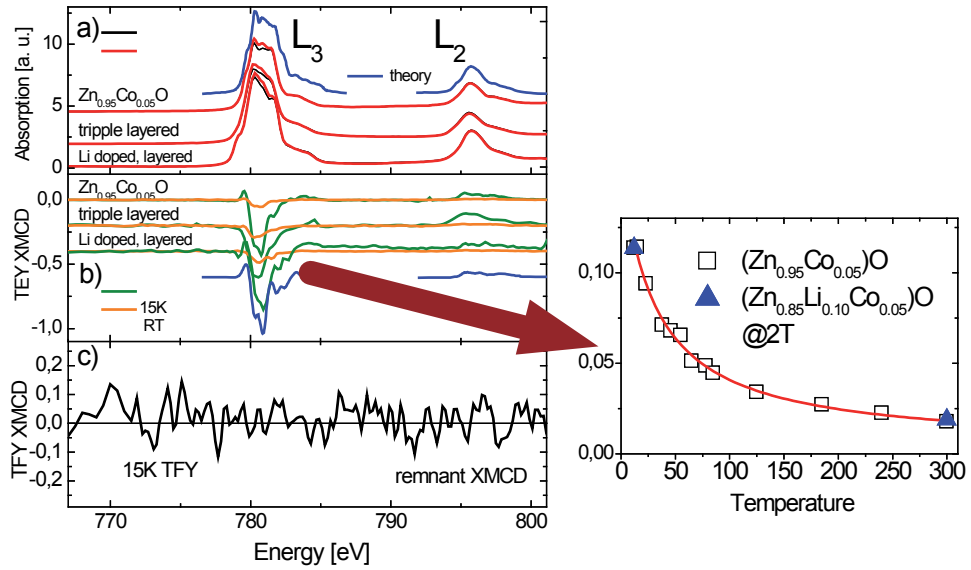

Fig. 2:
a) XAS spectra for opposite magnetizations of the Co doped, triple layered and Li co-doped samples (at 15 K and 2T external field).
b) Corresponding XMCD spectra at 15 K (olive) and RT (orange) and $3d^7$ multiplet spectrum (blue) [7].
c) Remnant Co fluorescence spectrum of the layered sample at 15 K. Inset: Temperature dependence of spin moments measured by XMCD.

Figure 2 shows the XAS (RT) and XMCD (RT and 15K) spectra at the Co $L_{2,3}$ edges for the single layered Co doped, the triple layered Co doped, and the layered Li co-doped sample. The Co $L_{2,3}$ edges are due to a Co 2p –> 3d transition, which provides information on the unoccupied density of the Co 3d states, probing the projected 3d magnetism of Co.

We found that the shape of the XAS and XMCD is not changing significantly for the different samples or detection modes and is consistent to the theoretical XAS multiplet spectrum (Co $3d^7$ in T_d symmetry [7]). This is the expected symmetry and valence for Co ions located at the Zn site. The XMCD sum rule derived magnetic moments are shown in the inset of Fig. 2. These small moments are in perfect agreement to pure paramagnetic Co with small antiferromagnetic correlations [8]. Also the non-vanishing orbital moment of about 25% with respect to the spin moment demonstrates the local character of the Co orbital. This provides clear evidence for the absence of metallic Co.

Similar experiments with higher signal to noise ratio have been performed at the O K edge (Fig. 3). We have performed a vast number of XMCD spectra at the O K edge at RT and 15 K, but we did not observe a significant and reproducible structure (pattern). Also, we did not find any ferromagnetism at the Co L_3 and O K edges in reflection mode (not shown), excluding interface related magnetism of Co and O at the ZnO/saphire [9]. A Zn based magnetization has been excluded in a previous paper due to the lack of a Zn $L_{2,3}$ XMCD signal [7,8].

So, where does the ferromagnetism derive from? Our detailed XMCD measurements on the Co $L_{2,3}$ and the O K edges found only paramagnetic Co for any kind of sample and any type of measurement with surface (TEY), bulk (TFY), and interface (reflection) sensitivity. We can definitely and without any doubt exclude Co as a possible origin for FM in such systems. Moreover, there is no sign of ferromagnetism for Oxygen or Zinc. Without finding any element specific signature of FM, we suggest oxygen vacancies as a possible carrier for ferromagnetism in doped ZnO [8,10].

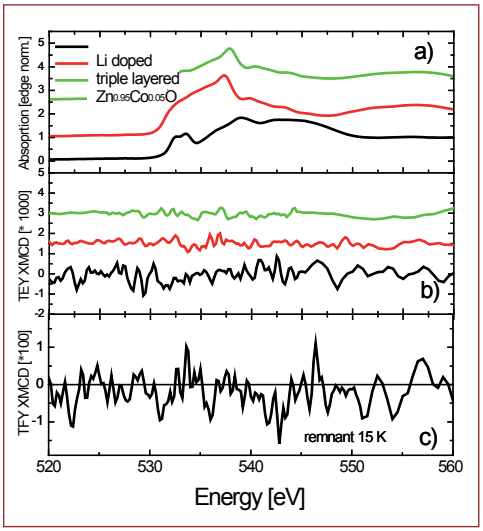

Fig. 3:
Room temperature TEY:
a) XAS and
b) XMCD oxygen K-edge spectra of single layered, triple layered, and Li co-doped samples, magnified by a factor of 1,000.
c) Remnant O K fluorescence spectrum of the layered sample at 15 K.

Contact:
Thomas Tietze
tietze@mf.mpg.de

Everybody has to check his tools...

Checking the tools.
Independent measurements of the pseudogap-driven Hall effect

D. V. Evtushinsky[1], S. V. Borisenko[1], A. A. Kordyuk[1,2], D. S. Inosov[1], V. B. Zabolotnyy[1], R. Schuster[1], B. Büchner[1], H. Berger[3], R. Follath[4]

1 Leibniz-Institut für Festkörper- und Werkstoffforschung Dresden
2 National Academy of Sciences of Ukraine, Kyiv, Ukraine
3 Institut de Physique de la Matiere Complexe, EPFL, Lausanne, Switzerland
4 BESSY

The era of simple materials is gone, modern life demands new materials with extraordinary properties. Such materials often possess a complex structure that requires very fine and accurate tools for investigation. The more accurate the tool, the more delicate it is. From time to time it is important to check, whether your tool is still appropriate. Concerning physics, it means that we should be sure that the results of an experiment are interpreted and understood fully and correctly. But how can we judge, whether the interpretation at hand is precise enough and looks deep inside the nature of the physical phenomenon? The natural way to refute any doubts would be to draw a comparison with another independent method. Here we present an interesting example of a successful comparison between two completely different experimental techniques – photoelectron spectroscopy and charge transport measurements.

Photoemission stems from the discovery and consequent explanation (Einstein, 1905) of the photoelectric effect. For the last few decades the method made a leap forward, which resulted in the development of angle resolved photoemission spectroscopy (ARPES). In ARPES we knock one electron out of a solid, measure its energy and momentum, and, applying conservation laws, obtain information about its state in the crystal. In charge transport measurements we study the integral motion of all electrons in a solid when placed in an external electromagnetic field. Early charge transport measurements date back to the 19th century, when the Ohm's law was discovered. Then, in 1879, experimenters were endowed with another phenomenon of voltage induced across the conductor carrying current when placed in the magnetic field that became known as Hall effect and will be one of the central issues of our 'tool check'. The simple explanation for the phenomenon would be the charge deflection by the Lorentz force, which finally results in the voltage, measured perpendicular to the current. Obviously, to get an insight into the effect on the quantitative level, one needs to have precise information on the dynamics of the particles that transport charge in the solid [1-3].

In crystals, charge carriers are organized in electronic bands, and the Hall coefficient, or in simple words the strength of the effect, can be calculated from the band dispersion. The required information is provided by ARPES, which makes it another complementary constituent of the discussion.

The ultimate step to perform the intended 'tool check' requires a valid theoretical link between the electronic structure and the charge dynamics. Electrons inside the crystal form essentially a quantum system, where dynamics comprise of transitions from one state to another. Since electrons are fermions, only transitions between occupied and unoccupied states are possible, and the dynamics are fully determined by events evolving in the narrow energy window – the temperature blurred boundary between filled and free states. Rigorous calculation of kinetic coefficients should take the wave functions explicitly, but a simple approach based on the solution of semi classical Boltzmann equation in isotropic τ approximation works well for a surprisingly wide variety of materials [1]. For quasi two-dimensional metals, compounds of our interest, the Hall coefficient within the mentioned approximation is given by the integral over the Fermi surface (FS):

$$R_H = \frac{4\pi^2}{e} \cdot L_c \cdot \frac{\int v_F^2(\mathbf{k})/\rho(\mathbf{k})\,dk}{\left(\int v_F(\mathbf{k})\,dk\right)^2}, \qquad (1)$$

where e is the elementary charge, v_F - Fermi velocity, d k - element of FS length, ρ - FS curvature radius, L_c - size of the elementary cell along the c axis. All quantities, except for the L_c, can be directly extracted from ARPES spectra as they are seen in the ARPES images and the FS maps per se.

Recently, much attention has been paid to a depletion of spectral weight near the Fermi level detected in numerous layered compounds and commonly referred to a pseudogap in the excitation spectrum. The most prominent examples are high temperature superconductors (HTSC) and charge density wave (CDW) systems. Since opening the pseudogap reduces the density of the states (DOS) near the Fermi level, i.e. the number of particles involved in charge dynamics, this as a consequence affects transport properties. Equation (1) implies that all energy bands are equally and uniformly populated by electrons. Though this assumption usually holds true, a complex

References:

[1] T. P Beaulac et al., Phys. Rev. B , **23**, 3617 (1981)

[2] H. N. S. Lee et al., J. Sol. State Chem., **1**, 190 (1970)

[3] M. Naito et al., J. Phys. Soc. Japan, **51**, 219 (1982)

[4] S. V. Borisenko et al., arXiv:0704.1544 (2007)

Acknowledgements:

We thank R. Hübel for technical support. Supported by the DFG under grant No. KN393/4.

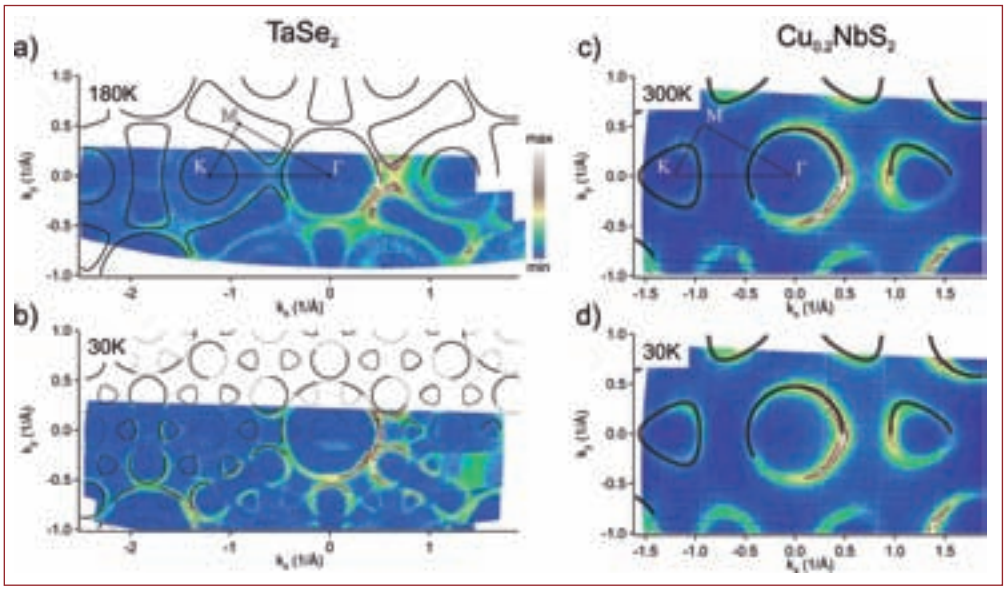

Fig. 1:
Evolution of the Fermi surface with temperature. Photoemission intensity at the Fermi level represents Fermi surface contours. The Fermi surface of $TaSe_2$ changes topology with cooling (a, b). The first signature of Fermi surface reconstruction is the opening of the pseudogap. In normal state, tight-binding fit shown (a, c, d). For CDW–reconstructed Fermi surface (b) different types of guidelines correspond to band "population", i.e. spectral weight distribution. Note the absence of changes and uniform spectral weight distribution in the spectra of NbS_2 (c, d).

picture of spectral weight distribution does not appear to be a rare occasion for unconventional materials. For such a case equation (1) can be modified introducing a factor that takes into account the distribution of the spectral weight:

$$R_H = \frac{4\pi^2}{e} \cdot L_c \cdot \frac{\int D(\mathbf{k}) v_F^2(\mathbf{k}) / \rho(\mathbf{k}) d\mathbf{k}}{\left(\int D(\mathbf{k}) v_F(\mathbf{k}) d\mathbf{k} \right)^2}, \quad (2)$$

where

$$D(\mathbf{k}) = \int \mathrm{DOS}_{\mathbf{k}}(\omega) \cdot \left(-\frac{\partial f(\omega)}{\partial \omega} \right) d\omega, \quad (3)$$

that is temperature weighted DOS at the Fermi level, $f(\omega)$ is a Fermi function, and ω is a binding energy. Note that in the simplest case $\mathrm{DOS}_k(\omega) = 1$, and $D(k) = f(-\infty) - f(\infty) = 1$, so we arrive back at formula (1).

The actual compound we use in our calculations is a CDW system 2H-$TaSe_2$. To account for the spectral weight redistribution, in addition to the band dispersion one should also know the magnitude of the pseudogap, which requires good quality data and careful spectra analysis [4]. Up to now, band calculations failed to precisely reproduce the FS geometry of $TaSe_2$. Moreover, the evolution of electronic structure from the normal to CDW state still remains an open issue. These are actually the reasons why transport properties cannot be calculated a priori.

To obtain temperature dependence of the Hall coefficient (Fig. 2b) we have studied the electronic structure of $TaSe_2$ at different temperatures and the reconstruction of its FS (Fig. 1a, b) in the CDW state. In the spectra of $TaSe_2$ a pseudogap is already present at room temperature, and begins to increase sharply upon the transition to an incommensurate CDW state (122 K) evolving to the band gap in a commensurate CDW. The magnitude of the pseudogap depends on the position in the Brillouin zone. In case of $TaSe_2$ the sheet of the FS around the K point is mostly affected by the pseudogap, so its contribution to the Hall coefficient has the strongest variation, which is the main reason for the Hall coefficient to change sign.

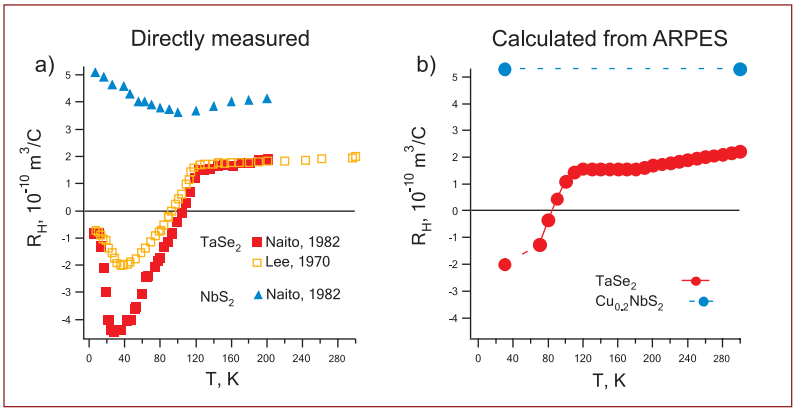

Fig. 2:
Temperature dependence of the Hall coefficient. The Hall coefficient in 2H-NbS_2 has weak temperature dependence, while in 2H-$TaSe_2$ the Hall effect changes sign (a). The discrepancy between two experimental curves for $TaSe_2$ is due to charge density wave suppression by impurities. The Hall coefficient of NbS_2, calculated in approximation of equally "populated" bands, agrees well with directly measured, while in case of $TaSe_2$ one should take into account spectral weight distribution and introduce the notion of the pseudogap (b).

2H-NbS_2 is a compound very similar to 2H-$TaSe_2$, but it exhibits no CDW, and possesses an 'ordinary' electronic structure with an uniform spectral weight distribution over the bands and no temperature dependence (Fig. 1c, d). The Hall coefficient of 2H-NbS_2 has a weak temperature dependence, as expected (Fig. 2).

The agreement of the Hall coefficient unambiguously derived from ARPES with the directly measured Hall coefficient indicates that our tool successfully passed through the 'check'. Such a fine, but nevertheless important, detail of photoemission spectra as a pseudogap finds reflection in the tangible properties of a solid.

Contact:
Daniil Evtushinsky
d.yevtushynsky@ifw-dresden.de

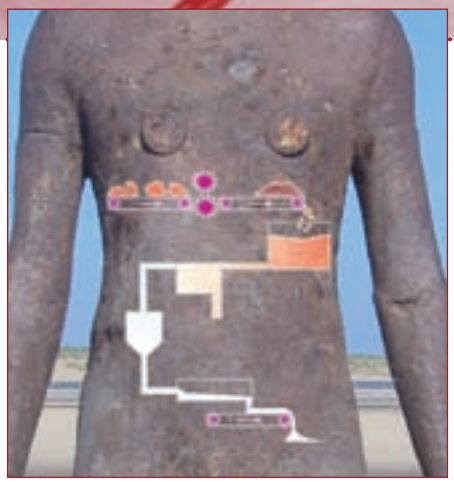

Looking inside Bayer's digestion

D. Croker[1, 2], K. Hodnett[1]

1
University of Limerick, Ireland
2
Aughinish Alumina Ltd., Co. Limerick, Ireland

Aluminium is one of the most important alloys in our civilized world. From beverage cans, kitchen foil to cars and aircrafts: Everyday life would look different without it. Production of aluminium begins with the Bayer process. Developed by Karl Bayer in 1888, the Bayer process is used to extract aluminium oxide from the raw ore bauxite. Aluminium oxide is subsequently electrolytically reduced in a smelting process to produce aluminium metal. The International Aluminium Institute put world production of aluminium oxide at 78 million tonnes in 2007 [1].

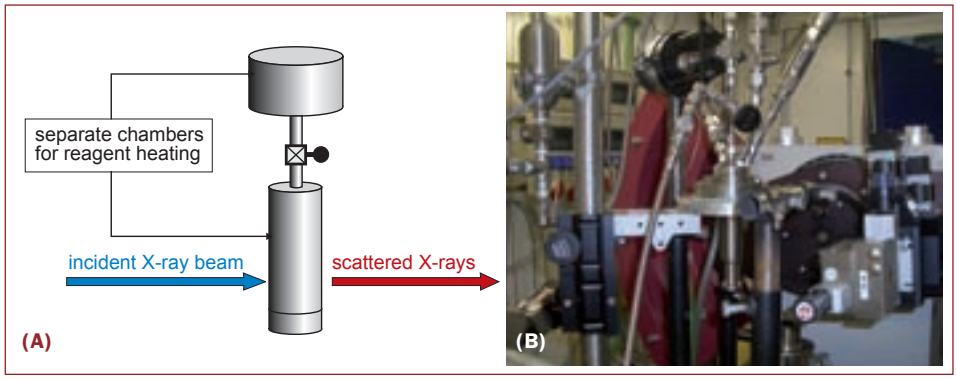

Fig. 1:
Schematic representation of the apparatus designed for use at BESSY (A). Pictured also is the vessel aligned at the 7T-MPW-EDDi beamline (B).

The Bayer process is based on the fact that aluminium-containing minerals within bauxite are soluble in sodium-hydroxide solution upon application of temperature, allowing the generation of an alumina rich alkaline solution and a solid waste that can be separated easily using settling and filtration. Precipitation of alumina trihydroxide from this solution and subsequent calcination produces aluminium oxide, which is used to generate aluminium metal at smelter plants.

The actual dissolution of the aluminium-containing minerals within bauxite is achieved in a stage of the Bayer process known as digestion. A number of secondary reactions are also possible at digestion conditions, about which relatively little is known. The extreme conditions required for digestion (up to 250°C, 42 bar) prevent one from 'peering' inside a digestor to ascertain the chemistry; up to this there have been no in-situ investigations of digestion chemistry. The objective of this work was to recreate the digestion process on a smaller scale for *in-situ* analysis using powerful X-ray radiation provided by the 7T-MPW-EDDI beamline in order to get a mechanistic insight into reactions on-going within the digestor. This high intensity radiation has the capability to penetrate reaction vessels, diffract off dissolving/growing solids within the vessel and give information on the reactions occurring.

A 'Mini-Digestor' reaction apparatus was designed for use in conjunction with the *in-situ* technique. The key requirements of this reaction vessel were to facilitate beam penetration and to provide for combination of solid and solution at 250°C. The reaction vessel itself is made from the nickel alloy inconel, a material with a high tensile strength. This material can adequately contain the digestion reaction at 250°C and 50 bar, even though the walls at the base of the reaction vessel are thinned to 0.3 mm to minimise beam attenuation. A simple representation of the apparatus is presented in Figure 1, along with a photograph of the vessel aligned in the experimental hutch. A typical experiment proceeded by placing the required solids/solution in their respective compartments and heating to a constant 250°C. After switching on the X-ray beam, solid and solution were combined and the reaction followed from the inception of reagent mixing.

In this manner, the dissolution of boehmite (AlO(OH)) in a Bayer process solution was investigated. Boehmite is a form of aluminium hydroxide commonly present in bauxite. Dissolution was rapid at 250°C, as demonstrated by the disappearance of the boehmite reflection at 6.11Å (Fig. 2A). The presence of titanium (a common impurity in bauxite) in digestion is reported to impede boehmite dissolution [2, 3]. This was confirmed by following boehmite dissolution in the presence of titanium dioxide (Figure 2B). The boehmite

References:

[1] P. A. Plunkert, Mineral Commodity Summaries 2006.

[2] A. Suss et al., The 6th International Alumina Quality Workshop, Darwin (2002).

[3] B. I. Whittington, Hydrometallurgy, **43**, 13-35(1996).

[4] J. Addai-Mensah et al., in R. Huglen, ed. Light Metals Orlando, Florida: The Minerals, Metals & Materials Society, 23-28 (1997).

[5] J. Zoldi et al., Light Metals: The Minerals, Metals & Materials Society, 105-111 (1987).

Acknowledgements:

Joe Murray, Marc Moreau and Doireann Funnell are thanked for assistance in performing the experiments. Financial support by Aughinish Alumina Ltd. and Enterprise Ireland Ltd. (grant number IP-2004-0191).

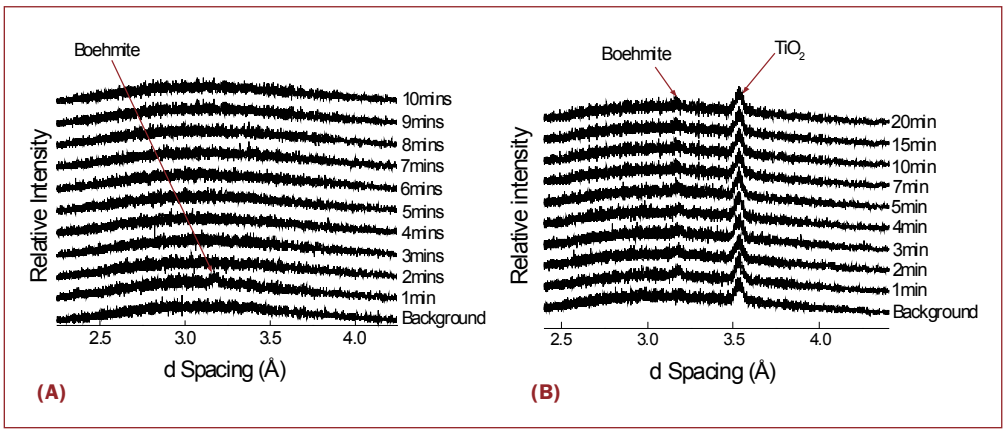

Fig. 2:
In-situ X-ray diffraction patterns demonstrating boehmite dissolution in Bayer solution at 250°C (A) and in the presence of titanium dioxide (B).

reflection was observed to persist for 20 minutes, accompanied by the titanium reflection at 3.5A° (Fig. 2B).

Bauxite also contains impurities in the form of the silica minerals kaolin ($Al_2O_3.2SiO_2.2H_2O$) and quartz (SiO_2). These minerals react in Bayer solutions to the sodium aluminosilicate compounds, sodalite and cancrinite [4]. Using the *in-situ* technique, sodalite growth was observed following the addition of kaolin to a Bayer solution at 250°C (Fig. 3). The kaolin peak is not observed as it is outside the range of detection but emergence of the sodalite reflection at 6.3Å demonstrates the rapid nature of the reaction. The behaviour of the iron minerals goethite (FeO(OH)) and hematite (Fe_2O_3), both present in significant amounts in bauxite ore [3,5], was also investigated. Figure 4 demonstrates the transformation of goethite to hematite in Bayer solution at 250°C in the presence of hematite seed.

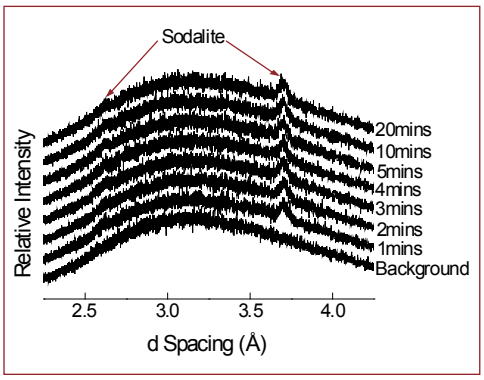

Fig. 3:
In-situ X-ray diffraction patterns demonstrating the precipitation of sodalite following the addition of kaolin to Bayer solution at 250°C.

Significant insight into Bayer digestion reactions has been obtained by application of the in-situ X-ray diffraction technique. This technique and the apparatus designed provide for fast collection of data from reactions occurring in real-time and can be applied to a wide range of chemical reactions. This is the first application of *in-situ* analysis, from the inception of reagent mixing *at temperature*, to the high temperature Bayer digestion process. We plan to continue the project using bauxite and simultaneously monitor the reactions in their entirety to generate a deeper understanding of what is going on in a digestor.

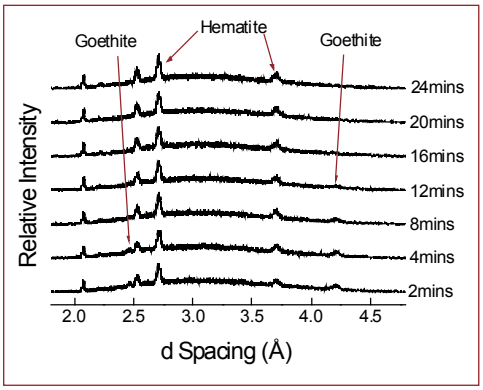

Fig. 4:
In-situ X-ray diffraction patterns demonstrating the transformation of goethite to hematite in Bayer solution at 250°C.

Contact:
Denise Croker
denise.croker@augh.com

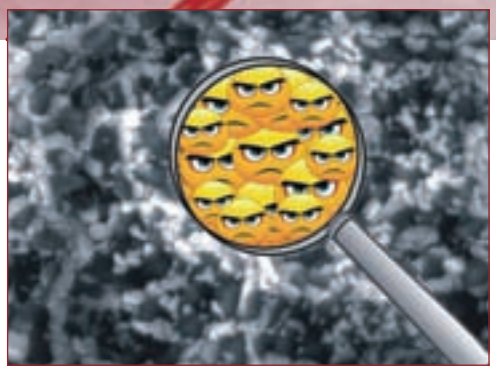

Stress on the surface?
EDDI can help!

P. Brito[1], H. Pinto[1], M. Klaus[2], Ch. Genzel[2], A. Pyzalla[1]

1 Max-Planck-Institut für Eisenforschung, Düsseldorf
2 Hahn-Meitner-Institut

In many industrial applications of metals, oxidation is a destructive and unwanted phenomenon that leads to significant economical losses worldwide. However, the ability to form a dense oxide layer can also be a desired feature in materials selection, in stainless steels, for instance. Here, a chromium oxide layer hinders the continuous destructive oxidation of the underlying steel substrate.

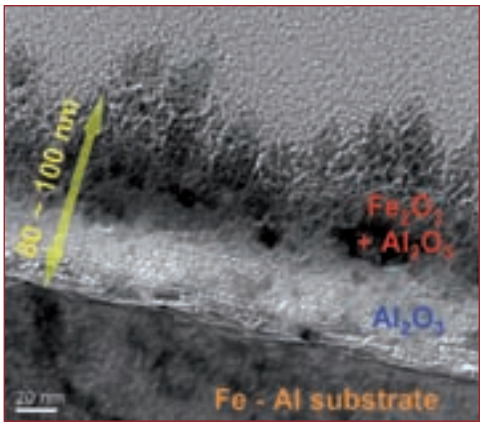

Fig. 1: TEM micrograph of oxide layer grown on an Fe-15at.%Al alloy after 5 h oxidation at 700°C.

Essential for high-temperature (HT) corrosion resistance is the formation of dense oxide layers, which protect metals by blocking the diffusion between the corrosive environment and the reactant [1]. If the substrate is subjected to both mechanical and thermochemical loads, oxidation resistance further requires surface layer integrity and adherence to the substrate. Thus, protective oxide scales need to have adequate mechanical properties to withstand internal and thermal stresses caused by oxide growth, and also any additional external load the metallic workpiece might be subjected to.

Fe-Al alloys are important materials for HT applications, such as gas turbines in power plants. This is partly due to the alloys' ability to form a slowly growing α-Al_2O_3 scale. However, at temperatures below 1,000°C metastable less protective aluminas might grow first and only later transform to the thermally stable α-Al_2O_3 [2,3]. This transformation is accompanied by a volume contraction, which can induce detrimental tensile stresses into the first-formed α-Al_2O_3 grains [4].

The evolution of phase composition and internal stresses in oxide scales can be best evaluated by using diffraction methods, which provide information on the phase constituents and their lattice distortion during oxidation. However, oxide layers formed on Fe-Al alloys grow very fast in the early stages, meaning that any *in-situ* study performed should rely upon an experimental technique which is able to detect eventual changes in the scale with sufficient time resolution.

Once the oxide film covers the entire substrate surface, diffusion is hampered and the oxide growth rate considerably slows down. This causes very thin oxide layers to grow on Fe-Al alloys. The overall layer thickness in Fig. 1 is of less than 100 nm. The oxide scale, however, constitutes of even thinner subscales: an outer intermixed scale of Fe_2O_3 and α-Al_2O_3, and an inner layer of pure α-Al_2O_3. This usually implies very long data acquisition times in traditional Angle-Dispersive diffraction experiments, making this method impracticable for the study of the initial oxidation stages related to the formation of less protective aluminas.

This experimental challenge led us to the beamline for Energy-Dispersive Diffraction (EDDI) in order to study the time-evolution of phase composition and internal stresses in nanostructured oxides grown on Fe-Al alloys. EDDI provides complete diffractograms for fixed positions of both sample and detector. Combined with the high photon flux of synchrotron radiation, EDDI is a valuable tool for time-resolved studies.

Fig. 2 shows diffraction data collected at the EDDI beamline during the oxidation of Fe-15at.% Al at 700°C. The acquisition time for a complete diffractogram amounts to only 3 min. After a few minutes, a double-layered oxide scale of Fe_2O_3 and α-Al_2O_3 grows with the volume fraction of Fe_2O_3 decreasing as the oxidation progresses. Metastable aluminas have not been observed. The internal stresses in the growing oxide layer were determined using the $\sin^2\psi$ method. This technique exploits the shallow penetration depth of X-rays to consider a bi-axial stress state in the near-surface zone. Under this assumption, the lattice spacing d_ψ measured

References:

[1] M. Schütze, Mater. Sci. Technol. **4**, 407-414 (1988).

[2] H. J. Grabke, Interm. **7**, 1153-1158 (1999).

[3] M. W. Brumm et al., Corr. Sci. **33**, 1677 (1992).

[4] G. V. Samsonov, The Oxide Handbook, Second Edition, p. 183, ed., IFI/Plenum, New York, 1982.

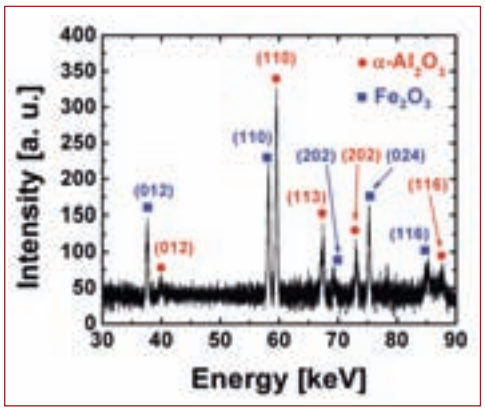

Fig. 2:
ED-Diffractogram collected during oxidation of Fe-15at.%Al.

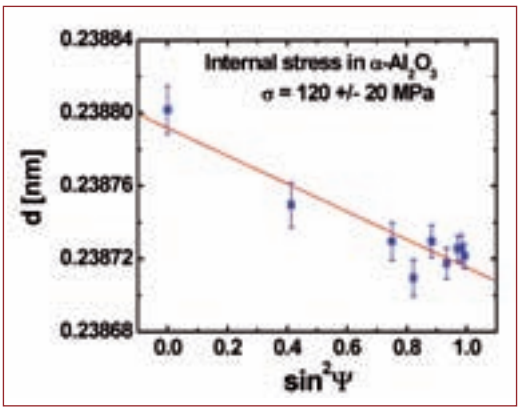

Fig. 3:
d-sin²ψ distribution for α-Al_2O_3 during oxidation at 700°C.

in isotropic materials at different inclination angles ψ varies linearly with sin²ψ. The in-plane stress is proportional to the slope of the d-sin²ψ curve.

For increasing the time resolution, energy dispersive diffractograms were recorded only for very high ψ-angles, where the gauge volume mostly encompasses the oxide scale. The strain-free lattice spacing d_0 needed for strain calculation was determined from additional measurements in the strain-free direction ψ* given by the biaxial stress state. Fig. 3 displays a typical d-sin²ψ distribution during *in-situ* oxidation.

The time evolution of growth stresses is shown in Fig. 4. α-Al_2O_3 grows under compressive stresses, which are counterbalanced by tensile stresses in the Fe_2O_3 sub-scale. The initial increase of compressive stresses in α-Al_2O_3 is also accompanied by an increase in tensile stresses in Fe_2O_3. After about 6.5 h, probably due to creep of the substrate, the internal stresses in both phases start to progressively release.

In conclusion, EDDI demonstrated its potential for in-situ characterization of microstructure and growth stresses in nano-layered oxides with unprecedented time resolution.

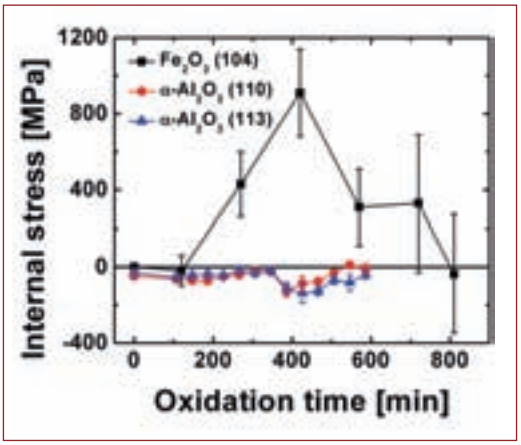

Fig. 4:
Internal stress evolution determined during *in-situ* oxidation using the ED diffraction.

Long-term aim of these investigations is to elucidate the connection between substrate microstructure, phase composition during the early stages of oxidation, growth stresses, and the oxidation resistance of Fe-Al alloys. The knowledge on the mechanisms of stress formation in these oxide scales will be essential for determining conditions necessary for the development of protective oxide layers on Fe-Al alloys.

Contact:
Haroldo Pinto
h.pinto@mpie.de

Pinning the catalytic centre: A new concept for catalysts development

K. Kovnir[1,2], D. Teschner[1], M. Armbrüster[1], P. Schnörch,[1] M. Hävecker,[1] A. Knop-Gericke[1], Y. Grin[2], R. Schlögl [1]

1 Fritz-Haber-Institut der Max-Planck-Gesellschaften

2 Max-Planck-Institut für Chemische Physik fester Stoffe, Dresden

Heterogeneous catalysis is 'perennially relevant, endlessly fascinating and deeply enigmatic' stated a text book on catalysis [1]. This statement might be biased, but there can be no doubt about its huge importance. After all, more than 90% of the chemicals in the world are produced utilizing catalysts. To fulfill raising demands, lower the production costs and to minimize the environmental impact, novel highly selective catalysts are required. Thereby, catalyst development based on experimental functional evidence rather than on trial and error becomes a viable alternative.

Supported bimetallic catalysts are widely used in industrial processes. These catalysts are complex objects for the preparation and characterisation and it is difficult to achieve a uniform particle composition and exclude strong metal-support interactions. A prediction for the nature of the active sites in such catalysts is strongly limited because the supported particles of the two metals may coexist as elements or form clusters of different compositions.

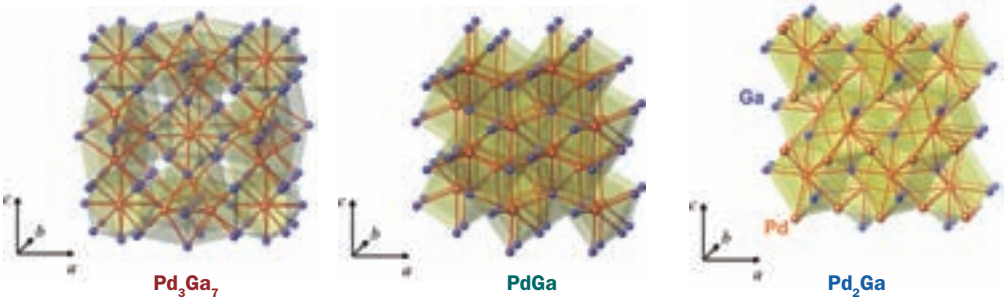

Pd_3Ga_7 PdGa Pd_2Ga

Fig. 1: The crystal structures of Pd_3Ga_7, PdGa and Pd_2Ga. Pd: orange; Ga: blue.

Materials that can surmount these drawbacks and be utilized for the development and testing of concepts are 'well-ordered unsupported intermetallic compounds (IMCs)'. Here, the atomic environment of the catalytically active metal is pinned in the crystal structure due to the partly covalent bonding. This leads to a homogeneous distribution of the active sites and to a significantly reduced segregation and to negligible sub-surface chemistry [2].

We chose the palladium-(Pd)-based catalyst involved in the production of polyethylene as candidate to validate the proposed concept. Polyethylene is a widely used polymer with more than 50 million tons produced worldwide per annum. During its synthesis the ethylene monomer feed needs to be cleaned from acetylene admixtures by selective hydrogenation. For this catalytic process selectivity is crucial since otherwise valuable ethylene is lost. Typical Pd-based catalysts show a limited selectivity and long-term stability, which is attributed to the formation of β-Pd-hydride and the presence of active-site ensembles [3]. In our study we tested three well-characterized intermetallic compounds – Pd_3Ga_7, PdGa, and Pd_2Ga (Fig. 1) – with different crystal structures, and thus with differently isolated Pd active sites.

In-situ high-pressure X-ray photoelectron spectroscopy (XPS) characterisation was performed at beamline U49-2_PGM-1. The IMCs are characterised by a significant shift of the Pd3$d_{5/2}$ X-ray photoelectron peak to higher binding energy compared to metallic Pd, and by a modified valence band (Fig. 2). Quantum chemical calculations suggest that their Pd *d*-band is further filled and shifted to higher binding energy by the chemical bonding between Ga and Pd (Fig. 3). Indeed, an increasing shift with lower Pd:Ga ratio is observed in XPS. In turn, the alteration of the valence band region leads to a different screening of the core hole, which is indicated by the changes of the Pd3*d* spectra.

In situ XPS measurements, performed at ~1 mbar pressure, showed a high stability of the Pd surface states (Fig. 4) without the appearance of any additional component or significant shift of the Pd3$d_{5/2}$ peak, when applying the reactive atmosphere and temperature (1.0 mbar of H_2 + 0.1 mbar of C_2H_2 at 400K). The metastable Pd-hydride phase, which is formed in conventional Pd-catalysts, is clearly not present in our system. Investigation of C and Pd depth profiles confirmed the absence of a sub-surface carbon-containing phase, distinguishing these materials from metallic palladium catalysts [4].

Filling of the Pd *d*-band and the covalent Pd-Ga interaction prevents the formation of sub-surface hydrides, as confirmed by the bulk-sensitive Prompt Gamma Activation Analysis

References:

[1] J. M. Thomas and W. J. Thomas, Principles and Practice of Heterogeneous Catalysis. VCH, Weinheim, 2005.

[2] K. Kovnir et al., Angew. Chem. Int. Ed. (2008), submitted.

[3] A. Borodzinski and G.C. Bond, Catal. Rev., **48**, 91, (2006).

[4] D. Teschner et al., J. Catal., **242**, 26, (2006).

[5] A.M. Doyle et al., Angew. Chem. Int. Ed. **42**, 5240 (2003).

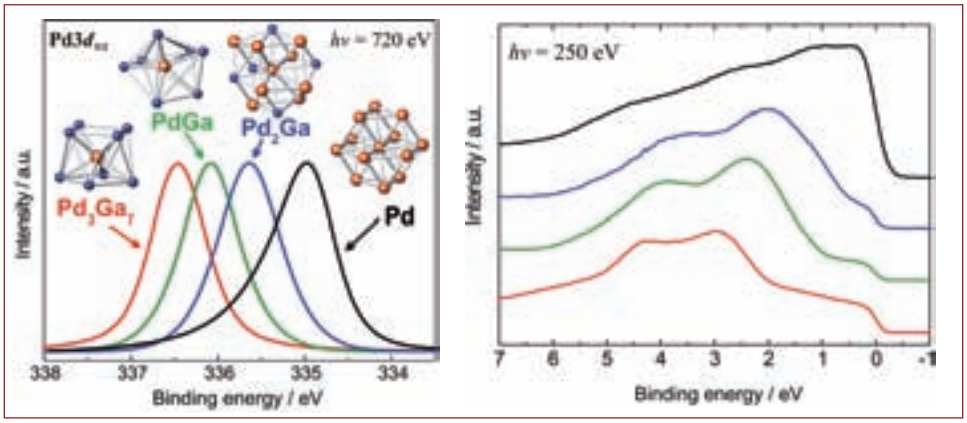

Fig. 2:
Pd3$d_{5/2}$ XP spectrum peaks (left) and valence band regions (right) of Pd_3Ga_7, PdGa, Pd_2Ga and elemental Pd. Spectra were recorded in UHV. The nearest neighbours of the Pd atoms in the structures are shown.

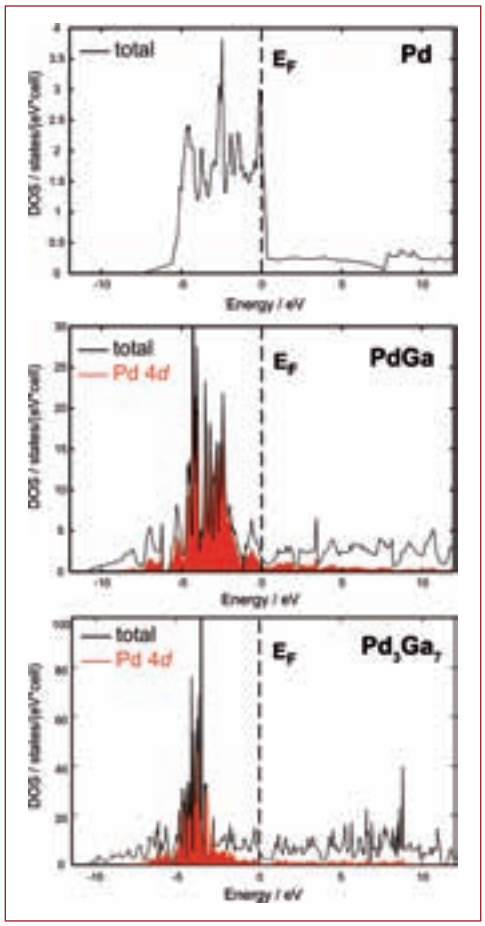

Fig. 3:
Electron density of states (DOS) of elemental Pd (top), PdGa (middle) and Pd_3Ga_7 (bottom).

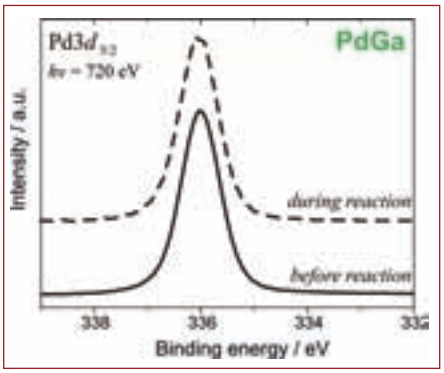

Fig. 4:
UHV and *in situ* Pd3$d_{5/2}$ XP spectra of PdGa does not reveal any modification of the surface.

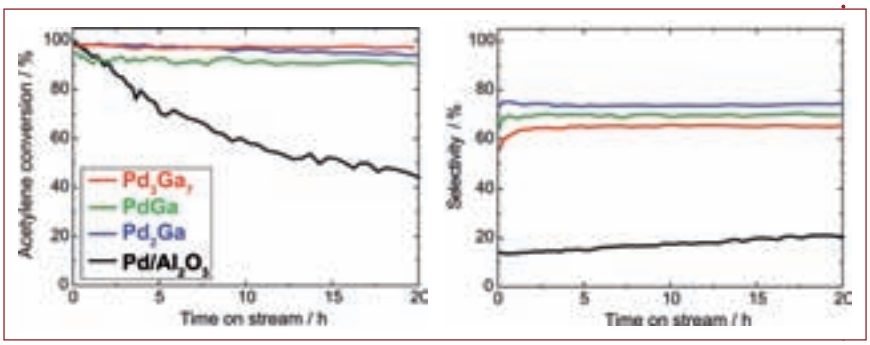

Fig. 5:
Acetylene conversion (left) and selectivity (right) at 473 K for Pd_3Ga_7 (50 mg), PdGa (20 mg), Pd_2Ga (10 mg) and a commercial 5%-Pd/Al_2O_3 (0.1 mg). Feed composition: 0.5% C_2H_2, 5% H_2 and 50% C_2H_4 in helium, total flow of 30 ml/min.

under reaction conditions. The absence of hydrogen incorporated in the catalyst is expected to diminish the hydrogen supply for the unselective, total hydrogenation, and thus to increase the selectivity [4,5]. Certainly, the Pd-Ga IMCs show considerably higher selectivity in the hydrogenation of acetylene to ethylene compared to the reference catalyst Pd/Al_2O_3 (Fig. 5). Moreover, the IMCs exhibit a remarkable catalytic long-term stability, because of the isolation of the active Pd sites bonding, thus preventing polycondensation side-reactions. The high selectivity observed for all compounds indicates that not only the surface geometric site isolation, but also the suppression of hydride formation through a covalent bonding interaction absent in conventional Pd alloys are important for achieving superior catalytic properties. Our results demonstrate that structurally well-defined intermetallic compounds exhibit a high potential in heterogeneous catalysis and are promising candidates for industrial applications.

Contact:
Marc Armbrüster
research@armbruester.net
Kirill Kovnir
kovnir@fhi-berlin.mpg.de

Nano-Jewelry:
Adamantane and higher diamondoids

K. Klünder[1], L. Landt[1], T. Richter[1], P. Zimmermann[1], T. M. Willey[2], T. van Buuren[2], J. Dahl[3], R. M. K. Carlson[3], T. Möller[1], C. Bostedt[1]

1 Technische Universität Berlin
2 Lawrence Livermore National Laboratory, USA
3 MolecularDiamond Technologies, USA

'Diamonds Are a Girl's Best Friend' sang Lorelei Lee in the famous movie 'Gentleman Prefer Blondes'. But nowa-days, particularly when you are a physicist, you might prefer a smaller version – nanodiamonds or diamondoids!

The first diamondoid, adamantane ($C_{10}H_{16}$), consists of the smallest possible single cage unit excised from the diamond lattice with the dangling bonds terminated by hydrogen atoms [Fig. 1]. Diamondoids are classified by the number of such closed diamond cages. Each subsequent diamondoid adds one additional face-fused cage. Higher diamondoids are a completely new form of ideal, surface-passivated nanodiamonds. Only recently have they become available in macroscopic quantities through extraction and isolation from petroleum resources, where they were formed on a geological time scale and survived due to their extraordinary stability under high pressures and temperatures [1].

In a broader scientific context the diamondoids are perfect clusters. They form the link between molecules on the one hand and semiconductor (nano-) crystals on the other hand. The unique combination of molecular and solid state properties makes diamondoids a very attractive candidate for a multitude of potential applications such as molecular electronics or as transport vehicles for pharmaceuticals.

From a cluster physics point of view diamondoids are ideal systems for the investigation of fundamental aspects about atomic structures on sub-nanometer and nanometer length scales. They are completely sp^3-hybridized, fully surface terminated, and they can be size- and even shape-selected. Due to their thermodynamic stability they can be brought into the gas phase allowing unique investigations on neutral, interaction-free, size- and shape-selected single clusters with bulk lattice structure. While such systems are the basis for virtually all theoretical investigations, nanoparticle electronic structure has never experimentally been investigated with this type of precision due to lack of availability of suitable monodisperse materials.

A fundamental question, both scientifically and technologically, is the evolution of the electronic structure of nanometer structures as a function of size. Surprisingly, the first X-ray absorption experiments showed that diamondoids behave very different than their group IV semiconductor relatives, silicon and germanium. For diamondoids the conduction band or lowest unoccupied orbitals (LUMO) were dominated by the particle surface and did not show any size dependence [2]. In contrast, the diamondoid highest occupied orbitals (HOMO) are theoretically predicted to be localized in the interior of the particle and therefore exhibit strong size dependence [3].

To obtain a more detailed insight we have investigated the occupied density of states of a series of diamondoids from adamantane to cyclohexamantane in the gas phase by means of photoelectron spectroscopy. The experiments were carried out at the MPG-beamline UE56-2_PGM-2, using a Scienta SES-2002 hemispherical analyzer. The high-resolution beamline and spectrometer in combination with the perfectly size- and shape-selected diamondoids did not only allow us to investigate changes of the highest occupied orbitals but also to probe the core levels. Therefore we could tackle long standing questions about initial and final state effects in the photoemission of nanoclusters.

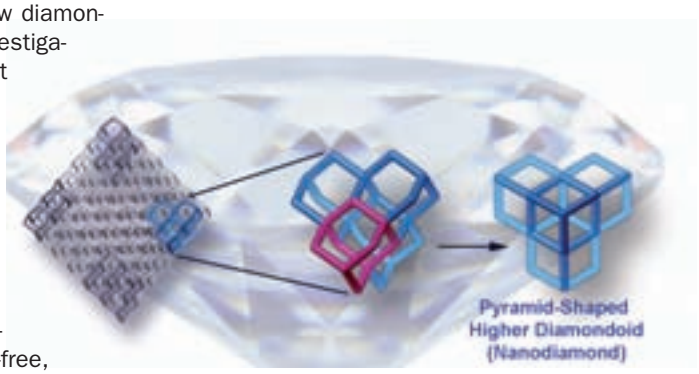

Fig. 1:
Each diamondoid is a hydrogen-terminated perfect sub-unit of the diamond crystal lattice. In the figure only the carbon framework is shown without surface hydrogen atoms for clarity. The smallest possible single cage unit (adamantane) is shown in red.

References:

[1] J. E. Dahl, et al., Science **299**, 96 (2003).

[2] T. M. Willey, et al., Phys. Rev. Lett. **95**, 113401 (2005).

[3] N. D. Drummond, et al., Phys. Rev. Lett. **95**, 096801 (2005).

Acknowledgements:

Supported by the DFG and the U.S. DoE, Basic Energy Sciences Division of Materials Science.

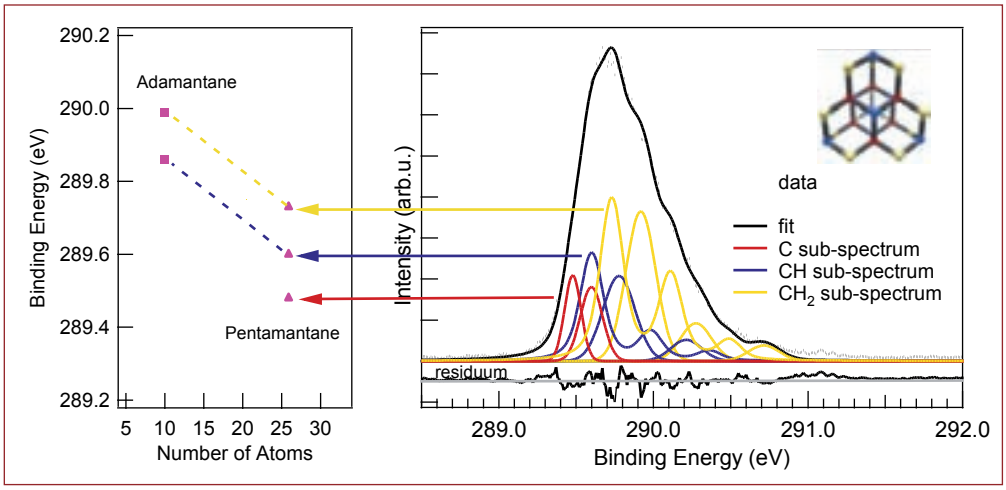

Fig. 2:
Core level photoemission (right) for [1(2,3)4]-pentamantane and binding energies (left) for some selected diamondoids.

As an example for the core level photoemission, the spectrum for [1(2,3)4]-pentamantane, a highly symmetric tetrahedral diamondoid with five cages, is shown in the right panel of Fig. 2. The data have been taken with a photon energy of hu=330 eV. With a resolution of 120 meV we are able to a resolve fine structure, similar to the best available data for related cyclic hydrocarbon molecules. With a fitting model it is possible to extract the binding and vibrational energies of the three possible chemical environments, i.e. carbon atoms bonded to one, two or three other carbon atoms in the cluster. The core level binding energies of pentamantane are compared to the findings of adamantane, the smallest diamondoid with a similar high symmetry (Fig. 2, left panel). The data show a clear shift with two contributions to the binding energies: First, there is the well known chemical shift for each atomic environment. Second, there is an additional shift between the diamondoid sizes. The second contribution can be related to a final state effect in the photoemission process, which describes how fast the system reacts and screens the created core hole.

In the left panel of Fig. 3 photoelectron spectra of the highest occupied states for some of the diamondoids are shown. The spectra have been taken with a photon energy of hv=80 eV. The joint beamline and spectrometer resolution has been determined to be better than 50 meV. The highest valence states shift over 1.5 eV to lower binding energies from adamantane to pentamantane. A comparison of the measured core level screening effects and valence band edge shifts for selected diamondoid sizes shows that the valence edge shifts are much stronger than the screening effects deduced from the core level photoemission (Fig. 3, right panel), a clear indication of existing strong size dependent changes in the diamondoid valence band.

In summary, diamondoids do show size-dependent changes in their electronic structure. While the LUMO is relatively fixed in energy, the valence band maximum generally shifts to lower energies with decreasing size. This change is much greater than screening effects determined from the core-level spectra, allowing the deconvolution of changes in the electronic valence states from final state effects in the photoemission process. These results are important for both, the comparison to theory on pristine diamond nanoclusters and for future integration of diamondoids in molecular electronics or biological applications.

Fig. 3:
Valence band photoemission for some selected diamondoids (left) and a comparison between valence band (red) and core-level shifts (blue) in the right panel.

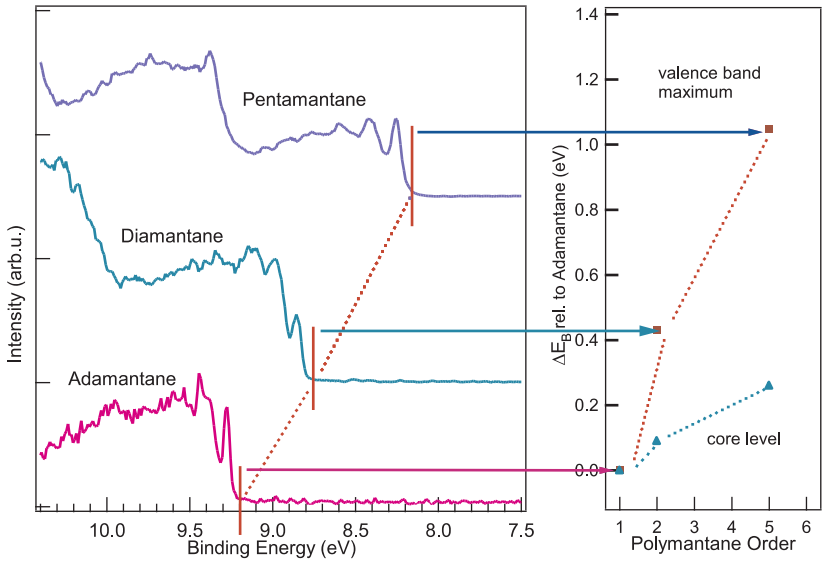

Contact:
Christoph Bostedt
bostedt@physik.tu-berlin.de

Under full control! The growth of luminescent gold and silver particles in glass

M. Eichelbaum[1], K. Rademann[1], A. Hoell[2], D. Tatchev[2], B. Löchel[3]

1 Humboldt-Universität zu Berlin
2 Hahn-Meitner-Institut
3 Anwenderzentrum für Mikrotechnik, BESSY

On the 5th of February 1857, Michael Faraday gave the groundbreaking Bakerian Lecture about 'Experimental Relations of Gold (and other Metals) to Light' to the Royal Society of London. For the first time, the various colours of gold suspensions, gold-ruby glasses or the 'Purple of Cassius', were interpreted in terms of the interaction of light with 'very minute' gold particles of different sizes [1]. 150 years later, noble metal clusters still reveal novel unexpected properties like catalytic activity or intense photoluminescence (PL) [2]. The investigation of 'minutest' molecular particles consisting of only few atoms is most interesting, because they represent the missing link between atomic and bulk properties.

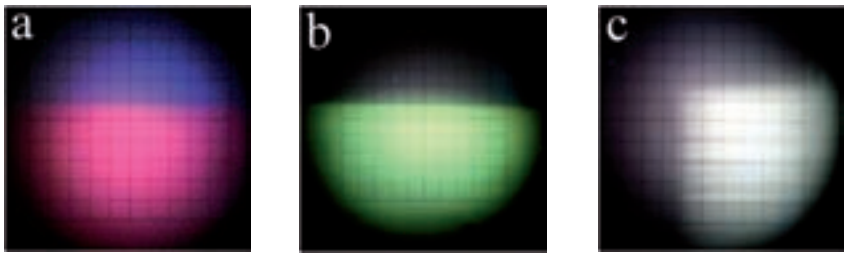

Fig. 1: Confocal fluorescence microscope images (λ_{exc} = 366 nm) of synchrotron activated gold- (a: no annealing; b: after 10 min at 550°C) and silver-doped (c: no annealing) glasses.

However, their direct experimental study is not straightforward. Large amounts of small clusters tend to aggregate and thus, rapidly form larger particles, whereas low cluster concentrations are difficult to be analyzed. Soda-lime silicate glasses can stabilize gold and silver nanoparticles, but the simultaneous nucleation, growth and ripening of the particles during the conventional preparation process has prevented the investigation of the PL of sub-nanometer sized particles.

Irradiation with highly intense synchrotron X-rays provides a way out of this dilemma [3, 4]. The synchrotron activation of Au^{3+}- or Ag^{+}-doped soda-lime silicate glasses creates defect centres like trapped holes and electrons in the glass network. X-ray generated electrons can combine with cationic noble metal ions and thus, neutral gold and silver species, respectively, are formed. A subsequent annealing process induces the growth of larger metal particles. In this way, nucleation (by irradiation) and growth (by annealing) can be separated allowing to control the cluster size and number density by simply changing the annealing time or temperature.

After activation with 'white' synchrotron light at the lithography beamline DXRL-1, silver-doped samples have been investigated by electron paramagnetic resonance (EPR) spectroscopy. The comparison with spectra of silver atoms isolated in solid argon matrices [5] indicates unambiguously that neutral silver atoms have been generated in activated silver-doped glasses. In contrast, no paramagnetic gold species like Au^{0} can be identified in activated gold-doped glasses. Instead, these samples show a characteristic red PL (Fig. 1a) peaking at 750 nm. A comparison of the PL and excitation spectra of gold particles isolated in solid argon matrices [6] points to the generation of gold dimers in the synchrotron activated glasses (Fig. 2). A comparably long luminescence lifetime of 30-40 µs was also measured for gold dimers in the gas phase by resonant two-photon ionization [7], which is a strong hint that the observed red luminescence is caused by an Au_2 triplet-singlet transition.

Annealing at 550°C induces the growth of larger gold particles. This process was studied by UV-Vis absorption, PL spectroscopy and small-angle X-ray scattering (SAXS) (Fig. 3). As a result, gold-containing samples, annealed for a very short time, emit exceedingly bright green light (Fig. 1b) with two maxima at 525 nm and 555 nm in the PL spectrum, which is not observed in as-treated pure soda-lime silicate glasses. Interestingly, an increasing annealing time is accompanied by a decreasing PL. Meanwhile the absorbance increases, and after approximately 30 min annealing the surface plasmon resonance characteristic for gold particles at 540 nm can be observed. SAXS measurements confirm the appearance of nanoparticles. With increasing annealing time, the mean gold cluster radius rises from 0.25 nm after 10 min, to 2.3 nm after 60 min. However, no gold particles can be detected in glasses annealed for less than 10 min. They consist only of a few atoms and are too small to be resolved by SAXS. Therefore, the light emission should be associated with molecular gold clusters (like Au_2).

References:

[1] P. P. Edwards et al., Angew. Chem. Int. Ed. **46**, 5480-5486 (2007).

[2] J. Zheng et al., Phys. Rev. Lett. **93**, 077402 (2004).

[3] M. Eichelbaum et al., Angew. Chem. Int. Ed. **44**, 7905-7909 (2005).

[4] M. Eichelbaum et al., Nanotechnology, **19**, 135701 (2008).

[5] P. H. Kasai et al., J. Chem. Phys. **55**, 1566-75 (1971).

[6] S. Fedrigo et al., J. Chem. Phys. **99**, 5712-5717 (1993).

[7] G. A. Bishea et al., J. Chem. Phys. **95**, 5646-5659 (1991).

[8] M. Eichelbaum et al., Gold Bull. **40**, 278-282 (2007).

Acknowledgements:

Funded by the DFG and VCI. We thank the BAM for technical and scientific support.

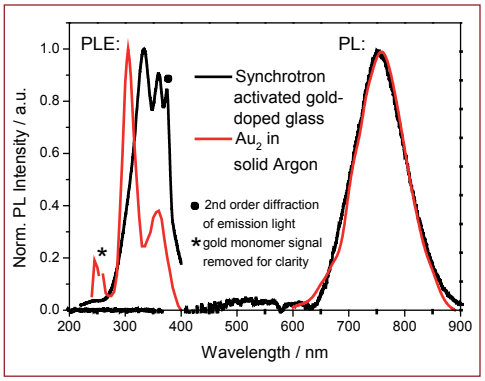

Fig. 2:
PL and PL excitation (PLE) spectra of gold-doped glasses compared with spectra of argon matrix-isolated gold dimers (after reference [6]).

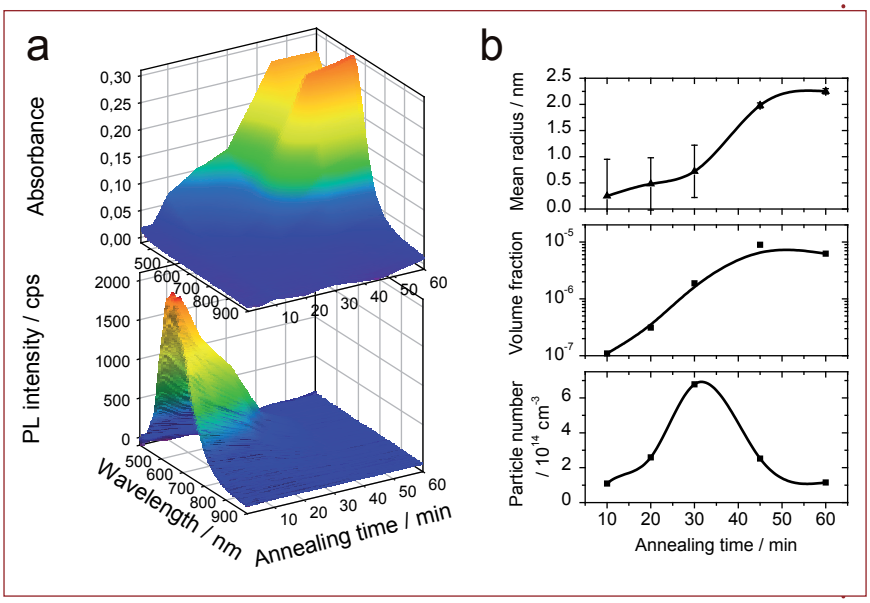

Fig. 3:
a) 3-dimensional plots of PL intensity (λ_{exc} = 337 nm) and UV-Vis absorption of an activated gold-doped glass during annealing at 550°C. b) Corresponding SAXS mean particle radii, volume fractions and particle number densities.

SAXS measurements show furthermore, that the number of particles initially increases, but decreases for longer annealing times. This is in accordance with a three stage phase separation process: After an approximately 10 min incubation period, smaller clusters grow driven by diffusion of isolated atoms through the glass matrix. Finally, after approximately 45 min, larger particles grow at the expense of smaller ones (called Ostwald ripening), which is associated with a decrease of the number of particles, a nearly constant volume fraction and a slow size increase.

Interestingly, annealing of synchrotron activated silver-doped samples induces a white luminescence (Fig. 1c) peaking at a similar range of 500-550 nm as in the case of gold-doped glasses. Further investigations have shown that in Eu^{3+}-doped glasses Eu^{3+} ions are partially reduced to Eu^{2+} ions by synchrotron irradiation, and that a green luminescence can be induced as well (Fig. 4). Because Eu^{2+} is an excellent donator in energy transfer processes, an indirect excitation of a luminescent glass center (like the localized state [Si-O-Na], called L-centre) via Eu^{2+} (or molecular gold and silver particles, respectively) could explain the appearance of the green luminescence in the activated samples. Because Eu^{3+} ions behave similar to L-centres and can emit a red luminescence, the hypothesis of an energy transfer process from molecular gold, respectively silver, could be confirmed by the investigation of gold- and silver-containing glasses co-doped with Eu^{3+}. After activation and subsequent annealing, the Eu^{3+} emission could be excited indirectly at 337 nm and enhanced this way by a factor of up to 250. This effect has not only proven the energy transfer mechanism, but could also open up new vistas for multicolour light sources like LEDs.

Moreover, by employing synchrotron X-ray lithography we can write luminescent and plasmonic microstructures (Fig. 5). This technique provides an opportunity for developing photonic devices in glasses [8].

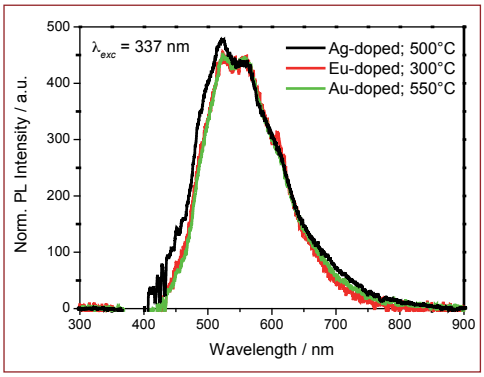

Fig. 4:
Comparison of PL spectra of activated glasses containing different dopants and annealed at different temperatures.

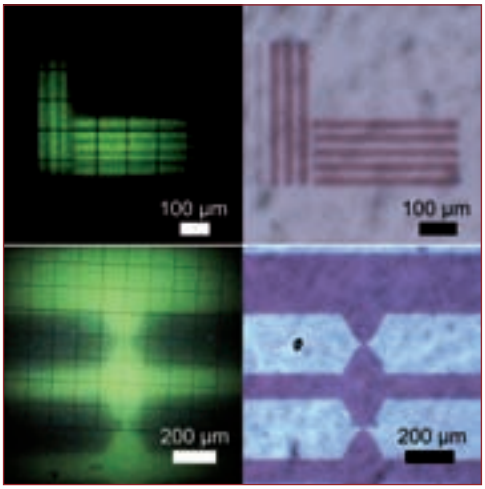

Fig. 5:
Confocal fluorescence (λ_{exc} = 366 nm; left images) and transmitted light microscope images (right) of X-ray lithographically structured gold-doped glasses after 5 min (left) and 45 min (right) annealing at 550°C.

Contact:
Klaus Rademann,
Klaus.rademann@chemie.hu-berlin.de

Looking beneath the surface: Standing-waves and hard X-ray photoemission

F. Kronast[1], S. Döring[2], M. Gorgoi[1], R. Ovsyannikov[1], A. Kaiser[3], C. Wiemann[3], S.-H. Yang[4], M. Huijben[5], A. Locatelli[6], D. E. Bürgler[3], R. Schreiber[3], F. Schäfers[1], W. Braun[1], H.A. Dürr[1], C. M. Schneider[3], C. Westphal[2], C. S. Fadley[3,5,7]

1 BESSY
2 Technische Universität Dortmund
3 Forschungzentrum Jülich
4 IBM Almaden Research Center, San Jose, USA
5 Lawrence Berkeley National Laboratory, Berkeley, USA
6 Elettra, Sincrotrone Trieste; Trieste, Italy
7 University of California, Davis, USA

Modern technological devices, as for example, the integrated circuits which carry out the logical operations in a computer or the device which reads magnetically-stored information from a computer hard drive, consist of multilayer structures whose dimensions have shrunk into the nanometer regime. The Nobel Prize in Physics for 2007 was in fact shared by a German scientist for work that led to the development of the current devices for reading information. For reference, one nanometer (nm) is about the length of five atoms in a row. Such 'nanodevices' consist of complex sandwiches of different materials. The individual layers and the interfaces between these layers are crucial to arriving at the desired performance. It is thus key in developing the next generation of high technology to be able to measure the properties of the different layers and interfaces in such structures, including their chemical composition, magnetic character, and precise electronic structure (e.g. metallic, semiconducting, or insulating).

Although many techniques have been developed in the past few decades for studying the first few surface layers of materials, the number of methods which can penetrate below the surface to look at buried layers and interfaces is quite limited. In our research at BESSY, we have explored, and combined, two new approaches for exploring such subsurface structures. Both are based on photoemission (photoelectron spectroscopy) in which an X-ray is absorbed and excites a photoelectron from the sample. Photoemission is a well known and very powerful tool for studying materials, but in its usual implementations, its probing depth is limited to the first few layers near a solid surface. However, it has recently been demonstrated in the 'HIKE' experiment [see BESSY Highlights 2006] and elsewhere [1] that, by exciting the photoelectrons with X-rays of significantly higher energies (up to ca. 4,000 - 10,000 eV, as compared to past studies with soft X-rays at ca. 20 - 1,500 eV) one can increase the average probing depth from ca. 1 nm up to about 10 nm or roughly 50 atomic layers. Various applications for such hard X-ray photoemission have been explored and suggested [1].

In addition, some recent soft X-ray studies have shown that, by growing the sample on top of a nanometer-scale multilayer (ML) mirror, the exciting radiation field can be 'tailored' into an oscillatory standing wave of the same scale. This standing wave (SW) can then be moved up and down in the sample layers on top of the ML in three ways: by scanning the incidence angle of the radiation around that satisfying the Bragg condition for reflection from the ML, by scanning the incident radiation energy around that satisfying the Bragg condition for reflection, and/or by sitting at the Bragg condition and moving the sample in the synchrotron radiation beam, with the latter method requiring one layer of the sample to be specially grown in a wedge configuration. Fig. 1a shows a schematic drawing of the third standing wave/wedge ('swedge') method [2].

We have for the first time applied these approaches, including the swedge method, to multilayer structures of interest in future magnetic data storage and logic technologies, or 'spintronics', using higher energy X-rays in the HIKE experiment to excite the photoelectrons. One system studied is an insulator on top of a ferromagnet (MgO/Fe), a combination that is important in current devices for magnetic data retrieval known as tunnel junctions (Fig. 1a). Fig. 1b shows clear oscillations of about 20% in the intensity of two Fe photoelectron peaks as the sample position is scanned in front of the beam, which effectively scans the SW through the Fe/MgO interface [2]. Via an analysis of these data using X-ray optical theoretical calculations, these data and other similar results obtained for photoelectrons emitted from other elements will permit determining the thickness and chemical composition of the MgO overlayer, as well as the nature of the buried Fe/MgO interface. A wide variety of applications of this hard X-ray photoemission approach seems possible.

Another important dimension of photoemission is its use as the imaging mechanism in a photoelectron microscope (PEEM). Such devices are now able to observe features along the two surface dimensions of x and y in Fig. 1a with resolutions of about 20 nm, and

References:

[1] Special journal issue dedicated to photoemission with hard x-rays: Nuclear Instruments and Methods A **547** (2005), edited by J. Zegenhagen and C. Kunz.

[2] S.H. Yang et al., Synchrotron Radiation News **17**, 24 (2004).

Acknowledgements:

Funded by the Land Nordrhein-Westfalen, the U.S. DoE, the Alexander von Humboldt Foundation, and the Helmholtz Association. The beamtime at BESSY was funded by the BMBF.

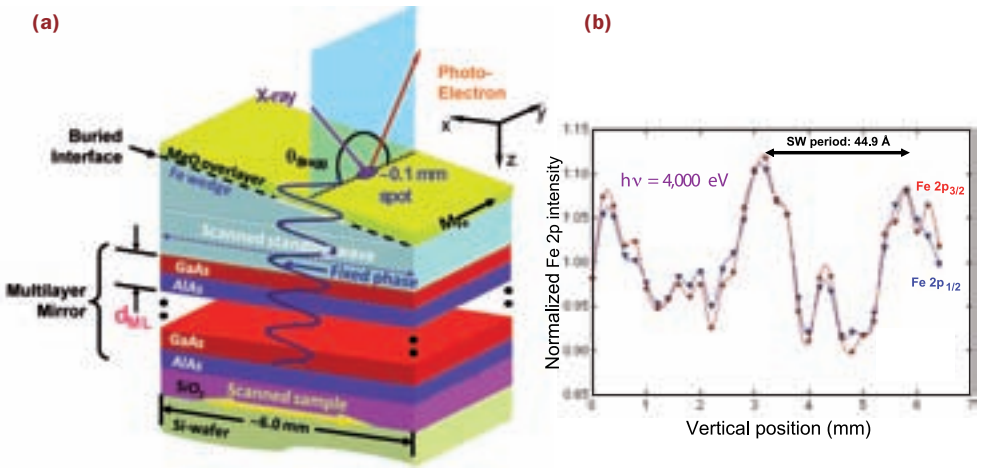

Fig. 1:
(a) Illustration of photoemission from a multilayer sample and the standing wave/wedge ('swedge') method for studying buried layers and interfaces. A movie illustrating the 'swedge' method is available at: www.physics.ucdavis.edu/fadleygroup. (b) Oscillatory intensity modulation of the iron photoelectron intensities as the standing wave is scanned through the iron/magnesium oxide interface shown in (a). The sample was scanned under the X-ray beam (Fig. 1a) and the hard X-ray excitation energy was 4,000 eV.

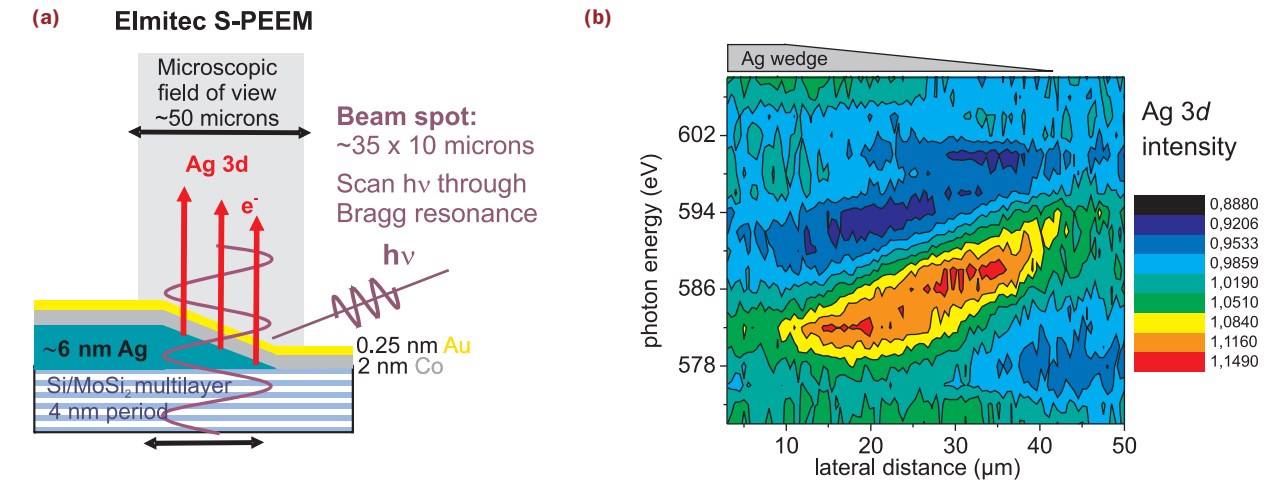

current developments at BESSY (e.g. the SMART project) promise resolutions in the few nm regime. However, PEEMs cannot resolve the third depth-related dimension z in Fig 1a. In order to add this important dimension to PEEM images, we have incorporated the swedge method into the S-PEEM endstation (for details see page 66), and studied a multilayer test structure consisting of a narrow wedge of silver (Ag) that is capped with layers of cobalt (Co) and gold (Au), as shown in Fig. 2a. In this case, the angle of X-ray incidence is fixed at the Bragg condition, and the radiation energy is scanned so as to move the SW through the Ag/Co interface. Plotting the Ag intensity in the images as a function of energy clearly shows the SW moving down the slope of the wedge, as summarized in Fig. 2b. These results thus represent a first proof-of-principle that the swedge method can be used to provide depth (or z) resolution in PEEM images, with many possible applications in the future.

Fig. 2:
(a) Illustration of the use of the swedge method in a photoelectron microscope, for the case of a Ag wedge below Co and Au layers. Here, 1 micron = 1μm = 1,000 nanometers. (b) Summary of images based on silver photoelectron intensities obtained as the soft X-ray energy is scanned over the multilayer Bragg condition, and showing clearly that the SW maximum moves down the wedge. A movie illustrating this movement is available at: www.physics.ucdavis.edu/fadleygroup

Contact:
Charles S. Fadley
fadley@physics.ucdavis.edu

Of Man and mice. Small-animal model of human listeriosis by rational engineering

T. Wollert[1], B. Pasche[1], A. Lengeling[1], A. D. Gruber[2], D. W. Heinz[1], W.-D. Schubert[1]

1 Helmholtz-Zentrum für Infektionsbiologie, Braunschweig
2 Freie Universität Berlin

Dairy products such as milk and cheese have not always been as safe as they are now. To prevent infectious diseases in humans, milk nowadays is generally pasteurized. One of the diseases transmitted by contaminated milk is 'listerioses'. Apart from humans, *Listeria monocytogenes*, the bacterium causing this disease also infects ruminants such as cows.

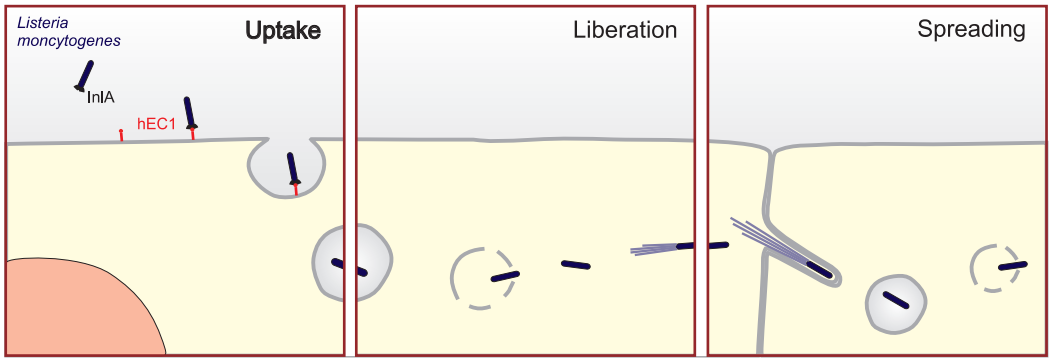

Fig. 1: Infection of cells by *Listeria monocytogenes*: Uptake, Liberation, Spreading

Most listeriae swallowed as part of contaminated food are killed in the stomach, but some occasionally survive and pass to the small intestine. From here they are able to initiate infections by forcing their way into the epithelial cells lining in the small intestine. Once they have overcome this barrier, they spread to other organs such as the liver and spleen. Being an intracellular pathogen, listeriae are able to cross two further physiological barriers, the blood-brain and the placental barriers. As a result, listerial infections give rise to highly divergent manifestations including sepsis, meningitis and fetal abort.

As part of its infection strategy, *L. monocytogenes* produces virulence factors to manipulate individual host receptors and associated signaling cascades to ensure its own survival. Many years of research have identified many of these with the result that *L. monocytogenes* is currently probably the best understood intracellular bacterial pathogens with respect to the underlying molecular processes. Especially well understood are its invasion proteins (Internalins A and B), the factors required for its liberation from primary phagosomes (after it has entered the cell), and the protein ActA required to re-organize the actin-cytoskeleton for intracellular bacterial motility and hence to spread to other cells (Fig. 1). Additional proteins have been found to be involved in pathogenesis but their precise involvement is still under investigation.

Investigations of listerial infections in humans has traditionally used either human cell lines or live mice to dissect the role of individual proteins, signaling pathways or entire tissues and organs during the infection. Work, on mechanisms of breaching the intestinal barrier has however been hampered by the fact that mice are not systematically infected via the oral route. Therefore we decided to have a closer look on the factors involved in invasion.

The protein Internalin A (InlA) is crucial for the very first step of listerial invasion, namely the recognition, adhesion and invasion of epithelial cells [1]. InlA is able to accomplish these three processes unaided by other bacterial factors. Its target in this process is epithelial cadherin (E-cadherin) [2], the major constituent of adherens junctions of epithelia, which normally interlocks neighboring epithelial cells through homotopic interactions with E-cadherin from these neighboring cells. Homotopic E-cadherin interactions involve only the N-terminal of five extracellular domains (EC1), and this domain is also the interaction partner of InlA. We have previously solved the high resolution crystal structure of the functional domain of InlA in complex with human EC1 (hEC1).

We could thereby describe the details of recognition between these two proteins and quantify. These analysis indicated that the complex though specific is rather weak (K_D = ~8 µM) [3]. However, the binding affinity to mouse E-cadherin (mEC1) is even weaker. The reason for this has been traced to the substitution of individual amino acids in mEC1 compared to hEC1. In particular, proline 16, a residue crucial to the recognition of hEC1 by InlA [3] is substituted by glutamate in mEC1 [4].

References:

[1] J.L. Gaillard, Cell **65**, 1127-1141 (1991).

[2] J. Mengaud et al., Cell **84**, 923-932 (1996).

[4] W.-D. Schubert et al., Cell **111**, 825-836 (2002).

[3] M. Lecuit et al., EMBO J. **18**, 3956-3963 (1999).

[5] T. Wollert et al., Cell **129**, 891–902. (2007).

[6] T. Wollert et al., Proc. Natl. Acad Sci (USA) **104**, 13960-13965 (2007).

Acknowledgements:

Funded by the Deutsche Forschungsgemeinschaft (DFG) as part of the Priority Program 1150 (SCHU 1560/1-1 and 1-2).

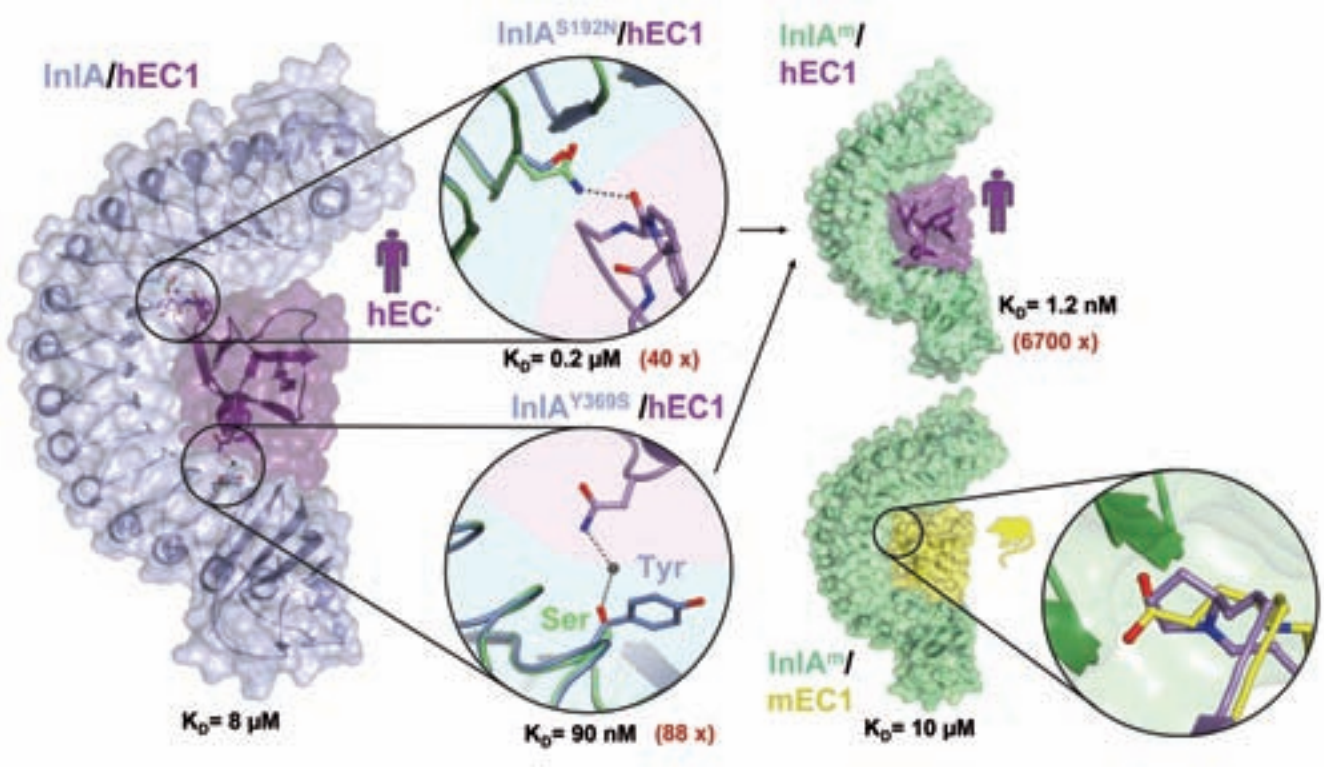

Fig. 2:
Rationally redesigning InlA: The complex of InlA (blue) and human E-cadherin (hEC1) (purple) [left] was used to increase binding affinity of hEC1 recognition. By combining only two substitutions [middle], the binding affinity of InlA^{m} (green) to hEC1 is increased 6,700-fold [top, right]. This compensates the repulsive force of glutamate16 in murine E-cadherin (mEC1, yellow) to InlA [inset, right] allowing InlA^{m} to bind mEC1 [lower, right].

We analyzed the complex of InlA/hEC1 in detail and identified individual amino acids in InlA whose contribution to recognition of hEC1 could be improved if substituted by other amino acids [5]. For example, tyrosine 369 of InlA collides with asparagine 27 of hEC1 during complex formation. In rotating away from its unbound conformation it disrupts the stacking of Phe348, Asp370 and His392 of InlA. By substituting Tyr369 by serine, this reorganization is eliminated and in addition a water-bridged hydrogen bond to Asp27 of hEC1 is created. Similarly, substituting Ser192 by asparagine allows for a direct hydrogen bond to hEC1 (carbonyl of Pro18). As a result of both these substitutions the binding affinity of InlA for hEC1 is increased by four orders of magnitude (K_D = 1.2 nM). This increase in binding affinity is able to overcome the repelling force of Glu16 in mEC1 with respect to InlA, with the result that mouse E-cadherin is now recognized by modified InlA (K_D = 10 µM) with a similar binding affinity as human E-cadherin by wild-type InlA (8 µM).

Introducing this modification into the genome of *L. monocytogenes* generates the variant strain Lmo-InlA^{m}. This bacterial strain is able to induce its own uptake into epithelial cells of mice and thereby simulate the early stages of infection in humans [6], the first step to study systemic listerioses in mice. Histological and immunohistochemical analyses of infected mice indicate that delayed infection via tips of intestinal villi represent the true route of infection in humans, instead of the previously suggested route via Peyer's patches.

Contact:
Wolf-Dieter Schubert
wolf-dieter.schubert@helmholtz-hzi.de

Do not touch! X-ray scattering of suspended proteins in acoustically levitated droplets

F. Delißen, J. Leiterer, R. Bienert, F. Emmerling, U. Panne, A. F. Thünemann

BAM Bundesanstalt für Materialforschung und -prüfung

Aggregation is a common feature of proteins. It occurs in healthy cellular assemblies and in pathological protein depositions (e.g. Alzheimer's disease). But it is also of importance in growth of protein crystals in vitro, which are generally used for structural studies, for the formation of protein fold and its assembly to larger functional complexes and nanoparticles. Aggregation processes can be studied with various methods, e.g. dynamic light scattering (DLS) and small-angle neutron scattering (SANS), but small-angle X-ray scattering (SAXS) with synchrotron radiation is the method of choice. SAXS allows an *in-situ* determination of changes in size, structure, and state of aggregation. It is further possible to look 'inside' small particles and aggregates, which is hardly possible with other techniques. However, SAXS is often hampered through a considerable background from the solvent (water) and the sample container. An isolated, 'untouched' droplet would improve the signal-to-noise ratio considerably. Therefore, we employed acoustical levitation of small droplets. Here, the scattering from any sample container is eliminated and solvent contributions are minimized.

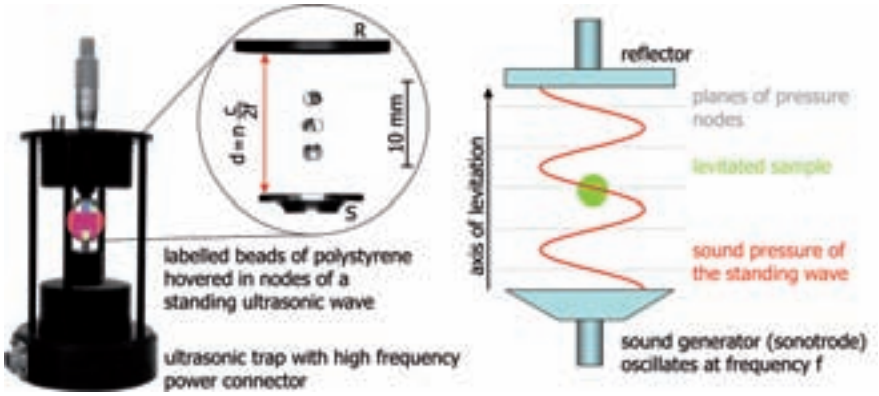

Fig. 1: Scheme of the principle and the set-up for the ultrasonic trap, which enables levitation in every node of the acoustic wave. Levitation of multiple samples is shown, as an example, with three polystyrene beads.

Liquid droplets can be utilized as miniaturized self-contained reaction vessels with the benefits of small and defined volumes and low reagent and/or sample consumption. Levitation of droplets prevents chemical contamination of the sample and interaction with container walls, while offering increased sensitivity with spectroscopic and scattering techniques otherwise hampered through sample containers.

Acoustic or ultrasonic levitation is one of the most useful approaches for containerless processing of small samples in analytical chemistry. It combines biological compatibility with stable and easy accessible sample positioning, requiring no specific physical property, e.g. electric charge or a specific refractive index of the sample.

In our study, we chose the protein apoferritin (APO) as a model system. APO has a well defined hollow sphere structure of 12 nm in diameter that produces a well structured SAXS pattern. All measurements were performed at the µSpot beamline [1] with initial APO concentrations in the range of 5-40 mg/ml. APO was dissolved in 150 mmol sodium chloride solution to minimize intermolecular interactions between APO molecules through electrostatic shielding.

Droplets with a volume of about 5 µl were suspended in the nodes of an ultrasonic standing wave. The wave is maintained in an acoustic levitator (Tec5, Germany) between a piezoelectric transducer and a concentric reflector (Fig. 1). More detailed experimental information was reported earlier and can be found in [2]. The levitated droplet was carefully positioned in the focus of a X-ray beam with a cross section of 100 µm at an photon energy of 12 keV.

Due to evaporation of the solvent, the volume of the droplet decreases continuously during the experiment. This can be controlled through a defined gas atmosphere and temperature. On-line infrared shadowgraphs were recorded by a CCD camera and allowed the calculation of the critical droplet volume and the analyte concentration in time intervals of 1 s. In combination with the known initial concentration of the dissolved sample at the time of injection into the levitator, the sample concentration was determined with an accuracy of 1 %. Fig. 2 illustrates the experimental set-up schematically.

We started with an APO concentration of 40 mg/mL, a concentration range typical for SAXS measurements. The APO scattering curves have four characteristic minima due to the monodisperse spherical shape

References:

[1] O. Paris et al., J. Appl. Cryst., **40**, S466-S470 (2007).

[2] J. Leiterer et al., J. Appl. Cryst., **39**, 771-773 (2006).

[3] L.A. Crum, L. A., J. Acoust. Soc. Am, **50** (1), 157-163 (1971).

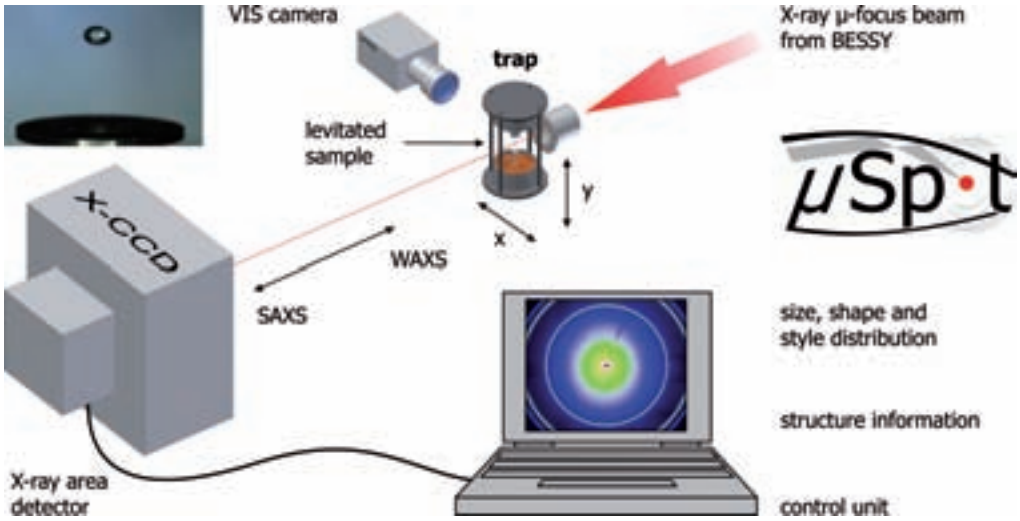

Fig. 2:
Schematically, the experimental set-up used for X-ray scattering experiments (WAXS and SAXS). At its center the ultrasonic levitator (trap) is implemented as a nouveau sample holder. The camera shows the levitated liquide sample

of APO (Fig. 3). For further data analysis, we processed the obtained scattering curves by using a core shell fitting function. Hence, from the best fit curves, it was verified that the apoferritin has a spherical structure with an outer diameter of 12 nm (± 0.4 nm) and a hollow interior with a diameter of 7 nm (± 0.3 nm). Smearing effects of the experimental set-up are of low significance; smearing effects would have flattened the depth of the minima significantly. For late levitation times, prominent changes in the low q-range indicate significant intermolecular interactions between the molecules of the protein. In addition, the changes at q-values smaller than about 0.4 nm^{-1} point to repulsive interactions. Due to the dominant agglomeration of APO at the end of the levitation experiment, the scattering curve is completely modified and similar to solid state scattering (Fig. 3, bottom curve).

The structure factor, S(q), of APO is a sensitive measure for protein interaction and agglomeration. It can be considered close to unity (i.e. no interaction) for lower concentration. Thus, structure factors are obtained for higher concentrations by dividing the measured intensity by the form factor determined for very dilute solutions. Structure factors for selected concentrations are displayed in Fig. 4. For the lowest concentration, S(q) is close to unity as expected. A characteristic change in the structure factors was observed with increasing concentration, while the maxima shifted to higher q values. This can be attributed to a decrease in the distances between single APO proteins with increasing concentration. Due to the controlled decrease in sample volume and increase in concentration, the SAXS measurements of APO could be carried out in a single experiment with the same sample. Note, that the structure factors can now be determined up to q-values of 3 nm^{-1}, which allows the detailed study of intermolecular interactions of the APO protein.

In conclusion, we found that ultrasonic levitation is a useful analytical tool for fast and precise in situ SAXS experiments of small sample amounts. The wide range of experimentally accessible concentrations in a single experiment, makes acoustic levitation a good approach to study agglomeration of (bio)macromolecules and nanoparticles via SAXS.

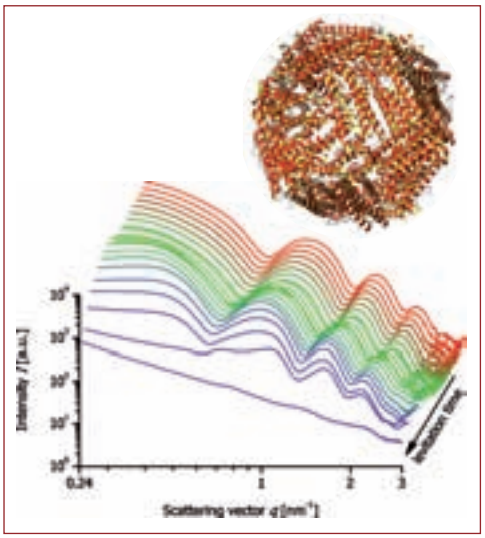

Fig. 3:
Small-angle X-ray scattering of APO as a function of time and concentration in a 0.15 mol sodium chloride solution. The concentration of APO increases from 40 mg/ml (top curve) to 1216 mg/ml (solid, bottom curve) while levitated in the ultrasonic trap for 36 min (time increases from top to bottom curve). A ribbon model of the hollow sphere APO is shown schematically.

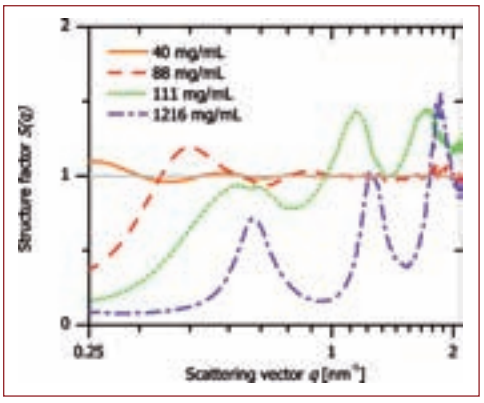

Fig. 4:
Change of the APO structure factor with increasing concentrations from 40 mg/ml to 1216 mg/ml (solid) in aqueous solution (0.15 mol/l sodium chloride). The structure factor is a measure for the interaction and aggregation of the protein molecule, the form factor for calculation of the structure factor was taken from a SAXS measurement at 5 mg/ml

Contact:
Andreas F. Thünemann
andreas.thuenemann@bam.de

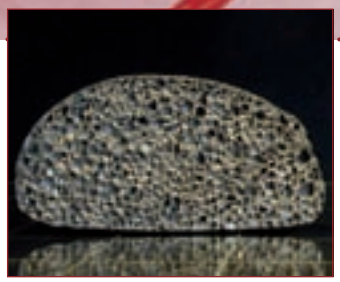

Nondestructive 3D insights into foamy metals and bioregenerative ceramics

A. Rack[1,4], S. Zabler[1] , H. Riesemeier[2], G. Weidemann[2], B. R. Müller[2], L. Helfen[4], M. Stiller[3], C. Knabe[3], J. Goebbels[2], J. Banhart[1]

1
Hahn-Meitner-Institut
2
BAM Bundesanstalt für Materialforschung und -prüfung
3
Charité
4
Forschungszentrum Karlsruhe

Micro-structured, multi-component material systems are of high interest due to their broad range of application fields. Within this article we focus on two representatives of these material systems and the insights we can obtain by employing X-ray microtomography.

Aluminum foams, with their high specific stiffness are of substantial interest for lightweight constructions e.g. for car bodies. But on the way to industrial applications there is still a need for basic approaches to control their final pore structure [1].

Something quite different are biodegradable ceramics (Fig. 1). These compounds can be used alternatively to autogenous bone grafts for supporting the bone regeneration in defects, which can occur after tooth loss for instance. Different biocompatible materials are available on the market. But there is still a demand for detailed investigations in order to optimise their properties for the various clinical applications [2].

In order to follow the pore formation in early stages of metallic foams and the biodegradation of bone substitute materials, we employed microtomography (µCT) using X-rays. This method is well established to image the inner structure of a sample in three dimensions in a nondestructive manner. µCT is particularly powerful when it is used in conjuction with synchrotron light sources like BESSY, since these sources offer a photon beam with a nearly parallel propagation, a high flux density, and a partial spatial coherence. The advantages are obvious: Resolutions up to sub-micrometer, different contrast modes (e.g. absorption contrast, holotomography, refraction contrast) and high data acquisition speed [3, 4, 5]. Furthermore, the high quality of volume images acquired with synchrotron-based µCT allows to perform a subsequent 3D image analysis [5, 6].

We used the excellent microtomography facility of the BAMline for our experiments [7] using monochromatic synchrotron radiation for our microtomography scans. This enabled us to distinguish between different phases of materials in the resulting volume images due to their different attenuation of the X-rays: e.g. the matrix and the blowing agent's particles in metallic foams or ceramic particles and bony tissue (Fig. 1, 2). In the subsequent 3D image analysis we separated different material phases within the images into Boolean images. These contain only the morphological information, marked with a Boolean '1' while the background is set to '0' [6].

By dilating the pore structure in successive steps we can determine the dependence of the blowing agent's (TiH_2) density on its distance to the pores space. Therefore, we are able to invest spatial correlations between the TiH_2 particles and the pores [8]. For aluminum foams produced from a prealloyed powder Al6061 (aluminum, silicon) it is known that pores and blowing agent's particles are spatially correlated in all foaming stages [9]. In AlSi6Cu10 and AlSi6Cu4 produced from a mixture of pure aluminum, copper and silicon powders we could prove spatial non-correlations between the TiH_2 particles and the early pores. This surprising result points out that there are different pore creation modes in the early stages of metallic foams which influence the spatial position of the first pores in the evolving foam matrix.

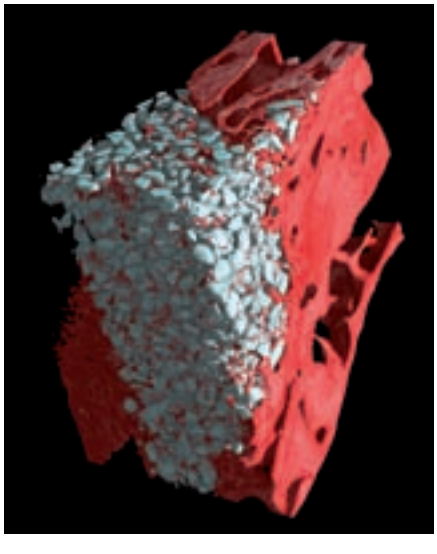

Fig. 1:
Bioceramic particles (white) three months after implantation in sheep bone (red) [8].

References:

[1] J. Banhart, D. Weaire, Physics Today **55** (2002).

[2] C. Knabe et al., Cellular response to bioactive ceramics (T. Kokubo, ed.), Woodhead Publishing Inc. (2007).

[3] U. Bonse, F. Busch, Prog. Biophys. Molec. Biol. **65** (1) (1996).

[4] A. Koch et al., J. Opt. Soc. Am. **15** (1998).

[5] J. Banhart (ed.), Oxford University Press (2008).

[6] J. Ohser, F. Mücklich, John Wiley & Sons (2001).

[7] A. Rack et al., Nucl. Inst. & Meth. in Res. A, **586**, (2008).

[8] A. Rack, PhD thesis (2006) http://opus.kobv.de/tuberlin/volltexte/2006/1370/

[9] L. Helfen et al., Proc. of SPIE **5054** (2002).

Acknowledgements:

The authors would like to thank K. Schladitz, J. Ohser (image analysis), T. Sych (volume rendering), C. Koch (histological images), A. Bütow (metal foams), H. Kropf (experimental support), T. Rack (patience).

Funded by the DFG, Grant KN 377/3-1.

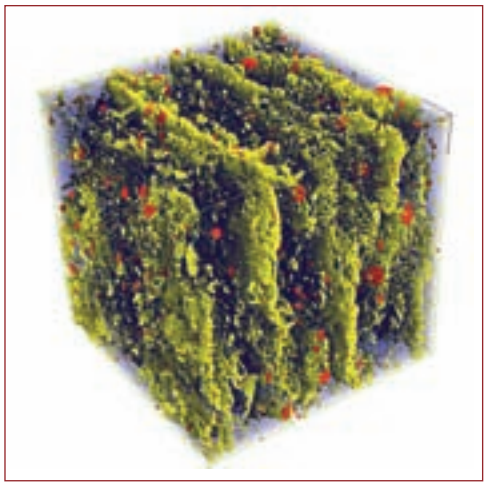

Fig. 2:
AlSi7 foam in early stage (6% porosity) with foam matrix (semitransparent blue), pores (yellow) and blowing agent (red).

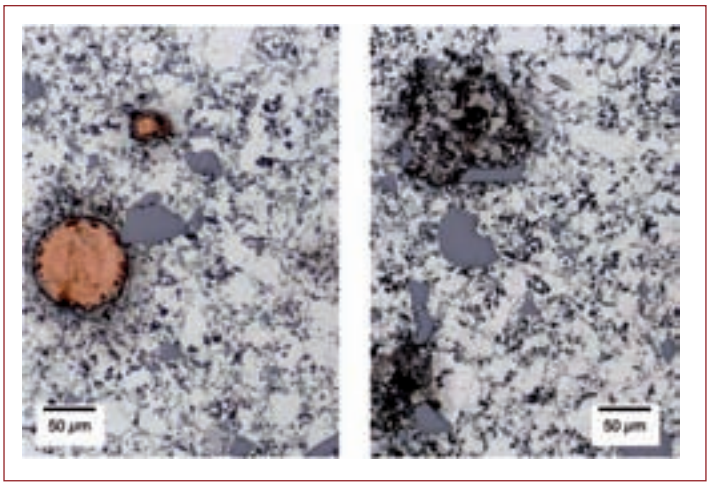

Fig. 3:
Metallographical photo of raw precursor AlSi6Cu4 (left) with Cu particles (brewn), Al (light grey), Si (blue) and tempered sample (right, same color code) [8].

The control mechanism behind this different behavior can be understood by examining etched and polished slices of the investigated samples (Fig. 3): the raw precursor contains pure copper, aluminum and silicon, the tempered sample only aluminum and silicon. Copper and part of the aluminum form an eutectic alloy already at lower temperatures. Here, gas set free from TiH_2 can nucleate most easy and form the first pores. In opposite to that precursors made of Al6061 are homogeneous due to the use of pre-alloyed aluminum with silicon. There are no 'weak' positions where a preferred pore creation can happen.

By masking the noise-reduced Boolean images of the bony tissue and the ceramics volume in the 3D image analysis, we obtained images which contain the morphology as well as density information of the different phases of material. Combined volume rendering of these data sets delivers excellent images which can be used for qualitative comparison with histological photos (Fig. 1). Samples were prepared as part of an animal study for comparing different bioceramics. We found a large difference in the amount of detected bone between the histological and the tomographical investigations (Fig. 4). The newly formed bone, if not fully developed, has a lower density and therefore is not visible in the µCT scans due to its low X-ray attenuation, while histology can detect it there due to the chemical sensitivity. This allows for a quality control of the bone regeneration depending on the bioceramic material used. The ceramic implanted in the specimen shown in Fig. 2 is degrading slowly: three months after implantation almost all ceramic particles are still left, only a small amount of bone tissue has formed. Bioactive ceramic materials with a higher biodegradability, which were also investigated in the context of this study resulted in an almost fully evolved bone structure after the same amount of time.

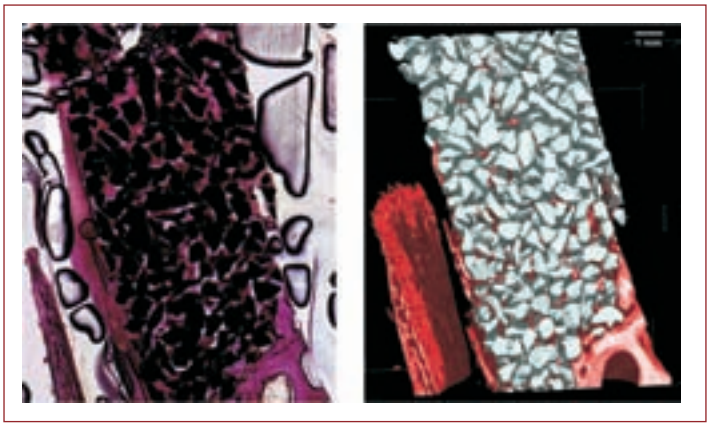

Fig. 4:
Left: histological image of bone substitute particles (black) in sheep sinus (bone in pink) and the rendered corresponding section from the segmented 3D data set (right) [8].

Our investigations show that heterogeneous precursors are one approach to control the pore structure of metallic foams as first pores start to grow on weak material positions. For the bioceramics we developed a novel approach to determine the stage of development of newly formed bony tissue by comparing histological with (synchrotron-)tomographical slices.

Contacts:
Heinrich Riesemeier
heinrich.riesemeier@bam.de
Alexander Rack
arack@snafu.de

Look through the lung book and don't miss a thing!

C. Kamenz[1], A. Staude[2]

1
Humboldt-Universität zu Berlin
2
BAM Bundesanstalt für Materialforschung und -prüfung

Fig. 1:
Ventral side of the scorpion *Hadogenes* sp demarcating the position of the book lungs (bright patches visible through cuticle: arrow heads).

Looking through lung books is like reading in old libraries, only that lung books are Palaeozoic ones. In fact, the lung book is nothing anthropogenic and it is much, much older than the Bible. The world already existed, and a few animals, too. It must have been whenever on the 5th day that the lung books appeared. According to modern time calculations it may have been about 400-450 million years ago. Nobody is responsible for the thing. Indeed, the lung book, respectively book lung is the respiratory organ of scorpions and spiders (Fig. 1, 2). Although this book does not contain any letters, it can tell us some interesting stories about something called 'evolution'.

The tricky thing is: How to get the information out. 'Leafing through' makes the first symbols readable although their meaning remains vague. Numbers of such book lungs must be compared to decode the symbols, which zoologists term 'characters', to understand their meaning. One, indeed the most striking, character is a stack of leaf-like lamellae, which give the lung its book-like appearance (Fig. 3).

Synchrotron radiation now offers the opportunity to 'read' the book lung, because we can look through all the fragile 'leaves' and gain a detailed view of their constitution. The µCT setup at the BAMline makes it possible to reconstruct book lungs in 3D with resolutions of below 2 µm. The high resolution allows very precise reconstructions in which individual lamellae are clearly visible (Fig. 3). This is exactly what we need to complete a look back in time at book lung evolution.

Different authors claimed that the lamellae stand vertically, others that they may be horizontal. But the orientation of the book lung lamellae varies, firstly, within the organ and, second, it may have changed during the evolution of scorpions and spider-like arachnids. However, the conventional methods to study the book lungs often introduce damages and artefacts to the sample. µCT leaves the entire specimen untouched. This guarantees that the natural conditions of the book lungs can be reconstructed without artificial alterations.

On the way towards reconstructions of such fragile biological material, two major methodical problems must be solved. First, it is necessary to stabilize the lamellae during the sophisticated process of ''scanning'. What we call scanning is actually a series of subsequent radiographies, while the book lung is rotated stepwise over 180 degrees. Embedding the book lungs into a solid material is the best way to fix all the structures permanently. Nothing else is done for histological (tissue) sectioning. Here, the same embedding substances were used, as in previous histological studies.

Contrast is the second point. Book lungs, i.e. the lamellae, yield no distinct signal in radiographies (Fig. 2). A contrasting substance might be helpful, which makes anatomical structures clearly visible. Just as staining in histology changes the light in the microscopic sections, we need substances changing X-rays. Heavier atoms work as strong absorbers of radiation from the X-ray spectrum.

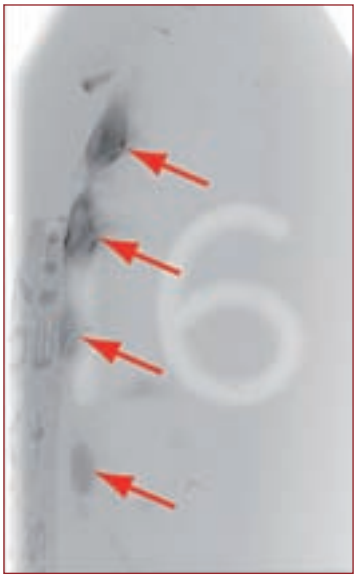

Fig. 2:
Radiography of half the mesosoma of the scorpion *Heterometrus* sp., delimited book lungs (red arrows) highlighted using a contrasting substance.

Acknowledgements:

The authors are grateful to Jason Dunlop, Gerhard Scholtz, Martin Watz and Nico Küntzel.

Funded by the DFG

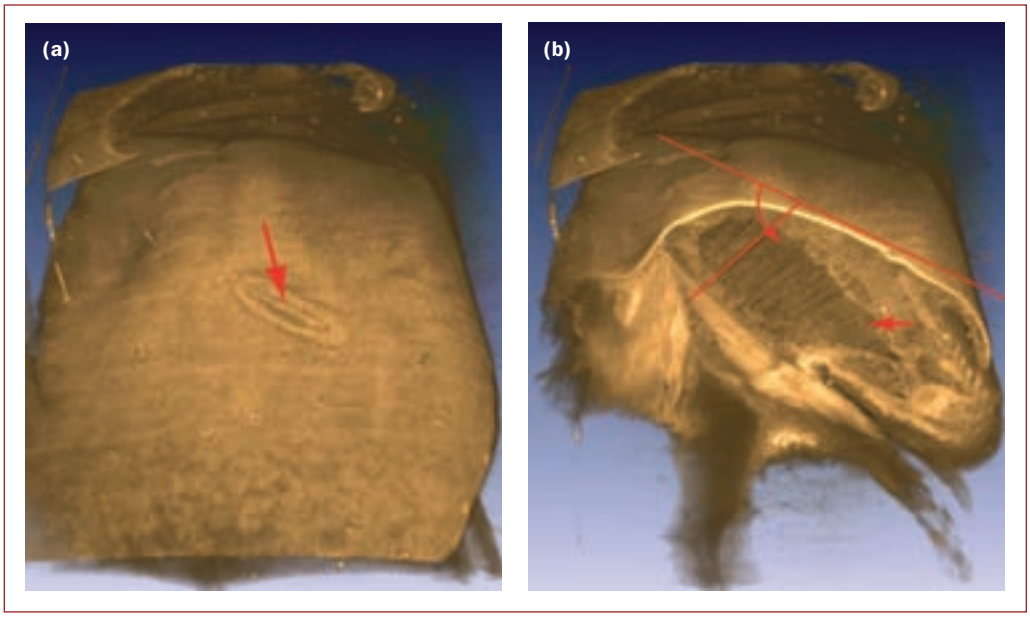

Fig. 3:
3D-reconstruction of the ventro-lateral part of the 5th opisthosomal segment of the scorpion *Nebo hierichonticus*. (a) showing the sternite with the respiratory opening (spiracle, red arrow) and (b) opened by a clipping plane to reveal book lung (red arrow). The angle demonstrates the inclination of the book lung lamellae.

We used osmium, which can be applied as the gaseous osmium tetroxide. Specifically applied to the respiratory organs, they fulfil the contrast function very well. The structures of the respiratory chamber are significantly shaded compared to the surrounding tissues using heavy metals, even in low concentrations.

In our study we intended to compare book lung reconstructions from a representative number of species amongst the arachnid branch of the tree of life. Previous studies on the structures on the lamellae clearly hint at a possible rotation of the book lung within one lineage of arachnid evolution. Those microscopic features of the book lungs are specifically situated on the opposite sides of the lung lamellae in scorpions on the one hand and spiders on the other. Maybe the lamellae rotated during scorpion evolution? It happened undoubtedly after the lineages of scorpions and spiders diverged from their common ancestor. In searching for this answer we are looking through the world's oldest 'books' very carefully.

Initial results are very promising since the contrasting approaches with osmium were successful. Osmium tetroxide enters through the respiratory opening and distributes very slow, remaining in the direct surroundings of the book lung structures (Fig. 3). The extended midgut diverticulum remains largely unaffected, which enhances the lung structures against any background structures. Ten species (eight scorpions and two spider-like arachnids) were analysed so far, yielding significant differences, although perhaps not as huge as expected. The gross morphology of all arachnid book lungs is fairly constant. All lamellae undergo torsion from the anterior, where they are roughly horizontal, towards the posterior end where they stand 'vertical'. Differences of the so-called 'vertical' edge seem specific for scorpion species and vary from almost 90° to ca. 45°. Our preliminary results give no hint that inversion by rotation of the book lung lamellae in the scorpion lineage occured.

Using µCT, we have made great progress in terms of two different subjects. We found a functional method to get almost artefact-free three-dimensional reconstructions of the extremely fragile features of respiratory organs. This improvement of tomographical imaging provides access to new morphological features, which will help 'classical' natural sciences, as per the Zoology. It is of great benefit, that µCT is now accessible for biologists. So we decoded a new essential character with micro-tomographical studies although arachnid lungs are not even books, which are easy to read.

Contact:
Carsten Kamenz
CarstenKamenz@gmx.de

NOBLE TRACES

NEWS & EVENTS

News

The eventful year 2007 saw a double climax in the summer with hosting the VUV-XV conference and the announcement that BESSY and the Hahn-Meitner-Institut will merge by January 2009 to the new 'Helmholtz-Zentrum Berlin für Materialen und Energie'. At the press conference on the 15th of August, the Federal Minister of Education and Research, Dr. Annette Schavan, and the Berlin Senator for Education, Science and Research, Prof. Dr. Jürgen Zöllner, said that the new centre will generate innovative and unique research opportunities by integrating two large scale facilities, the neutron source BER-II and the synchrotron radiation source BESSY-II. The focus of the centre will be on the complementary use of photons (light) and neutrons, and the design and development of modern materials in the fields of photovoltaics, functional and magnetic systems. With the merger BESSY will become a member of the Helmholtz Association, Germany's largest scientific organisation.

Three months earlier, Prof. Zöllner visited BESSY during his tour on the Science Campus Adlershof, acknowledging the success of the Adlershof site and its important role in establishing Berlin as a 'City of Sciences'. He encouraged even more marketing activities to raise its public awareness.

Prof. Zöllner was only one of some 2,900 visitors during 2007. Already in the beginning of the year, Prof. Krzysztof Kurzydlowski, from the Polish Ministry of Science and Higher Education, emphasized the intensified access of Polish researchers to the BESSY light source, and Honourable Steven Maharey, New Zealand's Minister of Education, Research, Science and Technology, was interested in the impact of Adlershof based institutes and companies on the Australian Light Source.

Among high ranking visitors we welcomed Prof. Hafeez Hoorani, the scientific director of SESAME, and Raleb Majadle, the Israelian Minister of Science, Culture and Sport. Many more national and international guests from politics and economy, delegations from Japan, China, Austria, the US, Slovenia, and the Czech Republic came for a visit. But BESSY remains particularly attractive to young people from schools and universities. They hold the majority of our visitors.

In the summer the 15th International Conference on Vacuum Ultraviolet Radiation Physics (VUV-XV) took place at the Konzerthaus at the Gendarmenmarkt in the centre of Berlin. More than 500 scientists from 32 countries all over the world working in the field of developing synchrotron, laser, or plasma based VUV and soft X-ray sources as well as applying photons in this spectral range participated at this very successful and inspiring meeting. The conference program was completed by an industrial exhibition, which allowed the participants to discuss technical requirements for future experiments and their possible realisation. Four plenary lectures covered topics of outstanding interest: Interferometry in the attosecond time regime by Paul Corkum (National Research Council of Canada), angle-resolved photoemission studies of high-Tc superconductors by Z.-X. Shen (Stanford University), electron spectroscopy in the analysis of functional surfaces by Robert Schlögl (Fritz-Haber-Institut Berlin), and charge transfer at interfaces for molecular electronics by William Salaneck (Universitiy of Linköping).

International visitors: Prof. Zöllner (Berlin), Prof Kurzydlowski (Poland), and the Ministers Maharey (New Zealand) and Majadle (Israel).

VUV-XV impressions

Events

Discussion at the ISISS inauguration

In April, the ISISS beamline celebrated its inauguration. Dr. Miquel Salmeron held the lecture on 'The pressure and materials gap in catalysis and environmental sciences'. Prof. Schlögl, long-term chairman of the Scientific Advisory Committee, highlighted the importance of the beamline for catalysis research. Dr. Hävecker explained the construction procedure and provided a first characterization of the beamline, followed by Dr. Knop-Gericke, who presented first results.

'Hahn-Meitner-Institut and BESSY – a new option for Berlin' was the slogan for the joint display of their activities during the 'Lange Nacht der Wissenschaften'. Researchers and staff members provided insights into their research from tiny elementary particles, applied sciences, up-to-date imaging techniques to solar energy. 4,300 visitors used the opportunity to have a look into the storage ring, enjoyed experiments and doing handcrafts for children, took a look into materials, and used the chance to discuss with Prof. Dr. Metin Tolan the physics that lies behind the adventures of James Bond. Pupils of the Goethe-Gymnasium provided with their C.O.M.B.O. the background music.

Archaeology and cultural heritage was the theme of a display for members of the parliament. Organised by the Leibniz Gemeinschaft some 30 institutes presented their research activities. BESSY and BAM summarized on the cultural objects, which have been studied so far by using the BAMline. Dr. Hahn and Dr. Rabin (BAM) gave an impression of their work on the Dead Sea Scrolls in numerous discussions.

Visitors at the 'Lange Nacht der Wissenschaften'

During the summer holidays we held another series of our Sunday morning 'Breakfast Physics'. Simple experiments show the character of light, what it is useful for and why physicists might prefer synchrotron light. More than 200 people from 8-80 attended the show and enjoyed BESSY-shaped food.

Following the very successful start of the Adlershofer Business Talk in October 2006 with 'Media meets Technology', the talks continued in 2007. 'Science2Business' communicated experiences made by outstanding companies and personalities about how to earn money with science. A second Adlershofer Business Talk focussed on photovoltaics, a growing business field on the campus. The 'Adlershofer Business Talk' is an event series organised by the campus management.

BESSY also attended the 'Industrietag' on imaging techniques of industrial relevance at the Hahn-Meitner-Institut. Organised by the HMI, this activity is dedicated to industrial users and to promote technology transfer.

Spin-up! Magnetism simulation at 'Breakfast Physics'

Dr. Rabin explaining her research project on the Dead Sea Scrolls

More visitors at the 'Lange Nacht der Wissenschaften'

Users' Meeting 2007

The audience listens to PD Dr. Birgit Kanngießer's key note lecture

The Users' Meeting was accompanied by the 4th Russian-German Workshop on 'Bilateral Research in Material Sciences at the Russian-German-Laboratory at BESSY'. The workshop focused on nanostructures, organometallic compounds, and electronic structure and X-ray methods. Participants used the opportunity to discuss new projects and perspectives for the Russian-German Laboratory at BESSY, in particular, regarding the proposed VUV-FEL project.

Almost 400 participants presented their scientific work on some 200 posters at the 26th BESSY Users' Meeting. The key note lecture 'Treasures from Art and Archaeology – Investigations at BESSY for Cultural Heritage' was held by PD Dr. Birgit Kanngießer (TU Berlin). Her lecture was followed by research highlights of various BESSY user groups.

The industrial exhibition featured some 40 companies, which also sponsored the traditional 'Berliner Buffet'.

The poster prize was awarded to Dr. Oleksandr Prokhnenko (HMI, SF2). 'Coupling of frustrated ising spins to the magnetic cycloid in multiferroic $TbMnO_3$' described the results of experiments, where only the complementary use of X-ray and neutron scattering helped to solve the underlying questions. The experiments using resonant X-ray scattering were accomplished at the MAGS beamline at the 7 Tesla Wiggler at BESSY.

Workshops

Cavity Meeting	February, 1 - 2
Workshop on 'Synergy of National Light Sources in Europe'	May, 21 - 23
Workshop on 'Quantifizierung der Röntgenfluoreszenzanalyse'	June, 4
15th International Conference on Vacuum Ultraviolet Radiation Physics (VUV-XV)	July, 29 - August, 3
Workshop on 'X-ray Diffraction Data Collection Using Synchrotron Radiation'	August, 23 - 25
Correlative Microscopy for 3-D Cell Imaging	September, 12 - 13
4th Russian-German Workshop	December, 5
26th BESSY User's Meeting	December, 6 - 7
Space Charge Effects in FELs	December, 12 - 14

Discussion at the Workshop on 'Correlative Microscopy'

Ernst-Eckhard-Koch Prize

The Ernst-Eckhard-Koch Prize is awarded annually by the Society of Friends and Sponsors of BESSY for an outstanding PhD thesis in the field of synchrotron radiation carried out at BESSY or HASYLAB. In 2007 the prize was awarded to two young researchers.

Dr. Justina Schlappa (II. Physikalisches Institut, University of Cologne) received the award for her thesis on 'Investigation of Electronic Order using Resonant Soft X-ray Diffraction'. Her thesis deals with the application of the quite novel technique of Resonant Soft X-ray Diffraction (RSXD) for the investigation of electronically ordered phases in transition metal oxides. The method was first systematically explored through application to a model system and later two real, more complex, systems were investigated: stripe phase in $La_{1.8}Sr_{0.2}NiO_4$ and orbital order in Fe_3O_4. The main focus of the work was on the spectroscopic potential of the technique.

Dr. Alexander Rack (HMI Berlin, Technical University of Berlin) was awarded the prize for his thesis on 'Untersuchung komplexer Materialsysteme mittels Synchrotron-Tomographie und 3D-Bildanalyse'. The thesis deals with synchrotron microtomography in combination with 3D image analysis to investigate microstructered, multi-component material systems. Selected applications are pore formation in metallic foams and biodegradation of ceramic particles in regenerating bone tissue.

Dr. Justina Schlappa one of the two Ernst-Eckhard-Koch awardees.

Innovation Award on Synchrotron Radiation

The Innovation Award on Synchrotron Radiation is awarded annually by the Society of Friends and Sponsors of BESSY for outstanding achievements that contributed significantly to the development of experimental methods, techniques or uses of synchrotron radiation.

Dr. Christian Brönnimann, Dr. Eric F. Eikenberry and Dr. Roland H. Horisberger from DECTRIS, PSI - Paul Scherrer Institut, received the Innovation Award for pioneering the technology of two-dimensional hybrid pixel array detectors in single photon counting mode for a range of X-ray application at synchrotron radiation facilities with unprecedented performance, notably protein crystallography with the 6 million pixel detector Pilatus 6M.

The winner of the Innovation Award: Dr. Christian Brönnimann, Dr. Eric F. Eikenbery and Dr. Roland H. Horisberger from Paul-Scherrer-Institut (left to right).

SPECIAL
NOBLE TRACES

This year's **HIGHLIGHT SPECIAL** is dedicated to two research fields - Magnetism and Surface Chemistry. One reason is, that both are hot topics for researchers using BESSY (I and II). The other reason is obvious: The Nobel Prizes for Peter Grünberg and Gerhard Ertl in 2007. Even though synchrotron radiation was not necessary for their brilliant work, both laureates have left important traces in both research fields for scientists employing synchrotron radiation. Two indispensable methods to study magnetism and surface chemistry on an atomic scale are Photoelectron Spectroscopy (PE) and Magnetic X-ray Circular Dichroism (MXCD). While researchers have continuously been pushing PE to new frontiers, MXCD only became readily available by generating circularly polarised X-rays in undulators. Let us follow the traces both laureates left. We are pleased, that we have Claus M. Schneider from the FZ Jülich and Robert Schlögl from the Fritz-Haber-Institut on board to give an idea of those 'nobel traces'.




Viewing Magnetism in a New Light

The sometimes mystified property magnetism is a fascinating phenomenon in condensed matter physics. On the one hand, it originates from the interplay of the myriad of electrons in a solid. As such, the very existence of magnetism represents a tangible manifestation of quantum physics, as it is tied to a specific quantum mechanical property of the electron, the spin. In a classical picture, the spin may be thought of as the angular momentum of an electron rotating around an axis, taking two discrete values 'spin up' (⇑) and 'spin-down' (⇓). On the other hand, magnetism plays a vital role in our everyday life. A rather mundane use in refrigerator door magnets is contrasted by highly advanced applications in information technology (magnetic data storage), electrical engineering (motors and generators) or even medicine (diagnosis and therapy).

All this has become possible by two major evolution pathways. First, during the last three decades we have developed an in-depth microscopic understanding of magnetism. In turn, this has triggered the discovery of a wealth of new effects and the development of novel magnetic materials with surprising properties. This success in magnetism was to a large extent made possible by a concomitant progress in the field of synchrotron radiation. Since the early 1980's vacuum ultraviolet and soft X-ray photons are increasingly employed in magnetism studies – a trend, which to some extent even stimulated the construction of dedicated light sources all over the world. Amongst others the scientific progress resulting from these studies helped to drive an impressive development in magnetic data storage technology (Fig. 1).

The very existence of magnetism is determined by electronic interactions, in particular, by the 'exchange' coupling. Being a many-electron effect it determines how electrons on neighbouring atoms will align their spins with respect to each other in a solid. The result depends on fine details of the atomic and electronic arrangement, resulting in a whole zoo of magnetic states. The most familiar and technologically relevant form is ferromagnetism, in which the majority of spins are oriented parallel giving rise to a macroscopic magnetization. Typical examples are Iron or Cobalt. The complement is called antiferromagnetism and describes a situation in which the spins are aligned along a given crystalline axis, but spins on neighbouring lattice sites are oriented oppositely to each other (Fig. 2). More complex spin structures such as ferrimagnetism or helical magnetism arise if the magnetic moments differ on neighbouring lattice sites or additional interactions are invoked. A long-known and famous ferrimagnet is the mineral Magnetite.

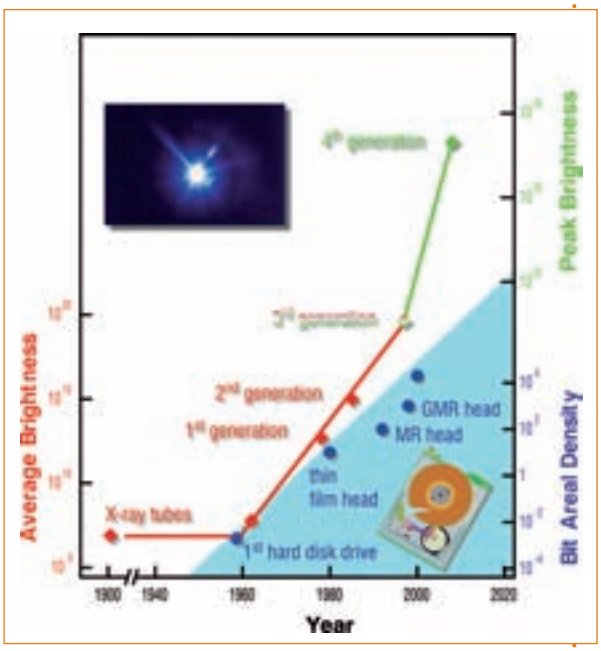

Fig. 1:
Evolution of the average (in photons/sec/mm²/mrad²/0.1% bandwidth) and peak brightness (in photons/pulse length/sec/mm²/mrad²/0.1% bandwidth) of X-rays produced in consecutive generations of synchrotron radiation sources. It is compared to the progress in storage density in hard disk drives (in megabit/inch²) marked by the market introduction of novel read head technologies. After [1].

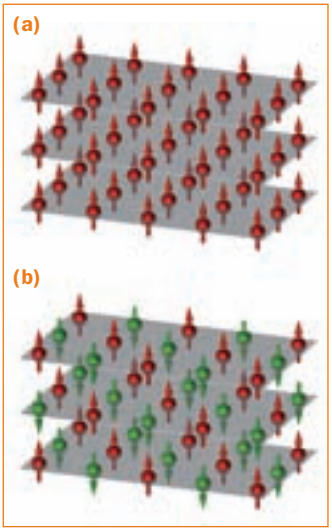

Fig. 2:
Spin arrangements corresponding to a long-range ferromagnetic (a) and antiferromagnetic order.

In order to unravel the quantum mysteries behind magnetism, we must understand its electronic origin. This is where synchrotron radiation comes into play. Already at the beginning of the 1980's it enabled pioneering experiments on magnetic systems using spin-resolved photoelectron spectroscopy [3]. Exploiting the high photon flux and tunability of synchrotron radiation this time-consuming technique allowed one for the first time to discriminate the spin-up and spin-down electronic states in ferromagnets. The breakthrough, however, which nowadays makes synchrotron radiation the most versatile probe in magnetism came with the discovery of X-ray magnetic dichroism [4, 5]. Based on circularly polarized (X-ray Magnetic Circular Dichroism) or linearly polarized light (X-ray Magnetic Linear Dichroism) these approaches have become seminal tools in spectroscopy and imaging studies of magnetic systems (Fig. 3). Whereas XMCD is a powerful probe of ferromagnets and enables a discrimination of spin and orbital contributions to the magnetic moment, XMLD is one of the few methods providing convenient access even to antiferromagnets [6]. Dedicated insertion devices in the storage ring – so called undulators – provide a fine control of the state and degree of light polarization and generate highly brilliant beams of synchrotron radiation. This results in an unparalleled sensitivity and enables experiments even on samples with only spurious magnetic response.

The second pathway of evolution in magnetism leads straight into the nanoworld. Scientific curiosity stimulates the question:

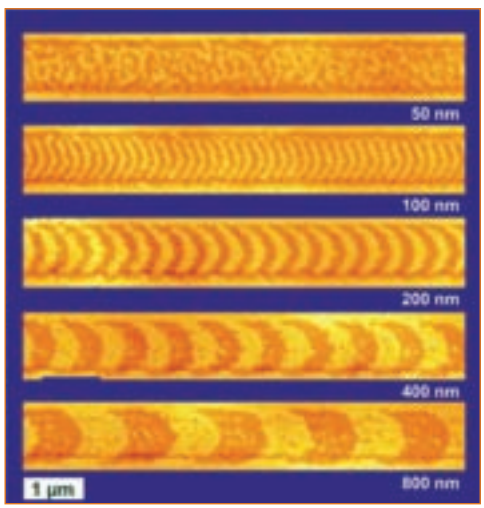

Fig. 3:
Magnetic domains of different length in a TbCoFe film imaged by X-ray transmission microscopy using XMCD at the Fe absorption edge. From [2].

How does a magnetic system behave, if it is made smaller and smaller, and which role do the boundaries play? This question applies to a wide variety of geometries, starting from thin magnetic films and surfaces and ranging from artificially created or self-organized nanostructures down to small clusters or and even individual atoms. In this course, also completely new magnetic structures with novel interactions may be created, for instance, by combining films of different magnetic or nonmagnetic elements into a sandwich or even multilayer. Magnetic multilayers form the basis for the Giant Magnetoresistance (GMR) effect, the discovery of which by the groups of Peter Grünberg (Jülich) [7] and Albert Fert (Paris) [8] was honored by the 2007 Nobel Prize in Physics. This discovery also initiated a new research field named 'spintronics', which currently drives the development in magnetism. Spintronics deals with the study and utilization of spin-transport phenomena and has already created a first high-impact application: GMR-based hard disk read heads, which revolutionized magnetic storage technology (Fig. 4). Moreover, spintronics is expected to make future key contributions to other areas in microelectronics and maybe even to quantum information technology.

The present challenges in magnetism and spintronics may be condensed in three key words: small, fast, and complex. The term small has two meanings. It refers firstly to magnetic phenomena appearing in systems with reduced dimensions, and secondly to micro- and nanomagnetic structures forming in extended samples. Examples for the latter are domain patterns, domain walls and other noncollinear spin configurations in ferromagnets (FM), antiferromagnets (AFM) or in heterosystems composed of different constituents. The last 15 years have seen the development of a number of high-resolution imaging methods based on X-ray magnetic dichroic phenomena and employing photons and electrons for imaging purposes. Photoemission microscopy in the soft X-ray regime (XPEEM) is one of these techniques, which pioneered in imaging domain structures in ferro- and antiferromagnets on an equal footing (Fig. 5). Combining element selectivity and surface-sensitivity in an ideal manner XPEEM has paved the way to understand magnetic coupling phenomena in FM/AFM thin film systems, for instance, the exchange biasing effect, which is crucial in defining a reference

magnetization direction in spintronics devices. At the same time, FM/AFM systems are also perfect examples for chemically and/or magnetically complex systems. In fact, the current studies in spintronics are addressing a wide variety of magnetic materials ranging from simple Cobalt to ternary halfmetallic alloys such as Co_2FeSi, from Silicon to diluted magnetic semiconductors such as Mn-doped GaAs, and from MgO to manganates, such as LSMO. Understanding the structural and electronic interplay of the individual chemical constituents and its role for the specific magnetic properties is an important step in making them usable for spintronics applications.

The high magnetic sensitivity of X-ray dichroism renders this approach uniquely suited for the study of very dilute systems, e.g. magnetic quantum wires or quantum dots, which are arranged on a substrate. Studying the properties of the individual wires or dots rather than their collective behaviour requires a sufficient separation between neighbouring entities, leading to a very small total amount of magnetic material to be probed. The findings on these 'nanomagnets' are spectacular and reveal a whole new world of effects, such as low-dimensional spin ordering, unexpected magnetic anisotropies, peculiar substrate-mediated coupling phenomena, or giant orbital moments, to name but a few. Magnetic molecules represent a peculiar class of low-dimensional magnets. They consist of one or several metal atom centres, which carry the magnetic moment and are surrounded by a cage of ligands. A monoatomic layer of these molecules on a substrate thus yields an extremely low density of magnetic centres. Nevertheless, the magnetic signal from these nanometric entities can be resolved giving unprecedented insight into spin-dependent molecule-substrate interactions. In Fe-porphyrines, for example, the ligands are found to promote an efficient exchange interaction between the molecules and a Ni substrate, causing the magnetic moments of the Fe centres to orient themselves parallel to the Ni magnetization direction even at room temperature (see this Highlights issue on page 8) [9].

The key word fast refers to the dynamic response of magnetic systems, among others addressing the fundamental question how fast the magnetization in a system can be reversed, i.e. switched. The magnetic switching is at the heart of applications in data storage and spintronics, which require information to be stored and read at high speed. As a natural property, the light generated in a synchrotron provides a well-defined time structure. It consists of evenly spaced light pulses of a few ten picoseconds width and is particularly suited to follow the time evolution of dynamic processes by so-called pump-and-probe experiments. The 'pumping' of a magnetic sample may involve a short magnetic field pulse (Fig. 6), a spin-polarized current or even a strong direct laser pulse. The dynamic response of the sample magnetization is probed by the soft X-ray pulse after a chosen time delay, capturing the state of the system at this moment in time, for example, in an XPEEM [10] or X-ray transmission microscope image. Repeating this pump-probe sequence in a synchronized manner is necessary to obtain a good signal-to-noise ratio. Thus, this stroboscopic approach is mainly sensitive to the reversible processes in magnetization dynamics. The time resolution attainable in these experiments is given by the width of the light pulses and may reach a few picoseconds at present. Investigating irreversible and stochastic processes requires a single-shot imaging with still shorter light pulses, which is not yet available today, mainly due to flux limitations and the lack of suitable detectors. But even today, this time-resolved approach yields important new insights into the magnetization dynamics in complex magnetic systems.

Fig. 4:
Modern miniature high-density hard disk drive with GMR read head.

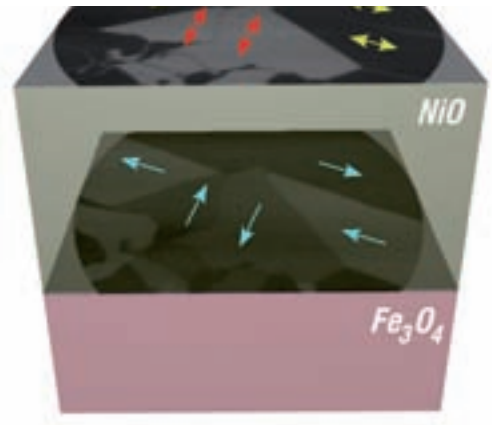

Fig. 5:
Coupled domain structures in a magnetic heterosystem consisting of a ferromagnet (Fe_3O_4) and an antiferromagnet (NiO). Arrows indicate the local magnetization (Fe_3O_4) and spin alignment axis (NiO), respectively. Images have been acquired at the Fe L_3 and Ni L_2 edges by means of photoemission microscopy.

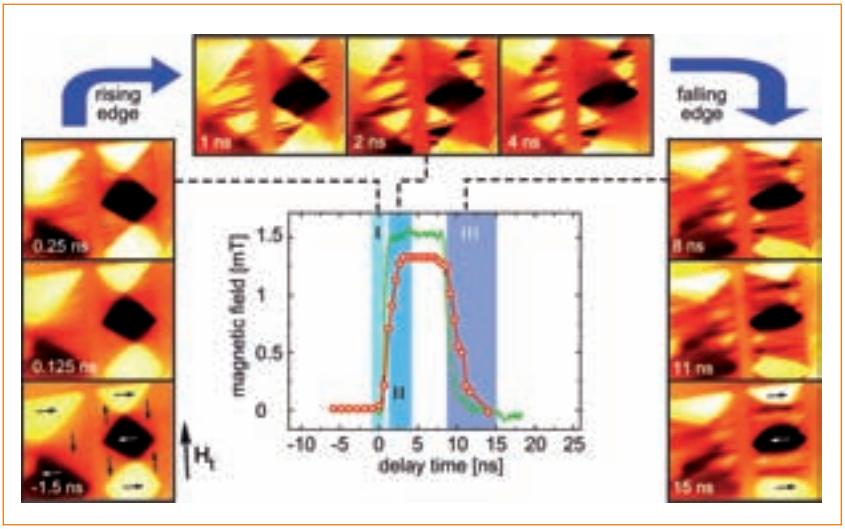

Fig. 6:
Time evolution of a magnetic domain structure in a Permalloy particle responding to a fast magnetic field pulse (centre). Dark and bright contrast in the XPEEM images is due to XMCD at the Fe L-edges and encodes the local magnetization direction (indicated by arrows). After [12].

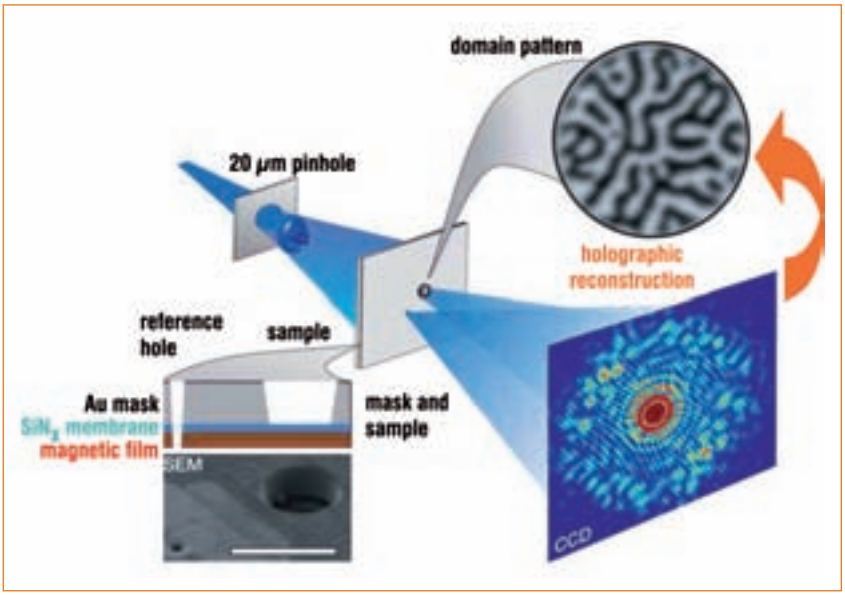

Fig. 7:
Magnetic X-ray holography from a CoPt multilayer. Interference of circularly polarized X-rays passing through the image and reference hole causes an interference pattern, which contains information about the magnetic domain structure. Fourier transforming the interference pattern yields the domain distribution. After [13].

The flux limitations of the current storage rings may soon be overcome by the 4th generation light sources – the so-called free electron lasers (FEL). Several projects are under way world-wide. An FEL generates light pulses of only 100 femtoseconds width or less and provides a several magnitudes higher peak brilliance (Fig. 1). Corresponding ultrafast pump-probe experiments will be able to address the electronic timescale in magnetism, i.e. the interplay between electronic excitations, spins and lattice, which governs the regime of spin dynamics. An example of the kind of dynamic phenomena that can be accessed with such short light pulses is the ultrafast demagnetization process, which occurs during the illumination by a strong femtosecond laser pulse. First results reveal a surprisingly fast energy transfer from the spin system to the lattice (see last years Highlight on Slicing) [11].

The light emitted from an FEL is not only very bright, but also strongly coherent. This property opens the pathway to a novel class of experiments involving optical interference phenomena. 3rd generation sources may provide photon beams of low angular divergence, which are partially coherent. Therefore, already today first steps in this direction can be made exploiting the coherence in dedicated X-ray holography experiments. Using the XMCD to obtain magnetic contrast, lensless imaging studies of magnetic domain structures have become possible and provide a complementary approach to high-resolution magnetic imaging (Fig. 7) [13].

The fields of magnetism and synchrotron radiation research have continuously cross-fertilized each other for the last 30 years. New discoveries in magnetism have become possible by novel experiments being enabled by an improved light quality. At the same time, the enormous success in magnetism investigations involving synchrotron radiation has initiated the construction of dedicated insertion devices and beamlines, providing a still better control of light polarization, coherence, and time structure. Light sources of the 4th generation will help to advance this fruitful 'symbiosis' also into the near future.

Towards the 'whole picture' of heterogenous catalysis

The 2007 Nobel Prize in Chemistry was awarded for fundamental studies of heterogeneous processes. Apparently diverse phenomena such as the generation of (nanostructured) materials and devices, corrosion, energy conversion, catalysis and batteries rest upon heterogeneous processes. Their complete understanding and quantitative description is still fragmented and can often not deal with levels of chemical complexity required in technological applications. Many important processes thus operate sub-optimal as they are based on empirical rather than on functional designs.

The concept of the Nobel laureate Gerhard Ertl was to separate the problem into a static part of material dynamics represented by single crystal terraces and steps and into a dynamic part of chemical reactivity allowing limited dynamics of adsorption, diffusion and reaction constrained by adequate temperature and low pressures. This concept was enormously successful in delivering quantitative data on thermodynamics and kinetics of elementary step reactions and triggered the evolution of surface science as well as the phenomenal development of ab-initio theory needed to rationalize and tie together experimental concepts and to describe non-observable parts of reaction sequences.

In the field of catalysis it was found that extrapolation from model studies with rigorously defined boundary conditions to chemically more complex situations was frequently not successful leading to the identification of 'science gaps'.

Work of the last decade indicates that the common origin of pressure and materials gap is the inadequacy of the separation of reaction dynamics and materials dynamics. The surface science approach describes boundary case situations in the limits of low reactivity and reduced complexity. Productive catalysts create themselves through interaction of reactants and products with the parent catalytic material establishing feedback between the geometric and electronic structure of the active phase and the chemical potential of molecular species present.

The resulting analytical challenge can only be met by studying reacting surfaces under adequate chemical potentials of reactants. The necessary in-situ techniques investigate surfaces for electronic and chemical structure under the working conditions of a catalytic process. Only few techniques like XPS and Auger-XAS meet the simultaneous requirements of surface sensitivity, chemical states selectivity and applicability to many chemical elements. Both techniques as photon-in-electron-out techniques are inherently incompatible with elevated pressures. Synchrotron radiation is an indispensable element in any strategy trying to overcome this barrier in the fields of catalysis, corrosion and battery development. Tuneable high intensity soft X-ray sources combined with suitable electron transfer optical instrumentation allow now to approximate in-situ surface analysis [14] to conditions where the full chemical dynamics of heterogeneous processes are unfolded and no more qualitative extrapolations need to be made about the state of the active phase.

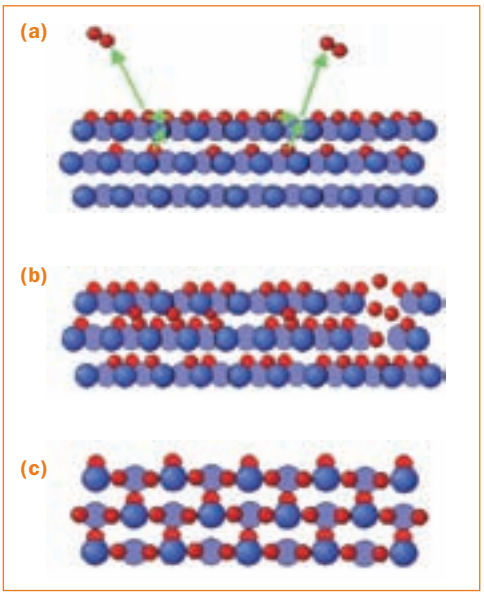

Fig. 8:
Schematic representation of the sequence of events during oxidation of Ru at gradually increasing chemical potentials. Step (a): adsorbate and sub-surface dissolution in equilibrium with oxygen recombinative desorption; Ru in metallic state. (b): defect formation in the metal into a disordered surface oxide (TSO); multiple metal-oxygen coordination but still metallic electron system. (c): stoichiometric an ordered RuO_2 crystallization; oxidic electron system and excess oxygen dissolved in bulk. The surface science experimental range ends between states (a) and (b).

The example addresses the reactivity of the element Ru in catalytic oxidation processes using CO and methanol as substrates. The target reactions are:

$2\ CO + O_2 \quad \text{---> } \quad 2CO_2$

'CO oxidation'

$2\ CH_3OH + O_2 \quad \text{---> } \quad 2\ CH_2O + 2\ H_2O$

'Selective methanol oxidation'

The CO oxidation reaction is well reviewed from the experimental [15] and theoretical [16,17] viewpoints. The active phase on single crystalline and on supported nanostructured Ru is a thin oxide film with a structure assumed to be RuO_2 [18,19].

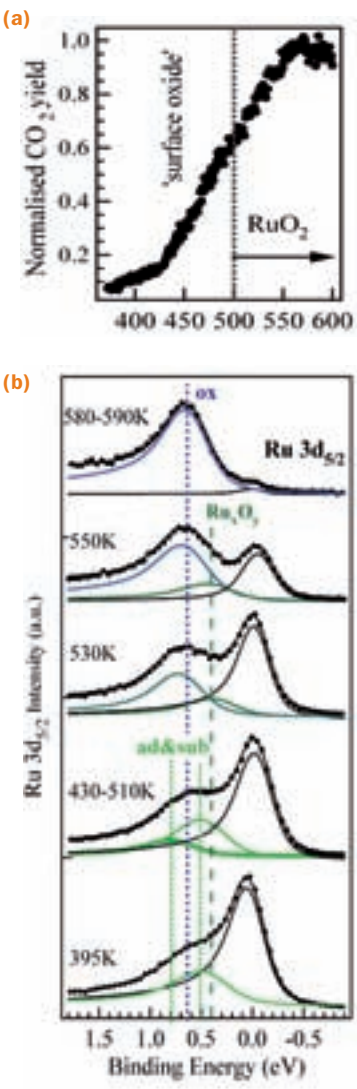

Fig. 9:
In situ oxidation of CO (stoichiometric feed mixture at 0.1 mbar pressure): (a) catalytic activity as function of temperature; the phase change was identified from combined Ru3d and O1s spectra. (b) typical Ru 3d spectra with a relative binding energy shift scale referenced to bulk metal at 280.1 eV. For state assignments see text.

Within the surface science conditions there is also a rich sub-surface chemistry of bulk dissolved and in-surface embedded oxygen species [20, 21].

This system was studied with high pressure XPS [21-23] in parallel to imaging photoemission microscopy that provides information about the lateral distribution of species. The fact that the experiments were carried out under 0.1 mBar reactant pressure without the need to transfer to a separate analysis chamber makes possible an accurate analysis of the different states, irrespective of their stable or metastable nature. Transfer of metastable species will lead to phase segregation and is seen as a major source of controversy in the literature.

In-situ photoemission allowed determination of binding energies of all relevant species with respect to the Fermi edge with a resolution of 0.05 eV. Good agreement with theoretical calculations of chemical shifts was obtained [24] as apparent from the original literature [22]. The sequence of events is sketched in Figure 8 [21-23].

The metal converts from an initial adsorbate state with increasing oxygen chemical potential into a surface oxide and a sub-surface dissolved oxygen species. The surface oxide grows in a thicker precursor layer being defective at low growth temperatures but forming with increasing temperature a thinner oxide film and additional sub-surface oxygen. At oxygen potentials allowing bulk equilibration, stoichiometric RuO_2 dominates the surface. The sensitivity of the Ru $3d_{5/2}$ core level is high enough to resolve [22, 23] shifts between Ru atoms in the top layer and in deeper layers.

Figure 9 summarizes the key results of the CO oxidation study. The evolution of the Ru $3d_{5/2}$ core level shows that the sequence of events is more complex than only formation of RuO_2 as assumed earlier [15] and that the transient surface oxide Ru_xO_y appears as intermediate. It becomes apparent when the state transformations are compared to the catalytic conversion curve (panel (a)) that the catalytic activity is insensitive to the phase transformation. This result is in agreement with theoretical predictions [17]. The adsorbate state of the system prevailing at low temperatures is weakly active. The maximum activity occurs when the surface energies of metal and oxide phases are comparable as occurring between 450 K and below 600 K. Only at temperatures above 600 K a stoichiometric RuO_2 layer (frequently assigned as the active phase) is produced with its formation coinciding with the deactivation of the catalyst. These observations are also in agreement with the atmospheric pressure data obtained on Ru nanoparticles [18, 19], which predict that a metastable thin film of oxidic nature should be most active rather than pure metal or RuO_2.

The results of the CO oxidation reaction indicate that the methanol oxidation reaction may show a complementary behaviour in structure-function relationship as methanol oxidation requires strongly bound basic oxygen as the active species. As this state is intermediate between oxide and metal, experiments were conducted starting from either the metal or oxide states of the same bulk-saturated Ru (0001) single crystal. The key results are collected in Figure 10.

The panels (a) and (b) exemplify the feedback coupling between the surface state of the active catalyst and the gas phase chemical potential of oxygen. Irrespective of the initial state being either bulk metal (a) or oxide (b) the final active material is the same as the oxygen chemical potential is the same. This can be concluded from the identical product yield curves seen in panel 3(c). The most active state is the transient surface oxide with a very similar spectral signature as the deactivated state for CO oxidation shown in Figure 9 (b). This inverse correspondence is explained by the different requirement of oxygen reactivity for CO oxidation (a weakly bound electrophilic species) and for methanol dehydrogenation (a strongly bound basic species in addition to an oxidizing weakly bound species for water formation). From the metallic initial state (panel 3a) it is more difficult to arrive at the transient oxide as first the perfect surface of the single crystal needs to become disordered by the action of subsurface oxygen (transition from states (a) to (b) in Figure 8). At low temperatures the

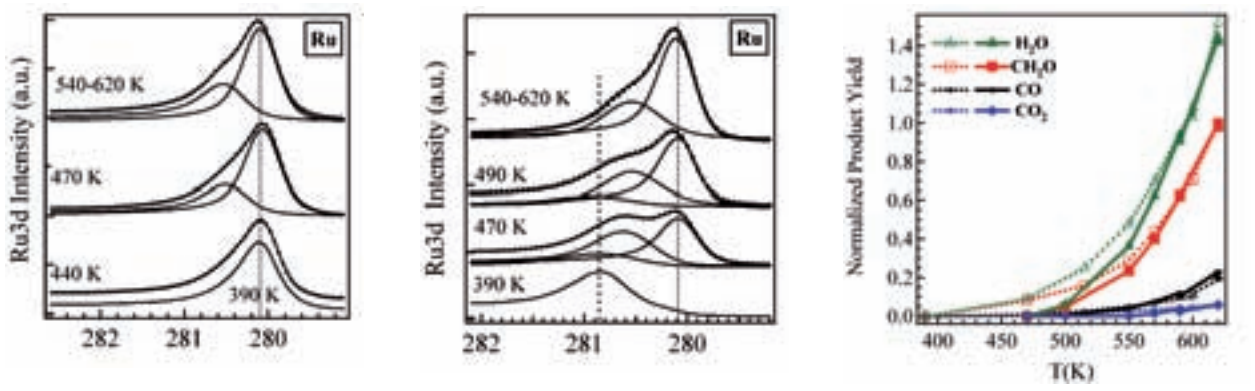

more active oxidic state begins working from defect sites and requires no structural transformation prior to action.

Synchrotron-radiation-based in situ analysis of catalytic processes allowed to directly identifying the active states. They are novel in nature being metastable with respect to metal and bulk oxide and form through stoichiometric action of activated oxygen upon a metallic precursor or through reaction of the carbon components with an oxidic precursor. The high spectral resolution of XPS data allowed further identifying the nature of the active oxygen as being different for electrophilic CO oxidation and nucleophilic methanol dehydrogenation. The ambiguities of low-pressure experiments were overcome in which static catalyst surfaces are studied followed by extrapolations into the regime of the dynamical catalyst.

The example illustrates that we are now in a position to analyze heterogeneous processes without having to omit critical aspects of the dynamics of the system. The new results are, however, only useful for understanding such processes if they are combined with elementary step reaction data from the surface science approach. The in-situ analysis is the experimental tool responding to the need of explicitly considering the material dynamics rather than having to extrapolate over qualitative changes of the active interface. The limited capacity of experimental infrastructure unfortunately precludes the fast and broad breakthrough of this technique. The as yet very rare additional application of X-ray microscopy and free electron laser studies will greatly expand the possibilities of synchrotron-radiation-based studies of heterogeneous processes. It is predicted that breakthroughs in the understanding of heterogeneous processes will occur in the near future using.

Fig. 10:
Selective oxidation of methanol over Ru metal (a) and RuO2 (b). Ru(0001) surfaces were first fully oxidized and then subjected to a MeOH – oxygen mixture. After this saturation of bulk-dissolved states the substrates were fully reduced by sputtering and annealing to the pure metallic state and subject to the same reaction mixture. The conditions were: total pressure: $2.4.10^{-4}$ mbar, P_{CH3OH}/P_{02} ratio = 1.5. Panel (c) reports the catalytic activities leading in both experiments to the same high-temperature activity for oxidative dehydrogenation (ODH) to formaldehyde and water. Full lines refer to experiment (a), dashed lines to experiment (b). The low activities for combustion and reforming (CO_2 and CO traces) indicate the presence of poorly active bulk oxide and metal at high temperatures.

References:

[1] J. Stöhr and H. C. Siegmann, Magnetism: From Fundamentals to Nanoscale Dynamics, (Springer-Verlag, Berlin, 2006).
[2] N. Takagi et al., Jpn. J. Appl. Phys., **40**, L380 (2001).
[3] R. Clauberg et al., Phys. Rev. Lett., **47**, 1314 (1981).
[4] G. van der Laan et al., Phys. Rev. B, **34**, 6529 (1986).
[5] G. Schütz et al., Phys. Rev. Lett., **58**, 737 (1987).
[6] F. Nolting et al., Nature, **405**, 767 (2000).
[7] G. Binasch et al., Phys. Rev. B, **39**, 4828 (1989).
[8] M. N. Baibich et al., Phys. Rev. Lett., **61** (1988) 2472.
[9] H. Wende et al., Nature Mat. **6**, 516 (2007).
[10] S.-B. Choe et al., Science, **304**, 420 (2004).
[11] C. Stamm et al., Nature Mat. **6**, 740-743 (2007)
[12] C. M. Schneider et al., Appl. Phys. Lett., **85**, 2562 (2004).
[13] S. Eisebitt et al., Nature, **432**, 885 (2004).
[14] M. Salmeron, R. Schlögl, Surface Science Reports 2008.
[15] H. Over et al., Science, 287, 1474-1476 (2000).
[16] K. Reuter, M. Scheffler, Phys. Rev. B, 68 (2003).
[17] K. Reuter, M. Scheffler, Phys. Rev. Lett., 90 (2003).
[18] H. Over, M. Muhler, Progress in Surface Science, 72, 3-17 (2003).
[19] J. Assmann et al., J. Phys. Chem. B, 108, 14634-14642 (2004).
[20] A. Böttcher et al., J. Chem. Phys., 112, 4779-4787 (2000).
[21] G. Rotaris et al., Surf. Sci., 359, 1-9 (1996).
[22] R. Blume et al., J. Catal., 239, 354-361 (2006).
[23] R. Blume et al., J. Phys. Chem. B, 109, 14052-14058 (2005).
[24] S. Lizzit et al., Phys. Rev. B, 6320 (2001).

Contact:
Claus M. Schneider
c.m.schneider@fz-juelich.de
Robert Schögl
acsek@fhi-berlin.mpg.de

NOBLE TRACES

FACILITY REPORT

Machine operation

In 2007, the accelerator complex consisting of the 50 MeV pre-injector microtron, the full energy booster synchrotron, and the storage ring operated reliable with one major exception: The failure of the storage ring septum magnet, which caused a three weeks loss of user beam time.

During a short shut-down in February, the storage ring was equipped with a new dipole chamber next to the UE112 insertion device, and the high temperature current feed-through of the PSF-WLS was repaired. The UE112 suffered from magnetic dust trapped in the vacuum chamber and no cure was found for that problem. Sudden strong lifetime reductions and particle losses required an exchange of the chamber, which took place in the long fall shut down. The new chamber is equipped with flat wires on the top and the bottom (Fig. 1). Carefully designed current distributions have been used successfully to compensate for some of the intrinsic field perturbations of the UE112 in the anti-parallel mode.

The main task of the fall shut down was the significant modification of the fs-slicing facility (Fig. 2). This project already started about two years ago with the ambition to provide an optimised path for the fs-laser to propagate through the modulator U139. It turned out that a large variety of crafts had to be incorporated, since the new laser beam path required significant changes to radiation safety measures, building services and cable work. Besides the adjacent beamline with its five new mirror chambers, we had to install new vacuum chambers for dipole and quadrupole magnets and the characterisation tools.

Water pipes had to be relocated, the 6.7° front end of the segment had to be removed, a hole for the beamline feedthrough had to be drilled into the slab of the storage ring tunnel, and quadrupole and sextupole magnets had to be opened before the new fs-slicing line could be installed inside the storage ring tunnel. A team of about ten people was busy inside and outside the tunnel. They pushed very hard to get work finished in time. Their job was really tedious (Fig. 3), but eventually, on late afternoon of the last day of the shut down, the beamline could be pumped down for recommissioning of the storage ring.

Instrumental improvements

The last year saw major improvements of the microtron, the synchrotron, and the transfer line mostly in connection with the planned top-up operation of the facility. The gun pulse is more intense and flat, and the synchrotron now operates at a higher horizontal tune in order to reduce the natural emittance of the beam injected into the storage ring. These improvements resulted in an increase of the accelerated charge. In addition, the fine-tuning of the quadrupoles and the RF-parameters leads to a complete deceleration of the beam in the synchrotron, if it is not extracted for injection. As a result, the radiation dose was noticeably reduced. The dynamical steering during the acceleration in the synchrotron allows a better extraction of the beam, and the resulting smaller vertical cross section of the beam in the transfer line increases the injection efficiency into the storage ring. Over the last years, the diagnostics in the transfer line was considerably modified. During the last shut-down, a set of stripline monitors was installed just in front of the septum magnets of the storage ring. It is now possible to measure the intensity as well as the position of the injected beam. The signals are acquired by a Tektronix oscilloscope, and the operating system of the scope has been used to directly analyze the data and transfer the extracted information to the EPICS control system. With the improved diagnostics, injection efficiency above 90% was achieved – one prerequisite for top-up operation.

Fig. 1:
New vacuum chamber for the UE112 equipped with flat wires along the chamber.

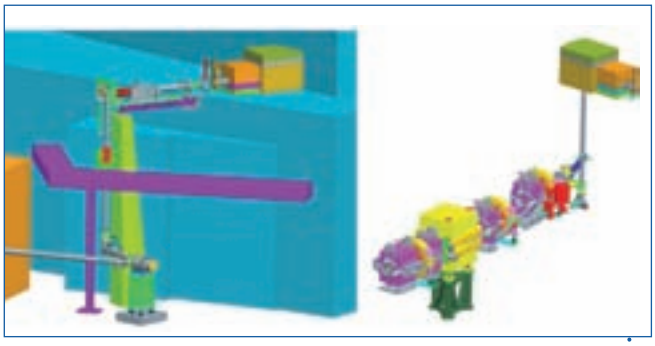

Fig. 2:
CAD-sketch of the new fs-slicing laser line. Left: outside the SR-tunnel; right: inside the tunnel.

Operational improvements

Routinely, injections take place every 8 hours. After the injections, the white-circuits of the synchrotron are switched to a standby mode. This reduces orbit and photon perturbations at 10 Hz and improves the quality of the beam delivered to the users.

The procedure for adjusting the horizontal orbit bump for the fs-slicing set up was finally settled. All details are cast in a single piece of software any operator can use easily. The injection procedure was dramatically relaxed by introducing a new type of RF-knock out technique for creating the desired fill structure with a hybrid single bunch in the middle of the 100 ns-long dark gap. The RF-clearing leaves the single bunch untouched and is capable of populating just one bucket. In the single bunch mode of operation this has led to a very high single bunch purity. In the normal mode of operation, the desired purity exceeds 1/1,000 routinely without permanent fine tuning of the gun timing. The RF-clearing technique was developed by Spring8, the ESRF, and the ALS in order to guarantee good single bunch purity also in future top-up mode.

Fig. 3:
The work inside the tunnel was really tedious.

Beamline developments

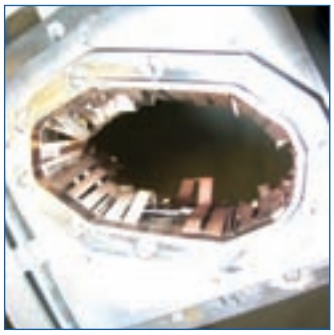

Fig. 4:
The broken beam dump.

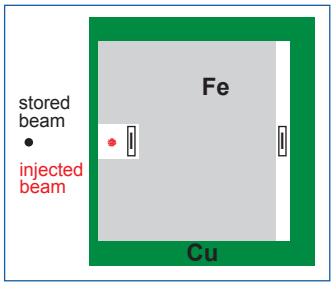

Fig. 5:
Cross section of the septum magnet.

Failures

The facility operated without dramatic or time consuming failures over the last ten years. However, last year two components created problems. The destroyed beam dump (Fig. 4) caused no noticeable delay for the users, because it happened just after the shut down during the re-commissioning. But when the septum magnet broke during the user beamtime on the 13th of October, we lost three weeks of user beamtime.

The septum magnet is a dipole, which bends the beam injected into the storage ring by 7° to become parallel to the already circulating beam. The stored beam is only a couple of mm away from the injected beam and should ideally not 'see' any perturbation at all from the septum. This field separation can be achieved by using a pulsed magnet with an eddy current sheet as shown in a cross section in Fig. 5. The pulsed current in the form of a back leg winding creates the desired bending field inside the laminated C-shaped iron core. Due to the induced eddy currents in the copper shield the fields outside the gap are suppressed. Nevertheless, the slowly decaying eddy currents produce a rather long lasting horizontal orbit distortion on the stored beam. This is incompatible with top-up operation and would have required modifications of the old septum in any case.

In October, a short circuit developed between the three circular wires in the slot and the iron core, which is at ground level. Due to the strong magnetic forces the wires were attracted to each other and the ceramic spacers moved in the longitudinal direction. After almost 10 years of trouble-free operation this septum suddenly gave up. Since no spare parts were available, we carefully moved the wires back in place and reassembled the septum (Fig. 6, 7). After the repair, a bake out over one week was required to get the rather complicated magnet back into ultra high vacuum. In total, it took a little more than two weeks and the septum was operational again.

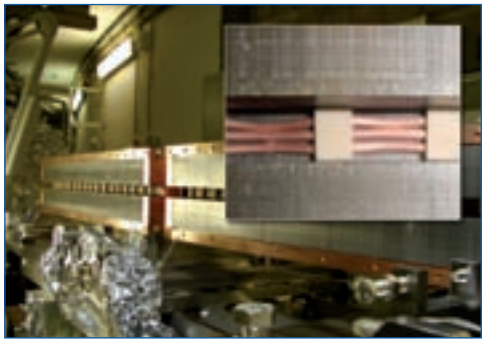

Fig 6:
The two dismantled injection septum magnets. The copper shields in the direction of the circulating stored beam have been removed. The insert shows the damaged coil inside the gap.

The modifications of the fs-slicing facility were not restricted on installing a new laser beam path. Since the photon flux available for the fs-slicing experiments is rather low, the development also concentrated on new or improved detection schemes. These efforts resulted in the fabrication of a new avalanche photo diode array, allowing parallel detection of a spectrum across the array. This new development has been tested successfully and will further improve the experimental conditions at the fs-slicing facility.

Earlier in 2007, the official inauguration of the ISISS collaboration was celebrated. ISISS is the acronym for 'Innovative Station for In-Situ Spectroscopy', an experimental station of Robert Schlögl's group at the Fritz-Haber-Institut in Berlin, dedicated to catalysis studies under ambient conditions. The beamline had already been commissioned in late 2006. In 2007, the first experiments were carried out with the new equipment. As for all other cooperating research groups, a part of the beamtime is allocated for common users. In this respect, an impressive result was obtained by investigating Cs_2Te, the cathode material for next generation free electron laser sources. Cs_2Te is known for its high quantum efficiency, but it is also known to have a poor life time between a few hours and a few days. The investigations revealed that the degradation is caused by fluorine atoms, coming from parts made of Teflon inside the cathode holder.

One month later, the commissioning of the new U41-SGM could be completed. This monochromator replaced the old plane grating monochromator, constructed by the X-ray microscopy group of the University of Göttingen for the use at the U41 X-ray microscopes. The new U41-SGM was the first beamline that could mainly be built from stock, with only a few components that had to be purchased for this project. Hence, the optics group needed only a few months to finish the construction and to achieve the desired performance regarding energy resolution, photon flux and spot size. The beamline is equipped with capillary optics, generating a hollow cone illumination for transmission microscopy experiments.

Two more X-ray microscopes will be installed at the UE46. This beamline will be equipped with another plane grating monochromator. The two branches are optimised for delivering coherent synchrotron radiation to the zone plates of the microscopes. One branch

will be used by a scanning transmission device, developed and operated by a group of the Max-Planck-Institute for Solid State Research in Stuttgart. For the second branch, a transmission microscope is planned, which will be operated by the BESSY X-ray microscopy group.

Associated with the preparation of the construction of the UE46 plane grating monochromator, we achieved another remarkable result: the best plane mirror ever delivered for the instruments at BESSY. Over a length of 310 mm, with an optical active area of 290 mm x 30 mm, a residual slope error of 0.025 arcsec was measured (Fig. 8). The extraordinary good result was obtained by combining the ultra high precision measurements at the metrology laboratory of the BESSY optics group with an ion beam polishing procedure, carried out at the IOM in Leipzig. The ion beam polishing is based on the height profile determined in the BESSY lab. The future challenge is now to extend the performance to the determination of sagittal radii between 2,000 mm and 50 mm, which will be required for the optical elements of microscopy applications at BESSY and for mirrors in FEL-beamlines, which demand a length up to 1,000 mm with a residual slope of about 0.01 arcsec!

At the UE52-PGM, the CRG operating the beamline and an experimental station for photoemission and near edge absorption spectroscopy, now also offers dispersive NEXAFS as an option. The reconstruction was required to be able to focus the dispersed light on the sample surface. The work was carried out during the shut-down period, and the subsequent commissioning could be successfully finished by the end of the shut-down. The area on the sample surface illuminated in this mode of operation has a height of about 7 mm. For a c_{ff}-value of 2.25, this leads to a dispersion of about 3.2 eV for the carbon K-edge (the full width at half maximum of the ID harmonic is about 3.8 eV in this case). Larger (smaller) dispersion can be obtained by operating the monochromator at lower (higher) c_{ff}-values. In combination with the Gammadata Scienta R4000 electron energy analyser, which offers both, position and energy sensitivity, intensity maps of photon and binding energy can be easily recorded in short time. Thus, changes on short time scales may be monitored with full spectroscopic information.

In addition, the monochromator is equipped with a second mirror that focuses the monochromatic synchrotron radiation in the common way on the exit slit. This allows for using the beamline for standard applications, which is of importance for a second experimental station that will be permanently installed at the UE52-PGM. GAMBIT, an acronym for 'Generalized Absorption of Magnetic moments at BESSY by Ion Trapping', is a project of a research team from the University of Kaiserslautern, the Technical University Hamburg and BESSY. In this experiment, XMCD and NEXAFS will be applied to investigate spin and orbital magnetic moments, and to derive electronic and geometrical structure information. The clusters will be stored in a penning-trap, which requires a 7T magnet to be installed subsequent to the dispersive NEXAFS experiment (Fig. 9).

Fig. 7:
Repair work of the septum magnets.

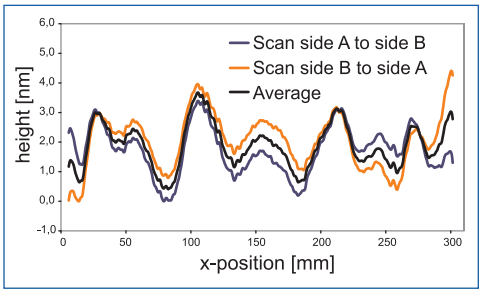

Fig. 8:
Profile of the residual height of a plane mirror for the UE46 PGM. The wiggles at an x-position of about 100 mm may be due to an instability during ion beam polishing.

Fig. 9:
CAD-sketch of the GAMBIT station at the UE52-PGM.

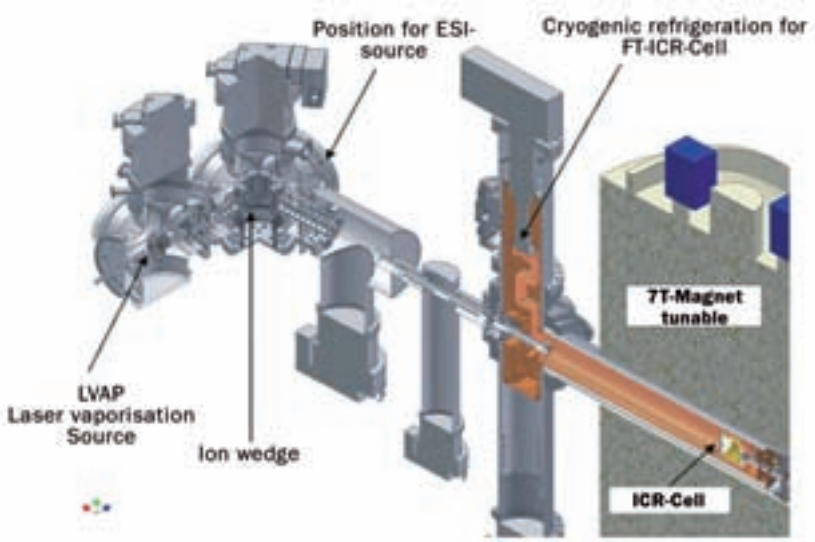

Developments for STARS – the FEL Project

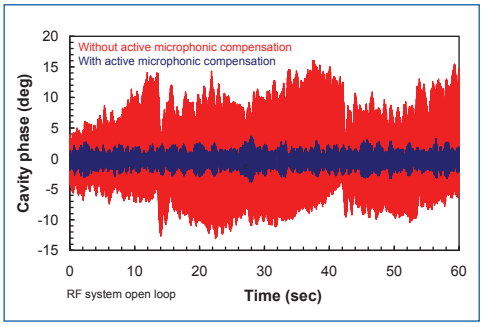

Fig. 10:
Mechanical lever system (tuner) mounted at the end of a TESLA cavity. This unit changes the cavity's frequency by stretching it via the lever arms. Two piezo elements are included for fast tuning capabilities. For the first time, such fast tuners have been used to actively reduce the detuning due to microphonics (mechanical noise) in a cavity.

Microphonics in CW TESLA cavities

Jitter-free FEL radiation (in time, energy and spectrum) is critical for the effective exploitation of future FELs. This requirement is one of the primary reasons the HGHG technique has been adopted for the BESSY FEL. However, for this technique to work effectively, the electron bunches must arrive with less than 70 fs time jitter at the undulators. This can only be guaranteed if the superconducting TESLA cavities achieve a phase stability better than 0.02 deg. A dominant source of noise in the cavities are mechanical oscillations caused by microphonics – even a cavity deformation on the nm scale is disruptive. Hence, schemes to actively compensate this mechanical noise by fast-acting piezo tuners have been investigated in the framework of the EuroFEL collaboration. A thorough understanding of the expected noise characteristics (spectrum) and the electro-mechanical properties of the cavity-tuner combination ('transfer function') has been gained by testing the system under cryogenic conditions in the HoBiCaT test facility at BESSY. Results demonstrated that only a few resonances contribute heavily. An 'intelligent' Piezo controller, that takes into account the transfer function, was then developed. For the first time, such a system has demonstrated the active reduction of microphonic phase noise, achieving an improvement of more than a factor of six (Fig. 10). The future implementation of an additional RF feedback system should thus be able to reduce the residual phase error of 1 deg to better than the required 0.02 deg phase stability.

Fig. 11:
BESSY's undulator at the HGHG-FEL on track to its final position at test facility at MaxLab.

HGHG test facility at MaxLab

Parallel to the development of new and the upgrade of existing insertion devices, the BESSY insertion device group has been actively participating in the construction of a single-stage HGHG-FEL test facility at MaxLab within the framework of the EuroFEL collaboration. These activities represent a first step towards realising the HGHG scheme for the BESSY FEL. In particular, BESSY's responsibilities included the undulators (Fig. 11) and the bunching chicane. The two magnet girders of the former UE56-1 double undulator, were integrated into a new support and drive system, which meets the geometrical constraints at MaxLab (beam height only 520 mm). This new device will now act as the FEL radiator. A 48-mm period planar magnetic structure loaned from the ESRF was installed into a similar support structure and will serve as the modulator.

Commissioning of the HGHG FEL began at the end of November 2007 with a thermionic gun, and the electron beam has been propagated all the way to the dump. More recent tests have commissioned an RF photoinjector, which will be used for the actual HGHG tests.

Superconducting gun at FZD

On November 12th 2007, a new superconducting electron gun was put into operation at the Forschungszentrum Dresden-Rossendorf. This project is a collaboration between BESSY, DESY, FZD and the MBI, and is supported by the BMBF. In the photoinjector a UV laser illuminates a cathode, which emits electrons. The photocathode is inserted into the backplane of a superconducting niobium RF cavity designed to operate at 50–60 MV/m peak field to rapidly accelerate the electrons, thereby forming a very-low-emittance electron beam. Since the power dissipation in the cavity is only a few watts, it can be run continuously (CW mode), rather than in the pulsed mode employed by present-day normal-conducting RF injectors. Such an injector thus represents a key component of the BESSY FEL and other next-generation light sources planned for CW operation.

BESSY personnel developed and installed the entire diagnostics and driver software to characterize the electron beam, when it exits the superconducting gun. In particular, knowledge of its bunch profile (both longitudinal and transversal) is critical for the efficient operation of a future FEL. The beamline, as shown in Fig. 12, consists of screens, slits and Cherenkov radiators, which can be moved into the electron beam, current monitors and an electron spectrometer.

Fig. 12:
Diagnostic beamline developed and installed by BESSY for the superconducting photoinjector at FZD. The RF cavity's cryomodule ends at the lower left corner of the picture.

Contact:
Jens Knobloch
knobloch@bessy.de

The Metrology Light Source is in operation!

The year 2007 was packed with milestones on the way towards the scheduled operation of the Metrology Light Source (MLS), the 600 MeV electron storage ring of the Physikalisch-Technische Bundesanstalt (PTB), dedicated to metrological and technological applications from the far-infrared to the extreme UV.

The set-up of the storage ring with its 100 MeV microtron injection system was finished as scheduled in February 2007. Soon after receipt of the preliminary operation permit, commissioning started in April 2007, and already one day later, the first beam circulated in the MLS. On **June 5th, the first beam was stored** and first synchrotron radiation was observed at the injection energy of 105 MeV. On August 14th, the first beam was ramped to 600 MeV. Thereafter, the commissioning rapidly proceeded, and by now an electron beam current of more than 100 mA at maximum energy with a life time above 4 hours is routinely reached (Fig. 13). Very important for the steady progress was the continuous, automated beam scrubbing during the night for conditioning the storage ring vacuum.

For the use of the MLS as a primary source standard for calculable synchrotron radiation, it is crucial to measure all storage ring parameters with high accuracy. The instrumentation for the measurement of the electron beam energy by Compton backscattering of CO_2/CO - laser photons was put into operation, and the electron beam energy was measured for the operation of the MLS at various energy values from 240 MeV up to 628 MeV (Fig. 14). The instrumentation for the controlled setting and measurement of the electron beam current over more than eleven decades is also operational. The electron beam current was purposefully reduced from the mA range down into the pA range. One circulating electron is equivalent to an electron beam current of 1 pA. So the loss of single electrons can be monitored (Fig. 15).

Also the set-up of the beamlines and experimental stations made considerable progress. The white light beamline for the use of calculable radiation was completed, and first measurements of the vertical photon distribution at different wavelengths were performed and a good agreement with theory was found.

The beamline for IR bending magnet radiation was also completed and saw the first light, including coherent synchrotron radiation in the far-infrared. Coherent synchrotron edge radiation was also observed from the fringing fields of the bending magnets adjacent to the undulator straight section.

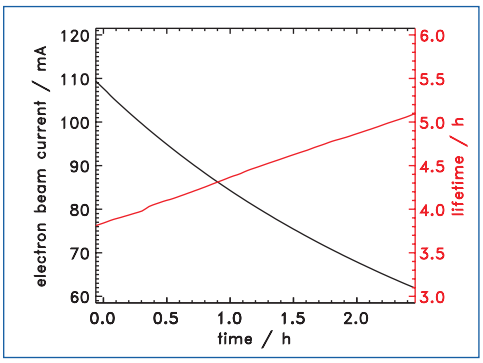

Fig. 13:
Typical electron beam current (black) and lifetime (red) as a function of time for operation at 600 MeV.

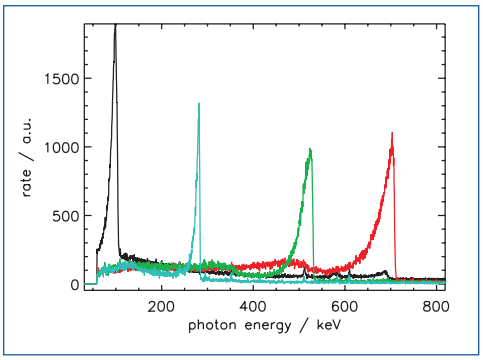

Fig.14:
Spectrum of backscattered CO_2/CO – laser photons for the MLS operated at electron beam energies of 240 MeV, 400 MeV, 550 MeV and 628 MeV (left to right).

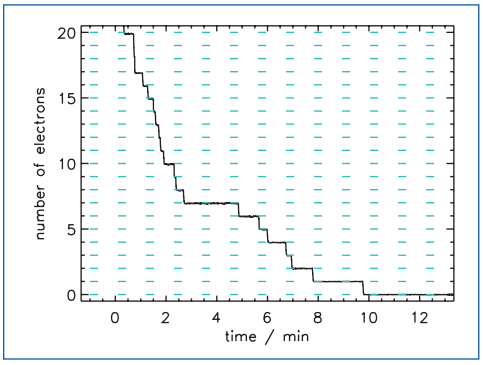

Fig. 15:
The number of electrons stored in the MLS is determined by the detection of the emitted synchrotron radiation by means of a photodiode cooled to LN_2 temperature. The single electrons have been intentionally kicked out by means of a scrapper.

Contact:
Roman Klein
Roman.M.Klein@ptb.de

Mimicking nature: Bionic activities at the Application Centre for Microtechnology (AZM)

Fig. 16:
Ultra-hydrophobic surface with water droplets.

The question concerning water repellent or **hydrophobic surfaces** is 'Why do we even care about things like this and why has this field evoked so much research and development attention in the last few years?' The answer for this is quite simple. First of all, there are many interesting effects related to such surfaces like water and oil repellency, anti-sticking, anti-fogging and anti-contamination or, as sum of all, self cleaning properties. The second reason is that nature has proven and used such surfaces for several million years now, by creating more than 200 plant and several insect species that show this particular behaviour.

The secret behind ultra-hydrophobic behaviour are rough structures. Rough in this spirit means feature sizes in the range of a few micro- and nanometers, which permit water to rest on top of the structures. The rough structures also prevent water from penetrating the spaces between them. Therefore, air is trapped under the water drops and the physical contact between drop, and surface is drastically reduced (Fig. 16).

As a part of the worldwide bionic research interests to copy natures' structures and create commercial products and applications, BESSY AZM developed a new procedure for the creation of ultra-hydrophobic surfaces based on lithographic processes. This new kind of lithographic procedure is based on the exposure of a photo sensitive polymer to UV light through a mask and a transparent substrate, which creates a several hundred micrometer proximity gap between the resist and the mask (Fig. 17). The result of these exposure conditions are the creation of diffraction and interference images, which gives the resist a special form. The high accuracy and perpendicular sidewalls known from standard lithographic procedures vanish and plant-like, naturally formed posts and structures can be generated (Fig. 18). Additionally, the photochemical behaviour of the polymer leads to the creation of nanoporous surfaces, which increase the hydrophobic behaviour even more.

Using this technique we were able to create structures, where water drops form contact angels between the water and the surface of more than 165° (Fig. 16). This value is even higher than that reported for the famous Lotus leaves.

Fig. 17:
Schematical process flow of the back side exposure.

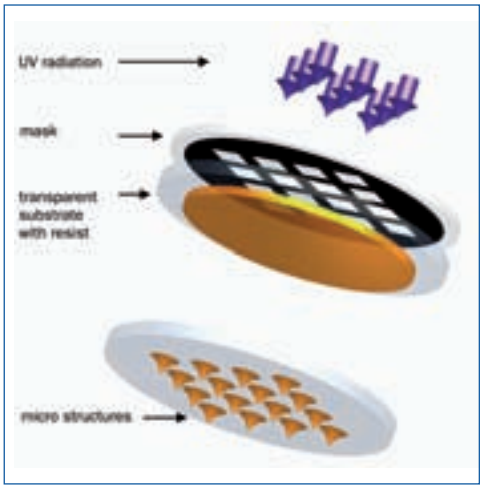

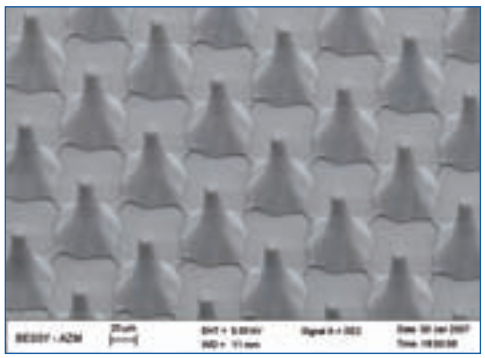

Fig. 18:
Details of lithographically created hydrophobic surfaces.

Contact:
Olaf Mertsch
olaf.mertsch@bessy.de

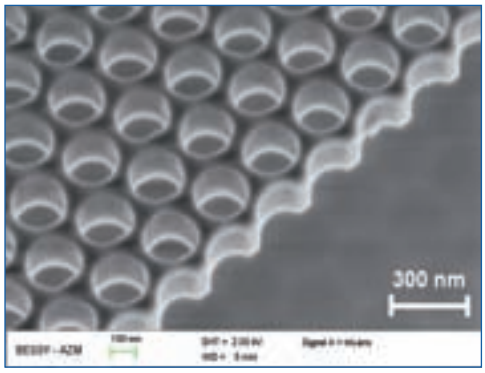

Fig. 19:
Scanning electron microscope of a fabricated silicon nitride photonic crystal sample showing a free standing Si_3N_4 photonic crystal membrane with hexagonal lattice of air holes with the lattice period of *a* = 270 nm and average hole radius of *r* = 90 nm. The thickness of the membrane is only *t* = 200 nm.

Another project is inspired by the nature of some butterfly wings or peacock feathers. Here **photonic crystals** are responsible for a blue iridescence. As one of only few groups worldwide, AZM succeeded in creating artificial photonic band gap materials (photonic crystals) for the visible wavelength range.

Due to their internal nanostructure, these artificial optical materials exhibit similar properties for photons as do the semiconductors for electrons, thus clearly illustrating their potential for the creation of extreme high density and high performance optical circuits. Furthermore, photonic crystals allow to strongly localize and confine light, resulting in large light-matter interaction. In order to obtain these properties we need fabrication techniques to pattern structures on a nanometer scale, since the material must exhibit a periodical internal arrangement on roughly half the scale of the operational wavelength.

We investigated two dimensional photonic crystals. These consist of thin membranes of silicon nitride, which are perforated with regular arrays of holes. In order to exhibit the photonic band gap properties, the thickness of the membranes must remain below 300 nm, while the holes need to be closely packed and as small as 150 nm in diameter (Fig. 19). The entire fabrication procedure developed in the AZM takes place in our lab and allows creating features as small as 25 nm.

Investigating various types of hole arrangements, we could experimentally show photonic band gaps in the visible range for the square and the triangular arrangement of holes. We further showed that by slightly changing the geometry of the holes, such as by changing the lattice constant of the radius of the holes, the position of the band gaps can be adjusted to the value required by the potential application (Fig. 20).

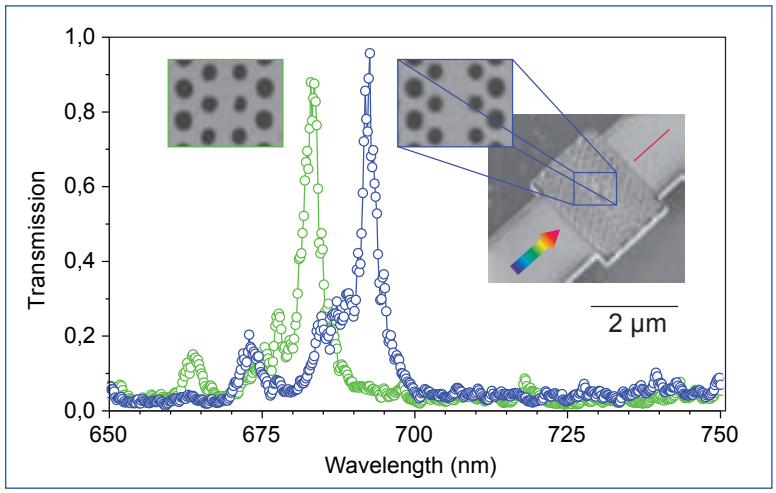

Fig: 20:
Measured transmission characteristics of the fabricated photonic crystal filters. The filter device as depicted in the upper right part of the spectra is only roughly 2 x 3 µm large and can be directly integrated into a film optical waveguide. High filter transmission as well as narrow transmission peaks can be achieved by optimizing the filter geometry as shown using examples of two fabricated devices.

Using the triangular hole arrangement, we further fabricated few demonstrators of highly potential applications, i.e. extremely compact photonic filters suitable for high density optical information processing. The devices were less than 2 x 3 µm in size and exhibited peak transmissions as high as 90% with typical values of the peak line width of only 3 nm. Among other examples of devices were high quality optical micro-resonators suitable for ultra small lasers or future lighting devices. These were created by omitting few consecutive holes in the regular crystal lattice and thus were typically smaller few λ^2. At the same time, the quality factor values of the resonators exceeded some 1,500, being so the best values reported up to date for corresponding systems operating in the visible range.

Contact:
Josef Kouba
josef.kouba@bessy.de
Daniel Schondelmaier
daniel.schondelmaier@bessy.de

NOBLE TRACES

USER PAGES

Operation Statistics

In 2007, we scheduled 38 weeks for user operation resulting in a maximum amount of 4,900 operation hours. In addition 7 weeks for machine studies and commissioning of insertion devices and beamlines were distributed over the whole year. In autumn, we have had a shutdown period of 5 weeks to install new storage ring components, insertion devices and a new laser guide system for the fs-slicing source. After almost 10 years of failure free operation, shortly after this shut-down period a short circuit in the injection septum of the storage ring caused a loss of almost 3 operation weeks (see also Machine Operation). Nevertheless, by the end of the year we had delivered 4,830 user operation hours, 98.6% of the scheduled amount.

In total 8,065 shifts of 8 h at 26 ID beamlines and 5,885 shifts at 18 bending magnet beamlines were delivered. The graphs show the distribution of the provided beamtime with respect to the different user institutions and funding programs.

In the two application periods of 2007 a total number of 970 proposals have been submitted via BOAT (BESSY Online Access Tool), for 746 projects beamtime could be allocated, 224 had to be rejected. The distribution of the proposals among the different scientific categories can be seen in the graphics. More than 1,230 researchers from 337 institutes visited BESSY to perform their studies. Among them were 22% from EU-countries and almost 10% from international institutes outside Europe. This ever increasing numbers indicate the international reputation of BESSY in the synchrotron radiation community.

Beamtime at BESSY

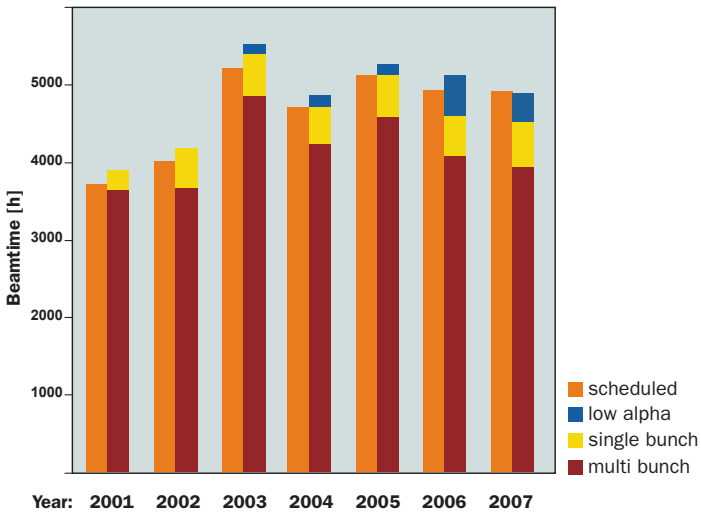

Main Research Areas

Number of Proposals

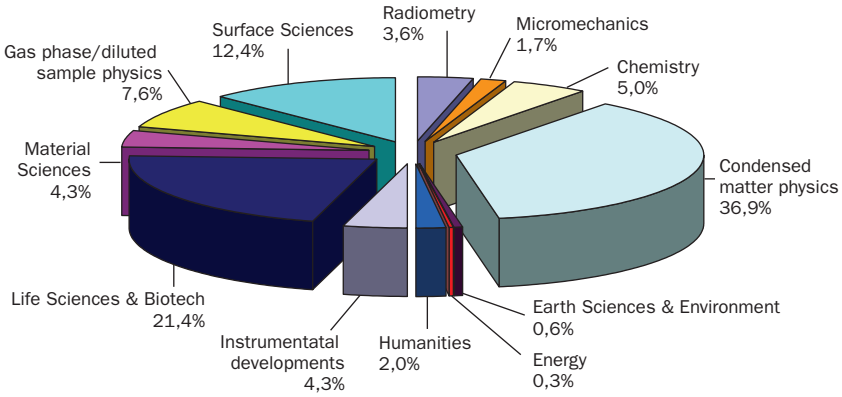

Beamtime allocation in 2007

Insertion Device Beamlines

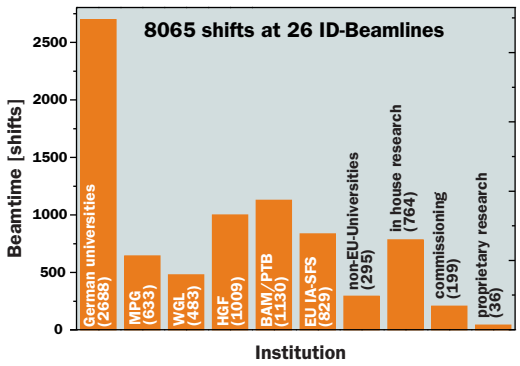

Bending Magnet Beamlines

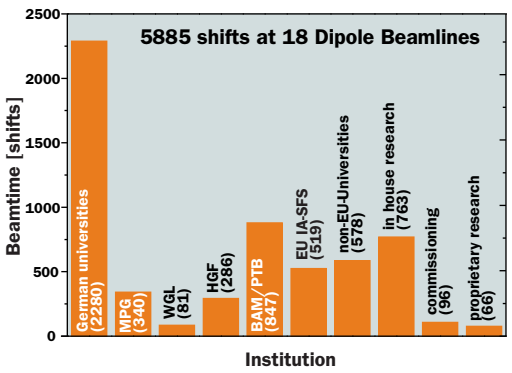

MPG
Max-Planck-Gesellschaft

WGL
Leibniz Gemeinschaft

BAM
Bundesanstalt für Material-forschung- und prüfung

PTB
Physikalisch-Technische Bundesanstalt

EU IA-SFS
Integrating Activity on Synchrotron & FEL

Improvements for Users

During the last year, we finalised installations in order to start with the detailed commissioning of our latest insertion device - the new UE112. In February, the dipole chamber subsequent to the UE112 was replaced by the new copper chamber. This chamber will serve the low energy, high resolution plane grating beamline for band structure investigations with variable polarisation. This was the final step required to enable the tuning the UE112 to deliver circularly polarised light.

The main contribution of the dynamic multipoles in the elliptical mode had already been removed in the magnet laboratory using L-shaped Fe-shims. During commissioning we studied the effect of the shims and performed a 'on-line' fine tuning based on dynamic aperture measurements. After three iterations the dynamic aperture was close to the value with gap open. In the inclined mode the L-shims are of no use. Thus, we had to develop an active dynamic multipole compensation technique. A total of 28 flat wires (3 mm wide and 0.3 mm high) were glued to the insertion device chamber. These wires can be independently powered by 14 power supplies. With the appropriate current settings for the individual wires, the dynamic multipoles generated in the inclined mode and the residual errors in the elliptical mode can be compensated. First preliminary results confirm the new concept (Fig. 1).

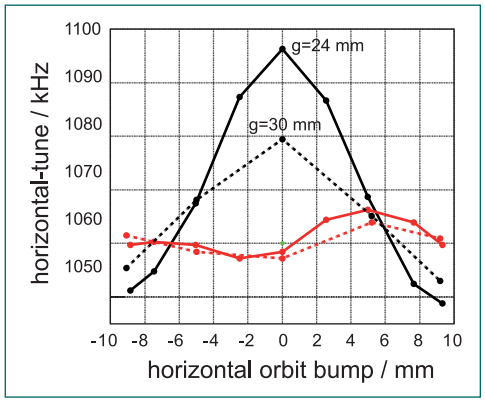

Fig. 1:
Horizontal tune shift versus horizontal beam amplitude at the UE112 for a shift of 28 mm (inclined mode, black curves) for g=24 mm (solid line) and g=30 mm (dashed line). The tune shift is reduced, if the flat wires are powered (red curves).

For the U125-2, our second long period insertion device, we further reduced its interaction with the stored electron beam by adding magic fingers at either end of the device. The dynamic multipoles of U125-2 are of minor importance and have not yet been shimmed.

The work spent on re-shimming the insertion devices and reducing their interaction with the stored electron beam is also crucial for exploring the conditions for top-up operation, since high injection efficiency is indispensable this operation mode. Although the electron storage ring BESSY-II has not been designed this specific operation mode, 'to-pup' is under consideration for several years. Up to now, we have identified several critical components that might limit the top-up operation, and we carried out appropriate modifications to be ready for a test run.

The decision about a possible topup operation is based on two critical issues: radiation

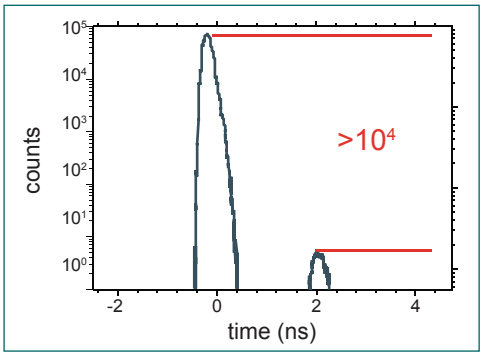

Fig. 2:
Improved bunch purity in the single bunch mode.

safety and easy access to the storage ring hall. The current operation licence of BESSY requires that all beam shutters are closed during injection, and all radiation safety measures are taken on this basis. The storage ring operation with beam shutters open during injection, as required for top-up operation, thus thus needs an adjustment of the radiation safety measures. In parallel, discussions concerning the feasibility of this operation mode for the experiments carried out at BESSY, in particular with respect to one our main user, the PTB, took place resulting in a variety of predictions. We therefore decided to run a one week of top-up test operation including real user experiments. After the modification of the interlock system to guarantee that only selected beam shutters could be opened during injection, we eventually got permission by the authorising agency to run topup test operation in week 3 of 2008: The results of this test phase and the conclusion derived will be presented to our users on the user's meeting in December 2008.

By the end of November 2006, one of the high-temperature superconducting feedthroughs of the 7T wavelength shifter, serving the macromolecular crystallography experiments broke down. Due to this accident, the beamtime allocated for the protein crystallography users had to be cancelled until the repair of the feed-through, which took place during the two commissioning weeks scheduled for mid of February 2007. Since then, the wavelength shifter has been operational without interruptions.

An improvement could be achieved for our single bunch users. As reported earlier, a new system was implemented in 2006 to determine the fill pattern of the storage ring, and, especially relevant for multi-bunch hybrid mode and single bunch operation, to keep the position of the single bunch injected constant from fill to fill. The system is based on time controlled single photon counting (TCSPC)

which proved to be a reliable tool. Using this tool, and after optimisation of the storage ring parameters and indroduction of a modified knock-out generator, we are now able to offer a purity of better than 10.000 for the duration of the fill of about 4-5 hours in the hybride mode (Fig. 2).

One of the most urgent claims derived from the 2006 workshop on Synchrotron Radiation in Art & Archaeology (SR2A), was the implementation of a climate control inside the experimental hutch of at least at one of BESSY's beamlines used for the investigations on cultural heritages and art works. As a consequence, we installed a climate control for the hutch at the µSpot-beamline, which is frequently used for this type of investigations. The parameter ranges for temperature and relative humidity were specified in close collaboration with users from museums and relevant institutes. The temperature can now be set to values in the range 17°C to 24 °C, with an accuracy of ±0.5°C. For the relative humidity, values between 40% and 60% can be selected, with an accuracy of ±1.25%. With the improved sample environment, ancient parchments like the dead-sea scrolls and delicate pieces of art can now be studied at BESSY.

We are prepared to improve our user services constantly. However, we need your feedback and your suggestions. BESSY has a couple of tracks to stay in touch with our users aiming at improving the quality of the support offered especially during your stay. The most powerful among them are the User Committee and the Technical User Feedback. The information obtained via these two channels is taken serious and we are anxious to react on these information. Of course, this instrument can only develop its full power, as long as we get input from as much of our users as possible.

Unfortunately, we had to realize that during the first beamtime period we received only 84 reports out of 435 user shifts, a participation of less than 20 %. (Fig.3). Among these, about 60 reports ranked "excellent" in all categories. Unbelievable – if true. Within the remaining reports, experimental problems with the sample or its treatment were identified to be crucial for the success of the work, but also the support offered by BESSY – beamline control, information, storage ring operation access to laboratories and mechanical workshops – as well as subsistence, lodging, transportation and missing recess rooms were topics of complaints. In order to further improve the user support, we kindly ask all our users to fill in the Technical User Feedback forms right after the end of their shifts. Also inform the user committee about complaints, suggestions and wishes.

During the last years, the BESSY Online Access Tools (BOAT) has developed to an important tool for handling the beamtime request and all the bits and pieces related to beamtime at BESSY. This includes the preparation of beamtime with the required Safety Declarations and the Radiation Safety Registration for dosimeters as well as reservation of lodging and safety instructions. In 2007, a new feature could be implemented which is supposed to make life easier for main proposers of beamtime. They now can delegate all the administrative work connected to BOAT like beamtime preparation and Technical User Feedback to an executive scientist of their group – if s/he agrees. This feature had been suggested by the User Committee in one of its regular meetings with the management. The members of this committee also helped testing and debugging the first version of the new feature, showing that there is a fruitful cooperation between BESSY and its users.

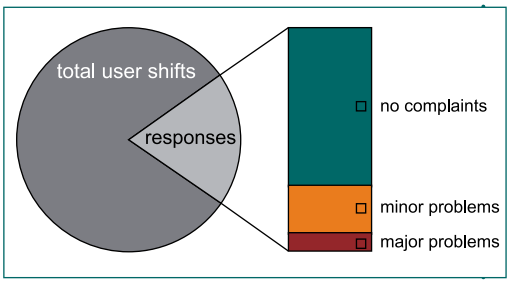

Fig. 3:
In 2007, only about 20% of our users gave a feedback on success and suggestions concerning their beamtime. Only a few of those sent us complaints, suggestions, whishes and desires.

It is the aim of BESSY to provide the infrastructure required to successfully perform experiments inside the complex area of the storage ring hall. This infrastructure covers a wide range of facets – beamline control, user support, Hallendienst and lodging are only a few of them. Although we intend to offer a complete service, gaps remain which then are filled by our users proactively. The resulting solutions often show a large amount of improvisation. But it is the result that counts.

Fig. 4:
Improvements by user.
Top: A coat hanger to stabilize the exhaust line of a differentially pumped feethrough at a manipulator; Bottom: A deck chair, making night shifts more convenient.

The **User Committee** is an important link between the users and the Scientific Director. The committee collects matters of concern to individual users working in the experimental hall, conveys an assessment summary of these matters and suggests appropriate measures.

Major topics discussed in 2007:

- user concerns on the planned top-up mode
- increase of the number of staff for user service,
- the need to inform users on new instruments,
- concerns on the merger of HMI & BESSY into a new Helmholtz Centre.

We need your feedback!
For many questions we require more user feedback. An important example is the plan for a replacement of the widely-used, but outdated, EMP data acquisition program. Here, users are asked to express their wishes for an improved software.

User Committee:

Tobias Lau	*Technische Universität Berlin*
Thomas Schmidt	*Universität Würzburg*
Christoph Cobet	*ISAS Berlin*
Thomas Seyller	*Universität Erlangen*

ID Beamlines at BESSY (January 2008)

ID	Beamline	Energy Range (eV)	Operated by	Contact	
7T-WLS-1	BAMline µSpot	5 k - 40 k 2 k -30 k	BAM/PTB BAM/MPIKG	H. Riesemeier, B. Müller (BAM) H. Riesemeier (BAM), O. Paris (MPIKG)	A. Erko I. Zizak
U125-2	U125-2_SGM U125-2_KMC U125-2_NIM	20 - 500 6 k - 12 k 4 - 40	BUS PDI/HUB Uni KI/BESSY	R. Püttner (FUB) W. Braun, P. Jenichen (PDI) G. Reichardt	G. Reichardt A. Erko I.Packe
7T-MPW	7T-MPW_EDDI 7T-MPW_MagS	10 k - 150 k 5 k - 30 k	HMI HMI	Ch. Genzel, I. Denks, G. Wagner (HMI) E. Dudzik, R. Feyerherm, G. Wagner (HMI)	 A. Erko A. Erko
UE56-2	UE56-2_PGM-1 UE56-2_PGM-2	60 - 1,300 60 - 1,300	MPG MPG	W. Mahler, B. Zada (MPG) W. Mahler, B. Zada (MPG)	
6T-WLS **0.4T-LFD**	DXRL-1	1,500 - 6,000	BESSY	B. Löchel, H.-U. Scheunemann	H. Köhrich
UE49	UE49_PGM a/b	100 - 1,800	BESSY	F. Kronast, M. Mast	J.-S. Schmidt
UE52	UE52_SGM UE52_PGM	90 - 1,500 85 - 1,600	BESSY Uni Wü	K. Godehusen, F. Senf D. Batchelor (Uni Wü)	T. Zeschke Ch. Jung
UE46	UE52_PGM-1 *UE46-XM* *UE46-STXM*	120 - 1,700 *120 - 1,700* *120 - 1,700*	HMI *BESSY* *MPIMF*	D. Schmitz, H. Rossner (HMI) *Under Construction* *Under Construction*	F. Senf
UE56-1	UE56-1_PGM a/b UE56-1_ZP UE56-1_SGM	60 - 1,300 715 / 786 / 861 55 - 1,500	BESSY BESSY FZJ	T. Kachel, J.-S. Schmidt A. Firsov S. Cramm (FZJ)	Ch. Stamm I. Packe
U41	U41-TXM / STXM U41-STXM U41_PGM	~ 250 - ~ 600 ~ 250 - ~ 600 170 - 1,800	BESSY/Uni Gö BESSY/Uni Gö BESSY	P. Guttmann (Uni Gö) P. Guttmann (Uni Gö) Ch. Jung	G. Schneider G. Schneider M. Mast
UE112	UE112_PGM-1 UE112_PGM-2 a/b	20 - 700 4 - 200	BESSY BESSY	O. Schwarzkopf R. Follath	F. Eggenstein J.-S. Schmidt
7T WLS-2	MX_Beamline 14.1 MX_Beamline 14.2 MX_Beamline 14.3	5 k - 15.5 k 5 k - 15.5 k 13.87	BESSY FUB BESSY	U. Müller M. Fuchs U. Müller	
U49-2	U49-2_PGM-1 U49-2_PGM-2	85 - 1,600 85 - 1,600	BESSY BTUC	O. Schwarzkopf P. Hoffmann (BTUC)	J.-S. Schmidt W. Braun

PTB Laboratory		Energy Range (eV)	Contact
U49-1	direct beam 13° PGM	direct beam 20 - 1,900	R. Klein (PTB) R. Klein, A. Gottwald (PTB) B. Beckhoff (PTB)

BAM Bundesanstalt für Materialforschung und -prüfung
BTUC Brandenburgische Technische Universität Cottbus
BUS Berliner Universitätsverbund Synchrotronstrahlung
FHI Fritz-Haber-Institut Berlin
FUB Freie Universität Berlin
FZJ Forschungszentrum Jülich
HMI Hahn-Meitner-Institut
HUB Humboldt Universität zu Berlin
Uni Gö Universität Göttingen
MPIKG Max-Planck-Institut für Kolloid- und Grenzflächenforschung
MPIMF Max-Planck-Institut für Metallforschung
MPG Max-Planck-Gesellschaft
PDI Paul-Drude-Institut
PTB Physikalisch-Technische Bundesanstalt
Uni KI Universität Kaiserslautern
Uni Wü Universität Würzburg

Dipole Beamlines at BESSY (January 2008)

Beamline	Energy Range (eV)	Contact	
Litho EUV	95	H.-U. Scheunemann	H. Köhrich
KMC-1	1.7 k - 10 k	M. Gorgoi	M. Mertin
IRIS	0.0006 - 1 0.1 - 300 THz*	U. Schade	
ISISS	80 - 2,000	M. Hävecker, A. Knop-Gericke (FHI)	T. Blume
DXRL-2	direct beam	B. Löchel, H.-U. Scheunemann	H. Köhrich
HE-SGM	200 - 700	A. Lippitz (BAM)	O. Schwarzkopf
Optics-Beamline	20 - 1,300	F. Senf	
KMC-2	5 k - 14 k	A. Erko	I. Packe
PGM-3	20 - 1,900	T. Kachel	F. Eggenstein
3m-NIM-A	2 - 40	G. Reichardt	I. Packe
3m-NIM-C	2 - 10	G. Reichardt	I. Packe
EDR	5 k - 40 k	W. Leitenberger (Uni P)	A. Erko
TGM 4	7 - 130	K. Godehusen	M. Mast
TGM 7	8 - 120	C. Pettenkofer, W. Bremsteller (HMI)	
RGBL	30 - 1,500	Y. Dedkov (Uni DD) S. Molodtsov (Uni DD	
CP-NIM	4 - 35	F. Schäfers	M. Mertin

*low-alpha operation mode

PTB Laboratory	Energy Range (eV)	Contact	
1m-NIM 1	3 - 35	M. Richter (PTB)	Moved to MLS
1m-NIM 2	3 - 35	R. Thornagel (PTB)	
white beam		R. Thornagel (PTB)	
KMC	1.7 k -10 k	M. Krumrey (PTB)	
PGM	30 - 1,800	F. Scholze (PTB)	

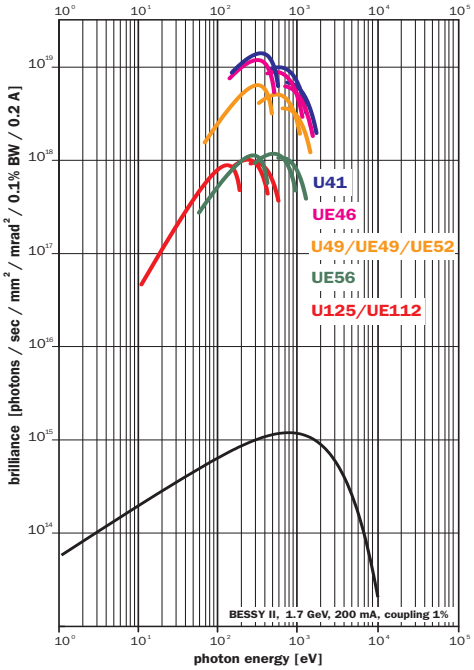

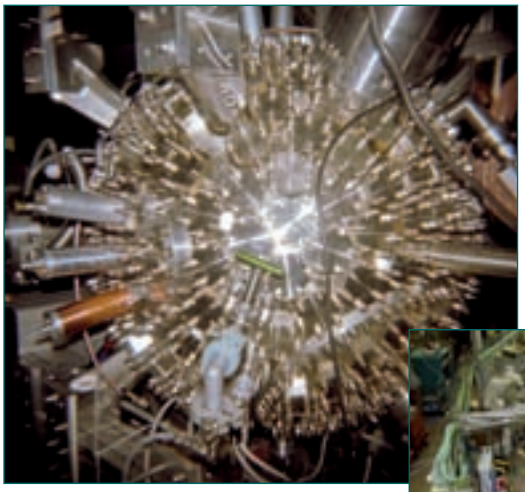

Experimental Stations

The MAGS endstation: the six-circle Huber diffractometer with cryostat.

The **MAGS** endstation is dedicated to **MAG**netic resonant X-ray **S**cattering and hard X-ray diffraction experiments. It was built by the Hahn-Meitner-Institut Berlin to study magnetism and other cooperative phenomena, but is used additionally as a versatile X-ray diffraction instrument. MAGS is accessible to external users and in-house researchers, and can provide support for users who wish to take advantage of the complementary nature of neutron and X-ray scattering experiments, where X-ray resonant scattering provides higher resolution, element selectivity and the possibility to separate magnetic and structural contributions.

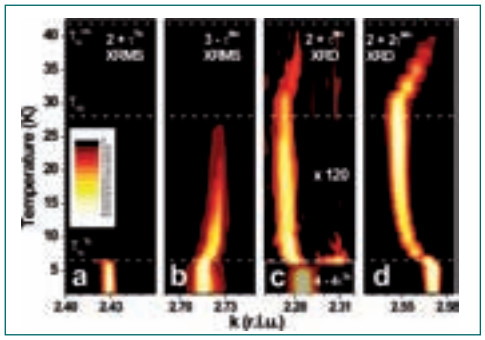

X-ray resonant and non-resonant temperature dependence of $TbMnO^3$ superstructure peaks (O. Prokhnenko et al., PRL 99, 188206 (2007)).

With a 7 Tesla multipole wiggler source, the beamline provides strong flux at photon energies between 4 and 30 keV. The optics consists of a pair of collimating/focussing mirrors and a Si(111) double crystal monochromator producing a horizontally and vertically focussed beam at the experimental endstation with fluxes of the order of 10^{12} photons/s at 10 keV.

The MAGS endstation consists of a 6-circle Huber diffractometer, which allows vertical, horizontal, and more complex scattering geometries. An additional three-circle polarisation analyser with a large set of crystals is optional. Available sample environments are a displex cryofurnace for temperatures from 6 to 800 K and cryostats with both 1.5 and 4 K base temperature. A 5 Tesla magnet is currently being commissioned. Samples can be mounted either on a standard goniometer head, inside the closed cycle cryostats or on an xyz-table mounted on the diffractometer. Two detectors are available: a Canberra Ge diode with an multichannel analyser for energy resolved detection, and a robust Oxford Danfysik scintillation detector. With an analyser in place only the smaller scintillation detector can be used. An off-line 4-circle diffractometer can be used for pre-aligning single crystal samples.

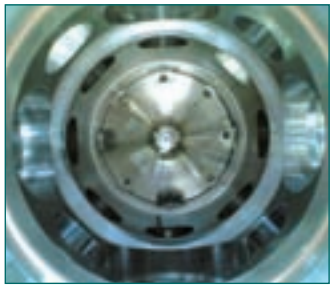

For electrons only! Looking on the objective lens of the SPEEM

This **SPEEM** endstation (**S**pin resolved **P**hoto-**E**mission Electron **M**icroscope) is dedicated to nano-spectroscopy of magnetic materials and nanostructures. It is equipped with a commercial PEEM (Elmitec GmbH) capable of 20 nm spatial resolution for synchrotron light excitation. The integrated imaging energy analyzer allows spatial resolved photoemission spectroscopy with an energy resolution of 0.48eV. A specialty of this new instrument is the integrated spin analysis. Using two electrostatic deflectors the photoelectron beam can be defected into one of the two attached Mott polarimeters. All three Cartesian components of the photoelectron spin can be measured using the Mott detectors. Confining the electron beam with an adjustable aperture in the last image plane of the microscope the spin polarization of areas with a minimum size down to 200 nm can be analyzed.

Samples can be investigated under various conditions, e.g. the temperature can be controlled between 110 K and 1,000 K and even magnetic fields up to several 10mT can be applied during imaging. To keep the exposure times in the microscopy mode as short as possible the SPEEM is permanently installed at a dedicated microfocus beamline, the UE49_PGMa. This beamline covers an energy range between 100 eV and 1,800 eV with full X-ray polarization control and a spectral resolution of about 10,000 ($E/\Delta E$) at 700 eV using the grating with 1,200 l/mm. A second grating with 600 l/mm is also available to provide higher photon flux at lower spectral resolution. The typical spot size on the sample surface is 8 x 32 µm (FWHM).

Time resolved experiments will become possible in the near future. A Titanium Sapphire laser-system with 5 MHz repetition rate and 300 nJ pulse energy will be set up during 2008 in order to perform pump-probe experiments.

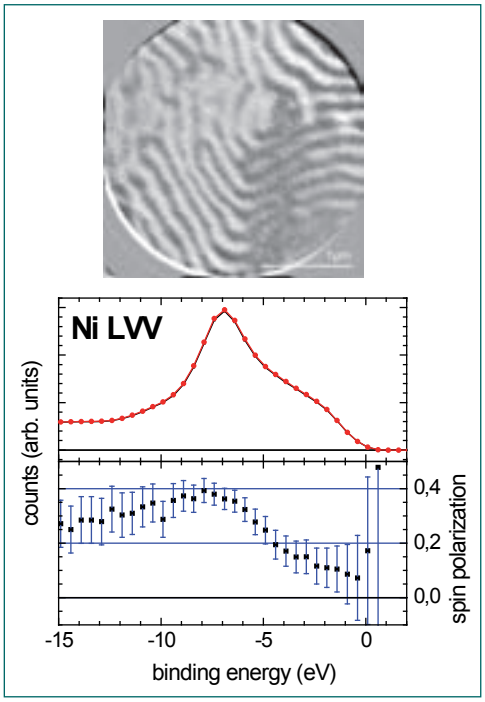

PEEM image of magnetic domains in a Nickel film recorded by using the X-ray circular dichroism at the L_3 edge of Ni. The lower side shows a spin-resolved resonant valence band photoemission spectrum of this Nickel film.

Permanent experimental stations

Experiment	Contact	Location
THz, THz-EPR spectroscopy	holldack@bessy.de	THz-Beamline
IR-/THz-spectroscopy and -microscopy[BioSR, Ind]	schade@bessy.de	IRIS
IR ellipsometry[Ind]	hinrichs@isas-berlin.de	IRIS
SURICAT - photoelectron and absorption spectroscopy	antje.vollmer@bessy.de	Optics Beamline
Femto-s-Pump-Probe - femtosecond slicing	hermann.duerr@bessy.de	UE56-1_PGM-A
One-Cubed ARPES - 1³-ARPES ultra high resolution photoemission	s.borysenko@ifw-dresden.de	UE112_PGM-2b
Two-Photon-Photoemission Experiment	weinelt@mbi-berlin.de	UE112 PGM 1
Dispersive NEXAFS	batchelor@uni-wuerzbug.de	UE52_PGM
GAMBIT - generalized absorption of magnetic moments by ion trapping	neeb@bessy.de	UE52_PGM
SPEEM - spin resolved photoemission microscopyplanned	florian.kronast@bessy.de	UE49_PGM a
SMART - spectro-microscopy with aberration correction	thomas.schmidt@physik.uni-wuerzburg.de	UE49_PGM b
7T High-Field Endstation - high magnetic field X-ray dichroism	schmitz@hmi.de	UE46_PGM
Reflectometry[Ind]	schaefers@bessy.de	Optics Beamline
XM - X-ray microscopy[BioSR, Ind]	guttmann@bessy.de	U41-TXM
ROSA - rotateable spectrometer apparatus	denecke@rz.uni-leipzig.de	U41_PGM
EUV-Scanner	scheunemann@bessy.de	Litho EUV
DEX-01[Ind]	loechel@bessy.de	DXRL-1
DEX-02[Ind]	loechel@bessy.de	DXRL-2
HIKE - high kinetic energy photoemission	mihaela.gorgoi@bessy.de	KMC-1
PHARAO - X-ray diffraction during MBE	braun@pdi-berlin.de	U125-2_KMC
mySpot - micro-XANES, -EXAFS, -fluorescence[BioSR]	zizak@bessy.de	mySpot Beamline
Diffraction	erko@bessy.de	KMC-2
MX-14-1 - Macromolecular Crystallography[BioSR, Ind]	umue@bessy.de	MX_BEAMLINE_14.1
MX-14-2 - Macromolecular Crystallography[BioSR, Ind]	fuchs@bessy.de	MX_BEAMLINE_14.2
MX-14-3 - Macromolecular Crystallography[BioSR, Ind]	umue@bessy.de	MX_BEAMLINE_14.3
BAMline - nondestructive testing in analytical chemistry[Ind]	heinrich.riesemeier@bam.de	BAMline
SAXS - ASAXS/GISAXS	hoell@hmi.de	7T-MPW-MAGS
MagS - resonant magnetic scattering	feyerherm@hmi.de	7T-MPW-MAGS
EDDI - energy dispersive diffraction	genzel@hmi.de	7T-MPW-EDDI

Variable experimental stations

Experiment	Contact	Location
HIRES - high resolution electron spectrometer	rader@bessy.de	Various
PHOENEXS - photoemission and near edge X-ray spectroscopy	varykhalov@bessy.de	U49-2_PGM-1
MUSTANG - multi-user stage for angular resolved photoemission	gavrila@bessy.de	Various
UVIS - protein circular dichroism spectroscopy[BioSR]	baumgaer@rz.uni-potsdam.de	3m-NIM-C, U125-2_NIM
High resolution spinpolarisation photoelectron spectroscopy	c.m.schneider@fz-jülich.de	UE56-1_SGM
Stored Nano Particels	ruehl@phys-chemie.uni-wuerzburg.de	UE52_SGM, U41_PGM
So-Li-AS - solid-liquid-analysis system	mayerth@surface.tu-darmstadt.de	TGM-4, TGM-7
VUV Ellipsometer - VUV/XUVellipsometry station[Ind]	esser@isas-berlin.de	3m-NIM-A
Scattering experiments in the VUV/XUV-range	eugen.weschke@physik.fu-berlin.de	UE46_PGM-1
Photoemission microscope for time resolved spectroscopy in the ps-regime[Ind]	schoenhe@mail.uni-mainz.de	UE56-1_SGM
LIQUIDROME - liquids and degassing samples equipment	emad.aziz@bessy.de	U41_PGM, U49-2_PGM-1/2
ISISS - innovative station for in-situ spectroscopy	knop@fhi-berlin.mpg.de	ISISS, U49-2_PGM-1/2
CISSY - CIS- diagnostic using Synchrotron radiation	cissy@hmi.de	U41_PGM
FLUORO - Fluorescence spectroscopy[Ind]	ruediger.mitdank@physik.hu-berlin.de	U41_PGM
Polarimeter - Polarimetry	schaefers@bessy.de	UE52_SGM, UE56-1_PGM-A

[BioSR] suitable for biological samples; [Ind] suitable for industrial users

Status of BESSY

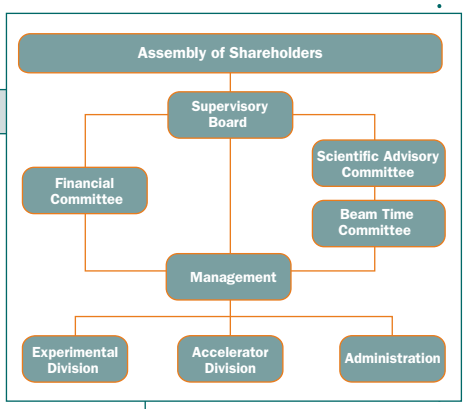

Supervisory Board

Prof. Dr. J. Treusch (Chairman)	Jacobs Universität Bremen
Prof. Dr. E. Umbach (Vice-Chairman)	Forschungszentrum Karlsruhe, KIT
Frau Dr. B. Vierkorn-Rudolph	Bundesministerium für Bildung und Forschung
Prof. Dr. E. O. Göbel	PTB Braunschweig
R. Willems	Max-Planck-Gesellschaft München
Prof. Dr. J. Schneider	DESY Hamburg
MinR. N. Barz	Bundesministerium für Wirtschaft und Technologie
Prof. Dr. M. Steiner	HMI Berlin
SenDir. W. Eckey	Senatsverwaltung für Bildung, Wissenschaft und Forschung Berlin
Prof. Dr. F.W. Scheller	Universität Potsdam
Prof. Dr. W. Wurth	Universität Hamburg

Scientific Advisory Committee

Prof. Dr. R. Schlögl (Chairman))	Fritz-Haber-Institut der MPG Berlin
Prof. Dr. M. Tolan (Vice-Chairman)	Universität Dortmund
Prof. Dr. H. Ade	North Carolina State University
Prof. Dr. V. Bonacic-Koutecký	Humboldt Universität zu Berlin
Prof. Dr. R. Brinkmann	DESY Hamburg
Prof. Dr. T. Elsässer	Max-Born-Institut Berlin
Prof. Dr. R. Falcone	ALS Berkeley (Institutional Member)
Prof. Dr. - Ing. N. Langhoff	Institut for Scientific Instruments Berlin
Prof. Dr. N. Martensson	MAXLAB, Sweden
Prof. Dr. E. Rühl	Freie Universität Berlin
Priv.-Prof. Dr. I. Schlichting	Max-Planck-Institut für medizinische Forschung Heidelberg
Prof. Dr. H.-P. Steinrück	Universität Erlangen-Nürnberg

Permanent Guests

Dr. J. Feldhaus	HASYLAB/DESY Hamburg
Prof. Dr. M. Stutzmann	Technische Universität München
Prof. Dr. W. Salz	BMBF
Dr. R. Schuchhardt	Senatsverwaltung für Bildung, Wissenschaft und Forschung Berlin

Beam Time Committee

Prof. Dr. W. Wurth (Chairman)	Universität Hamburg
Prof. Dr. L. Singheiser (Vice-Chairman)	Forschungszentrum Jülich
Prof. Dr. S. Blügel	Forschungszentrum Jülich
Prof. Dr. R. Claessen	Universität Würzburg
Prof. Dr. T. Elsässer	Max-Born-Institut Berlin
Prof. Dr. K. Horn	Fritz-Haber Institut der MPG Berlin
Prof. Dr. W. Kuch	Freie Universität Berlin
Dr. M. Meyer	Centre Universitaire Paris-Sud
Prof. Dr. A. R. Pyzalla	MPI für Eisenforschung Düsseldorf
Prof. Dr. W. Reimers	Technische Universität Berlin
Prof. Dr. L. Hao Tjeng	Universität zu Köln
Prof. Dr. H. Zabel	Ruhr-Universität Bochum

Sub-Committee Protein Crystallography

Prof. Dr. R. Ficner	Universität Göttingen
Prof. Dr. P. Lindley	Universität Lissabon
Dr. M. Wilmanns	EMBL Hamburg

Financial Committee

Ass.jur. S. Lettow (Chairman)	Forschungszentrum Karlsruhe
R. Kellermann (Vice-Chairman)	Forschungszentrum Jülich
Dr. W. Buck	PTB Berlin
M. Schleier	Max-Planck-Gesellschaft München
Dr. R. Schuchardt	Senatsverwaltung für Bildung, Wissenschaft und Forschung Berlin
H. Görres	Bundesministerium für Bildung und Forschung

User Committee

Dr. T. Lau	Technische Universität Berlin
Dr. T. Schmidt	Universität Würzburg
Dr. C. Cobet	ISAS Berlin
PD Dr. T. Seyller	Universität Erlangen

CONTACT:

Scientific Director
Prof. Dr. Dr. h.c. Wolfgang Eberhardt
Secretary: Ines Maupetit
phone +49 (0)30 / 6392 4633
fax +49 (0)30 / 6392 2989
wolfgang.eberhardt@bessy.de,
ines.maupetit@bessy.de

Technical Director
Prof. Dr. Eberhard Jaeschke
Secretary: Dr. Nikoline Hansen
phone +49 (0)30 / 6392 4651
fax +49 (0)30 / 6392 4632
eberhard.jaeschke@bessy.de,
nikoline.hansen@bessy.de

Administration
Thomas Frederking
Secretary: Katrin Rosenblatt
phone +49 (0)30 / 6392 2901
fax +49 (0)30 / 6392 2920
thomas.frederking@bessy.de,
katrin.rosenblatt@bessy.de

Beamtime Coordination
Dr. Walter Braun, Dr. Gerd Reichardt
Secretary: Stine Mallwitz
phone +49 (0)30 / 6392 2904
fax +49 (0)30 / 6392 4673
beamtime@bessy.de

User Office
Ines Drochner, Cornelia Stürze,
Daniela Theile
phone +49 (0)30 / 6392 4734
fax +49 (0)30 / 6392 4746
useroffice@bessy.de

Public Relations
Gabriele André, Sandra Fischer,
Dr. Markus Sauerborn
phone +49 (0)30 / 6392 4921
fax +49 (0)30 / 6392 4972
pr@bessy.de

Credits

For providing photographs and drawings we would like to thank:

Bernhard Schurian

Cartoonstock.com

Get In The Hole Golf Company, Holmdel, Ireland

Gary Sova

Forschungzentrum Jülich

Fritz-Haber-Institut

Hahn-Meitner-Institut

Heiko Wende

Kai Godehusen

media.nasaexplores.com

Pedro Brito

www.aboutpixel.de

I would also like to thank my colleagues Gabriele André and Sandra Fischer who kept me free form other tasks and K., A. and P.

BESSY